Tectonics®

RESEARCH ARTICLE
10.1029/2022TC007366

Key Points:

- Three sets of microfolds (Foliation Inflexion/Intersection Axis, FIA) preserved within garnet porphyroblasts of the Betic-Rif orogen record changes in crustal shortening direction
- New Sm-Nd garnet ages reveal Eocene to Miocene tectonism in the Nevado-Filabride complex
- Integration of FIA data with garnet geochronology shown powerful tool for reconstructing past plate motions

Supporting Information:

Supporting Information may be found in the online version of this article.

Correspondence to:

D. G. A. M. Aerden,
aerden@ugr.es

Citation:

Aerden, D. G. A. M., Farrell, T. P., Baxter, E. F., Stewart, E. M., Ruiz-Fuentes, A., & Bouybaouene, M. (2022). Refined tectonic evolution of the Betic-Rif orogen through integrated 3-D microstructural analysis and Sm-Nd dating of garnet porphyroblasts. *Tectonics*, *41*, e2022TC007366. https://doi.org/10.1029/2022TC007366

Received 3 MAY 2022
Accepted 14 SEP 2022

Author Contributions:

Conceptualization: Domingo G. A. M. Aerden
Formal analysis: Domingo G. A. M. Aerden, Thomas P. Farrell, Emily M. Stewart, Alejandro Ruiz-Fuentes
Funding acquisition: Domingo G. A. M. Aerden, Ethan F. Baxter
Investigation: Domingo G. A. M. Aerden, Thomas P. Farrell, Ethan F. Baxter, Emily M. Stewart, Alejandro Ruiz-Fuentes, Mohamed Bouybaouene

Refined Tectonic Evolution of the Betic-Rif Orogen Through Integrated 3-D Microstructural Analysis and Sm-Nd Dating of Garnet Porphyroblasts

Domingo G. A. M. Aerden[1,2], Thomas P. Farrell[3,4], Ethan F. Baxter[3,5], Emily M. Stewart[5,6], Alejandro Ruiz-Fuentes[1], and Mohamed Bouybaouene[7]

[1]Departamento de Geodinámica, Universidad de Granada, Granada, Spain, [2]Instituto Andaluz de Ciencias de la Tierra (CSIC-UGR), Granada, Spain, [3]Department of Earth and Environmental Sciences, Boston College, Chestnut Hill, MA, USA, [4]Now at Department of Geoscience, Boise State University, Boise, ID, USA, [5]Department of Earth and Environment, Boston University, Boston, MA, USA, [6]Now at Department of Earth, Ocean and Atmospheric Science, Florida State University, Tallahassee, FL, USA, [7]Département de Géologie, Université de Rabat, Rabat, Morocco

Abstract High-resolution microstructural analysis of porphyroblast inclusion trails integrated with Sm-Nd garnet geochronology has provided new insight into the tectonic history of the Betic-Rif orogen. Three principal age groups of porphyroblasts are demonstrated with distinctly oriented inclusion-trails. Inclusion-trail curvature axes or "FIA" (Foliation Inflexion/Intersection Axes) are shown to represent "fossilized" crenulation axes from which a succession of different crustal shortening directions can be deduced. The regional consistency of microstructural orientations and their geometric relationship with multiple sets of macroscopic folds reveal the composite character of the Gibraltar Arc formed by a superposition of different folding directions and associated lineations. Bulk-garnet ages of 35–22 Ma obtained from five micaschist samples of the Alpujarride-Sebtide complex (ASC) and of 35–13 Ma from four micaschists of the Nevado-Filabride complex (NFC) allow to deduce NNE-SSW directed shortening in the Late Eocene changing to NW-SE shortening in the early Oligocene, alternating with suborthogonal NE-SW shortening during the Miocene. These directions can be related to a major swing in the direction of relative Africa-Iberia plate-motion known from kinematic modeling of magnetic seafloor anomalies, and subsequent dynamic interference between plate convergence and suborthogonal "tectonic escape" of the Alboran Domain. Coupled to previously established P-T-t paths, the new garnet ages support a common tectono-metamorphic evolution of the ASC and NFC as laterally equivalent orogenic domains until, in the Miocene, the second became re-buried under the first.

Plain Language Summary A 3D microstructural analysis of tectonic foliations preserved within garnet porphyroblasts combined with radiometric dating of these crystals has allowed reconstruction of a complex tectonic history experienced by the Betic-Rif orogen, the strongly curved mountain belt connecting southern Spain and Morocco. Multiple porphyroblast age groups can be linked to differently oriented microfolds preserved within these metamorphic crystals. The specific ages and orientations of these microstructures measured using conventional thin sections and X-ray tomography can be matched to known changes in the direction of convergence of the African and Iberian plates, thus demonstrating a powerful new tool for reconstructing past plate motions.

1. Introduction

The detailed deformation history of the Betic-Rif orogen (Figure 1) and its relationship with distinct metamorphic events recognized in this belt are still ambiguous as is reflected in disparate tectonic models that still differ on such fundamental aspects as the timing and polarity of subduction zones, the role of crustal extension versus compression, or the emplacement history of several peridotite massifs exposed in the belt (e.g., Bessière, Jolivet, et al., 2021; Jabaloy Sanchez et al., 2019; Michard et al., 2002; Platt et al., 2013; van Hinsbergen et al., 2020; Vergés & Fernàndez, 2012). This paper aims to improve this situation by examining the kinematic and geochronological record represented by metamorphic porphyroblasts and their internal tectonic fabrics (inclusion trails). Forty-four oriented samples of porphyroblastic schists from the Nevado-Filabride and Alpujarride-Sebtide complex (NFC and ASC) have been studied in precisely oriented thin sections and X-ray computed microtomographies. This 3D microstructural analysis has been integrated with Sm-Nd (thermal ionization mass spectrometry,

Methodology: Domingo G. A. M. Aerden, Ethan F. Baxter
Resources: Domingo G. A. M. Aerden, Ethan F. Baxter
Supervision: Domingo G. A. M. Aerden, Ethan F. Baxter
Visualization: Domingo G. A. M. Aerden
Writing – original draft: Domingo G. A. M. Aerden, Thomas P. Farrell
Writing – review & editing: Domingo G. A. M. Aerden

TIMS) dating of garnet porphyroblasts of 10 samples (5 from each complex) as a well-established accurate and precise method to constrain the timing of tectonometamorphic processes (e.g., Baxter et al., 2017).

The kinematic significance of porphyroblast inclusion-trails has been intensely debated particularly between 1990 and 2010 (e.g., Bell et al., 1992; Bons et al., 2009; Fay et al., 2008, 2009; Passchier et al., 1992) and since these microstructures play a central role in our study, it is appropriate to briefly outline how ideas about them have evolved. More than 100 years ago, Peach (1912) described spiral garnets from the Caledonides and already perceived what seemed an obvious explanation when they wrote: "*The garnet was rotating under the impulses received from streams of material flowing with unequal velocities past its two sides. It was being rolled along, and was growing larger, like a snowball, during the process*." During much of the twentieth century, the "snowball" model remained unquestioned and was further refined (Zwart, 1960; Spry, 1963; Rosenfeld, 1968 amongst others). Three simple predictions of the model are (a) that the curvature sense of inclusion-trails (from the center outward) is opposite to the shear sense, (b) that the curvature axes lies normal to the shearing direction, and (c) that the amount of curvature is related to the amount of shear strain. McLachlan (1953) was probably the first to apply these principles to a regional tectonic problem. It was debated at the time whether a fold-axes parallel lineation in the Moine schists (Scottish Caledonides) formed parallel or perpendicular to the direction of regional tectonic transport. By cutting thin sections parallel and perpendicular to the lineation in several samples hosting spiral garnets, McLachlan (1953) determined that the spiral axes were subparallel to the lineation. Consequently, he concluded tectonic transport (i.e., thrusting) orthogonal to the lineation and fold axes. Interestingly, a similar conclusion will be reached later in this paper concerning the Betic-Rif orogen.

During the 1980s, a radically different interpretation of "rotational" inclusion trails was proposed (Bell, 1985; Bell & Hayward, 1991; Bell & Johnson, 1989; Bell et al., 1986) recognizing the control of deformation partitioning on foliation development and porphyroblast growth. Porphyroblasts were shown to preferentially nucleate within microlithon domains during early stages of crenulation-cleavage development. Depending on the relative rates of porphyroblast growth and deformation, straight to sigmoidal inclusion trails can then develop by overgrowth of crenulations without porphyroblast rotation. It was further claimed that spiral-shaped inclusion-trails form by repetition of the same process during alternating crustal shortening and gravitational collapse generating successions of steeply dipping and subhorizontal foliations.

Although initially highly controversial, the "non-rotational" model has been increasingly supported by studies revealing remarkably consistent orientations of inclusion trails in folds, shear zones (Bell & Forde, 1995; Evins, 2005; D. G. A. M. Aerden et al., 2010; Fyson, 1980; Hickey & Bell, 1999; Jung et al., 1999; Steinhardt, 1989; Timms, 2003) and across large metamorphic regions (Ali, 2010; Ali et al., 2016; Bell & Mares, 1999; Bell et al., 1998; D. G. A. M. Aerden, 1994, 1998, 2004; D. G. A. M. Aerden et al., 2013; Kim & Ree, 2013; Rich, 2006; Sanislav, 2011; Sayab, 2005; Sayab et al., 2016; Shah et al., 2011; Skrzypek et al., 2011; Yeh, 2007; Yeh & Bell, 2004). Several of these studies documented sub-orthogonal preferred orientations of inclusion trails apparently witnessing shortening-collapse cycles in the Northern Appalachians (Hayward, 1992), the Lachlan fold belt (Johnson, 1992), the Mount Isa inlier (Sayab, 2005), the Himalayas (Bell & Sapkota, 2012; Shah et al., 2011), the European Variscan belt (D. G. A. M. Aerden, 1994, 1995, 1998, 2004), or the Betic Cordillera (D. Aerden & Sayab, 2008; D. G. A. M. Aerden et al., 2013). This data suggests that ductile deformation processes in natural rocks are considerably more complex as the simple mechanics of viscous fluid flow. Indeed, advanced modeling techniques have already identified various mechanisms that potentially reduce (Griera et al., 2013; ten Grotenhuis et al., 2002), prevent (Fay et al., 2008; Johnson, 2008) or even reverse (Gardner & Wheeler, 2021) porphyroblast rotation. These studies highlight the dependency of model results on a particular rheology and boundary conditions chosen, apart from the incompleteness of our knowledge of the deformation mechanisms that operate at geological strain rates in natural rocks.

The present work extends earlier research by D. Aerden and Sayab (2008), D. G. A. M. Aerden et al. (2013), and D. G. A. M. Aerden and Ruiz-Fuentes (2020) in the NFC to the overlying ASC. These previous papers already documented multiple porphyroblast age groups associated with specifically oriented inclusion trails. They drew attention to the fact that inclusion-trail orientations can be matched to Africa-Iberia plate-convergence directions deduced from paleomagnetic data. This intriguing link between microtectonic and plate-tectonic processes is further explored in this paper. The scale gap between these extremes is bridged by detailed analysis of selected outcrop-scale structures and a comprehensive compilation of over 15,000 field data (including 571 new data) for lineations and fold axes measured across the Betic-Rif belt. Finally, we will consider implications of our new

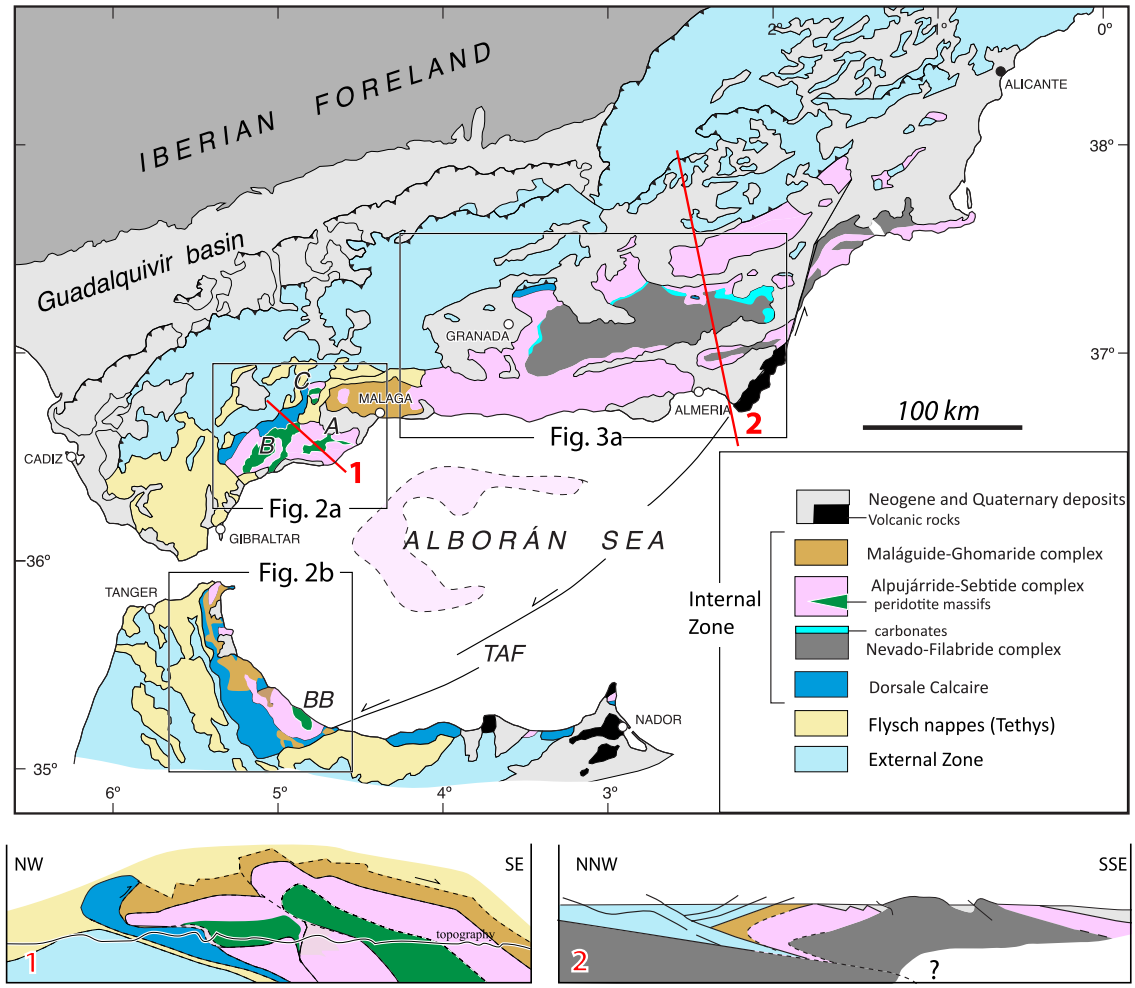

Figure 1. Geological map showing the principal tectonic units in the Betic-Rif orogen. Peridotite outcrops are labeled BB: Beni-Bousera massif, B: Bermeja massif, C: Carratraca massif, A: Alpujata massif. TAF: Trans Alboran Fault. Cross sections slightly modified after Mazzoli and Martin Algarra (2011) and Vissers et al. (1995).

geochronological and (micro)structural evidence for the tectono-metamorphic evolution of the NFC and ASC, the timing of peridotite emplacement, and the paleogeographic evolution of the western Mediterranean.

2. Geological Setting

2.1. The Betic-Rif Orogen

The Betic-Rif orogen geologically connects Europe and Africa across the Gibraltar Arc at the westernmost end of the ca. 12,000 km long Alpine-Himalayan system. It features an external fold and thrust belt (External Zone) of Miocene age developed at the expense of Mesozoic and Cenozoic sediments of the Iberian and North-African forelands. The Internal zone mainly comprise Paleozoic to Triassic sediments that were deformed and metamorphosed during the Variscan and Alpine orogenies as well as several large peridotite exposures (Figure 1). In the Late Cretaceous, the Iberian plate included the Baleares-Sardinia-Corsica block and another continental fragment know as "Alkapeca" (Bouillin, 1986) or "Mesomediterranean terrain" (Guerrera et al., 1993) which was located further south or southeast, either attached to Iberia (e.g., Stampfli & Hochard, 2009) or separated from it by a narrow strip of Tethyan oceanic crust (Handy et al., 2010; Leprêtre et al., 2018; Michard et al., 2006; van Hinsbergen et al., 2020). Paleogene Africa-Eurasia convergence, subduction and crustal shortening created a mountain belt continuous from the Betics to the Alps. In the Early Miocene, the southern part of this orogen experienced a dramatic extensional collapse associated with the opening of the western Mediterranean basins, volcanic activity and development of the Gibraltar and Calabrian Arcs. The synchronicity of this crustal extension

affecting the metamorphic core of the orogen and thrusting in the External Zone has been attributed to various combinations of back-arc spreading driven by roll-back or delamination of a northwest dipping subducted slab (e.g., Jolivet & Faccenna, 2000; Lonergan & White, 1997; Royden, 1993) and/or gravitational spreading within the orogen after loosing part of its lithospheric root (Calvert et al., 2000; Platt & Vissers, 1989; Platt et al., 2013). Crustal extension led to breakup of Alkapeca and outward migration of different pieces to their present positions in the Betics and Rif (Alboran Domain), the Kabylias, Peloritani Mountains of Sicily and Calabria (hence the name Al-Ka-Pe-Ca).

The Internal zone contain three principal nappe complexes arranged from bottom to top as the NFC, the Alpujarride Complex called Sebtide complex in the Rif, and the Malaguide complex called Ghomaride complex in the Rif. The lower two complexes have similar lithostratigraphic columns including pre-Permian sediments metamorphosed into schists and quartzites and a cover sequence of Permo-Triassic phyllites and Mesozoic marbles. In the largely non- or low-metamorphic Malaguide-Ghomaride complex, a similar succession is still overlain by Paleogene carbonates and Oligocene to Early Miocene synorogenic clastics (e.g., Chalouan & Michard, 1990; Mazzoli & Martin Algarra, 2011). The three complexes appear thrusted over the "Dorsale Calcaire" unit or "Frontal Units," a stack of steeply dipping to overturned thrust slices of Mesozoic carbonates cropping out mainly in the western Betics and Rif (Mazzoli & Martin Algarra, 2011; Vitale et al., 2014). This unit is generally interpreted as the detached sedimentary cover of "Alkapeca" since it is separated from the External Zone by the so called "Flysch unit," Upper Cretaceous to Miocene deep to shallow marine sediments of the Alpine Tethys.

2.2. Alpujarride-Sebtide Complex

The Alpujarride Complex of the western Betics (west of Malaga; Figures 2a and 2b) has been subdivided into an upper Los Reales unit and Lower Blanca unit. The first includes a several km thick basal peridotite slab overlain by a strongly condensed crustal sequence, in ascending order, composed of granulitic and migmatitic gneisses, pre-Permian (sedimentary age) high to medium-grade schists (Jubrique schists), and a thin level of low-grade Permo-Triassic phyllites and carbonates. Several thrust imbrications on top of this sequence, mainly of Permo-Triassic rocks, have been differentiated as the "Benarraba Imbrications" or subunit (Balanya et al., 1997).

The Blanca Unit comprises a similar lithostratigraphic succession, but with a notably thicker Triassic marble formation and a particular HT/LP migmatitic aureole widely attributed to tectonic emplacement of hot peridotites either in the Early Miocene (e.g., Platt et al., 2013; Tubía et al., 1997) or during the Variscan orogeny (e.g., Montel et al., 2000; Rossetti et al., 2020). Note, however, that Sanz-de-Galdeano and López Garrido (2016) and Sanz-de-Galdeano (2017) recently reinterpreted all Blanca-Unit outcrops as structurally overlying the peridotites. In their view, the contact aureole correlates with the migmatitic gneisses of the Los Reales crustal sequence. Bessière, Augier, et al. (2021) recently called for further exploration of this model after reinterpreting a small tectonic window of Blanca-Unit rocks as a Los Reales klippe (Robledal Klippe).

Low thermal gradient parageneses preserved in Permo-Triassic phyllites (Azañon et al., 1997) of the Los Reales and rare eclogite lenses in the Blanca unit gneisses (Tubía et al., 1997) witness early subduction stages in the Eocene (Bessière, Jolivet, et al., 2021; Marrone, Monié, Rossetti, Aldega, et al., 2021; Platt et al., 2005). Higher-grade rocks preserve medium gradient (Barrovian) assemblages (garnet-staurolite-kyanite-sillimanite) from which conditions have been derived of ca. 10 kbar/550°C in the schists (Balanya et al., 1997) up to 13–14 kbar/800°C in the migmatitic gneisses (Massonne, 2014) of the Los Reales unit. The age of this metamorphism has remained poorly constrained and will be discussed in the light of our new Sm-Nd garnet ages. Indeed, most radiometric ages in the ASC correspond to an Early Miocene (~22 to 18 Ma) low-pressure/high-temperature (LP/HT) metamorphic overprint (3–4 kbar; 650°C) related to the opening of the Mediterranean back-arc basin.

Virtually all outcropping rocks of the Sebtide Complex (Internal Rif) are equivalent to the Los Reales unit and have also been assigned to two subunits. The upper subunit or "Federico unit" contains several thrust slices of mainly Permo-Triassic rocks and is comparable to the Benarraba subunit of the western Betics (Figure 2a). The lower subunit includes the Beni-Bousera peridotite massif and the overlying "Filali" schists and gneisses. Only a small orthogneiss outcrop in the Ceuta peninsula possible correlates with the Blanca unit as it is overlain by a small peridotite sliver.

The Federico unit preserves similar high-pressure/low-temperature (HP/LT) assemblages as Permo-Triassic phyllites in the Betics with conditions up to 18 kbar/550°C reconstructed for the deepest levels (Homonnay

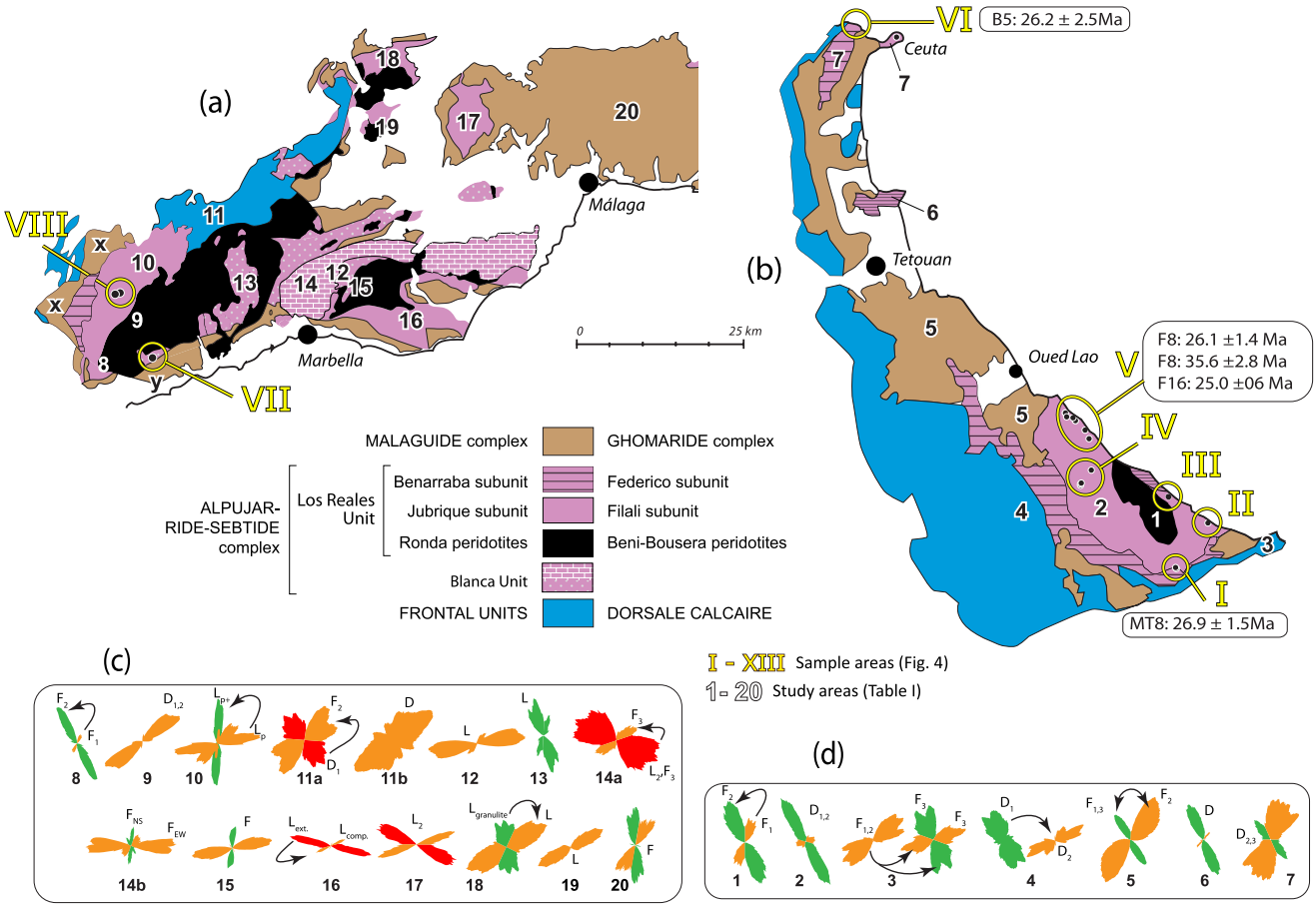

Figure 2. Internal zone of the western Betics (a) and Rif (b) with indication of sample areas, field areas of previous workers (Table 1), and Sm-Nd garnet ages. The locations of the maps are shown in Figure 1. (c and d). Rose diagrams for lineation- and fold-axes from the works listed in Table 1 for study areas numbered 1 to 20. Small black arrow point from older structural trends to younger ones as interpreted by the original authors of the data. The original nomenclature of different structural elements is also indicated: "F" for fold axes, "L" for lineations, and "D" for both.

et al., 2018; Marrone, Monié, Rossetti, Lucci, et al., 2021; Michard et al., 2006). The Lower Sebtide, in contrast, preserves early Barrovian assemblages (Grt, Ky, St, and Ru) formed at relatively low pressure in the micaschists (6 kbar/550°C; Gueydan et al., 2015) but up to 18 kbar/800°C recorded by metabasite lenses hosted in granulitic gneisses immediately overlying the Beni-Bousera peridotite body (Bouybaouene et al., 1998). These early parageneses are pervasively overprinted by Miocene HT/LP assemblages (biotite, andalusite, sillimanite, cordierite, and K-feldspar).

Correlation of Alpujarride (sub)units from the western Betics to the central and eastern Betics is complicated by a ca. 40 km long intermediate patch of Malaguide Complex and a lack of peridotite outcrops east of Malaga (Figure 1). Sanz-de-Galdeano (2019) distinguishes three main units (lower-, middle-, and upper) that, in ascending order, display successively higher metamorphic grades and lower proportions of Permo-Triassic rocks. This author correlates the upper unit with the Los Reales unit of the western Betics. In contrast, Williams and Platt (2017, 2018) consider all Alpujarride outcrops of the central- and eastern Betics equivalent to the Los Reales unit and attribute tectonic subdivisions to syn- and post-metamorphic recumbent (F3) folds and (D4) extensional detachments. Another group of workers, however, interprets the same folds and part of the D4 detachments as products of a late crustal shortening and thrusting following (D2) crustal extension (Azañón & Crespo-Blanc, 2000; Rossetti et al., 2005; Simancas, 2018).

2.3. Nevado-Filabride Complex

The Alpujarride—Nevado-Filabride contact is a brittle-ductile detachment demarcated by lenses of brown-yellow carbonate-breccia. It places blueschist facies (carpholite-chloritoid-kyanite bearing) Permo-Triassic phyllites of the Alpujarride Complex on top of amphibolite-facies Mesozoic marbles and schists of the NFC. This combination of a stratigraphic repetition with a metamorphic gap has been explained in terms of an extensional detachment cutting earlier contractional structures (e.g., Martínez-Martínez et al., 2002), or a thrust reactivated as an extensional decollement (e.g., D. Aerden & Sayab, 2008; Platt et al., 2013; Vissers et al., 1995). The contact is associated with a subhorizontal crenulation cleavage that sharply cuts upright (F3) folds in the footwall deforming the principal (S2) foliation. Shear-sense criteria associated with the contact vary significantly in detail but a large westward movement is generally assumed.

The NFC is traditionally subdivided into a lower Veleta or Ragua unit, and an upper Mulhacen Unit. The latter has been further subdivided into two or three thrust slices or subunits, which are from bottom to top, the Calar-Alto- and Bedar-Macael units of García-Dueñas et al. (1988), or the Caldera-, Ophiolite-, and Sabinas-units of Puga et al. (2002). The nature, location and even existence of the bounding contacts are still debated though (Ruiz-Fuentes & Aerden, 2018; Sanz-de-Galdeano & Santamaría-López, 2019).

The Veleta unit together with the lower part of the Mulhacen unit comprises a several km thick package of dark schists and metapsammites of Devono-Carboniferous sedimentary origin. The Mulhacen portion of this package appears more strongly deformed and hosts orthogneiss lenses derived from late-Variscan granites and associated HT/LP minerals. These Variscan basement rocks are overlain by Permo-Triassic (sedimentary age) light-colored schists and quartzites and Mesozoic marbles (Poulaki & Stockli, 2022 and references cited therein). Mafic and ultramafic lenses with Jurassic protolith ages that appear concentrated near the base of the marble formation have been interpreted as marking an ophiolitic suture between Iberia and Alkapeca (e.g., Porkoláb et al., 2022; Puga et al., 2017) or a hyper-extended continental margin (e.g., Pedrera et al., 2020).

Ar-Ar ages for white-micas and amphiboles were originally interpreted to indicate HP/LT metamorphism in the Paleocene-Eocene, followed by reequilibration under greenschist to amphibolite conditions in the Oligocene to Early Miocene (Augier et al., 2005; Jabaloy et al., 1993; Monié et al., 1991). But subsequent Miocene Lu-Hf garnet ages (13–18 Ma; Platt et al., 2006) and similar Rb-Sr multimineral ages (Kirchner et al., 2016) suggested that Ar-Ar ages are significantly offset by excess argon, and this led to reinterpretation of the tectono-metamorphic evolution of the NFC as largely postdating that of the Alpujarride Complex, related to subduction of the Iberian margin below an extending Alboran Domain. Li and Massonne (2018), however, revived the possibility of a Paleogene high-pressure event based on two texturally and chemically distinct groups of monazite grains in two samples of the Ragua and Calar-Alto units yielding mean (EMPA U-Pb) ages of 40 and 24 Ma. These ages were linked to initial burial of the complex along a low geothermal gradient to 17 kbar/530°C, followed by near-isothermal decompression and then re-burial and heating to ca. 9 kbar/650°C. Such a bi-cyclic evolution starting in the Eocene appears further supported by recent Ar-Ar dating of white micas revealing two age populations (38–27 and 23–12 Ma) associated with different tectonic fabrics (Porkoláb et al., 2022), and Eocene U-Pb zircon-rims (Poulaki et al., 2020). Also our garnet ages will be shown to confirm a protracted history of Late-Eocene to Miocene metamorphism in the NFC.

3. Samples and Microstructural Methods

3.1. Sampling Strategy

A total of 44 oriented micaschist samples were studied containing garnet, and/or staurolite, and/or plagioclase, and/or andalusite porphyroblasts with well developed inclusion trails. A list of these samples stating geographic coordinates, rock type and index minerals can be found in Supporting Information S1. Mafic lithologies were not investigated as these are relatively rare and fine-grained rocks lacking large porphyroblasts with inclusion trails.

Thirty-six samples are dark schists and metapsamites belonging to the Variscan basement of the ASC. All contain garnet, biotite, white-mica ± staurolite, plagioclase, andalusite, or sillimanite. One sample is a dark schist from the Variscan basement of the Veleta unit already studied in significant microstructural detail by D. G. A. M. Aerden et al. (2010). The remaining seven are light-gray colored schists from the Permo-Mesozoic cover of the Mulhacen nappe complex.

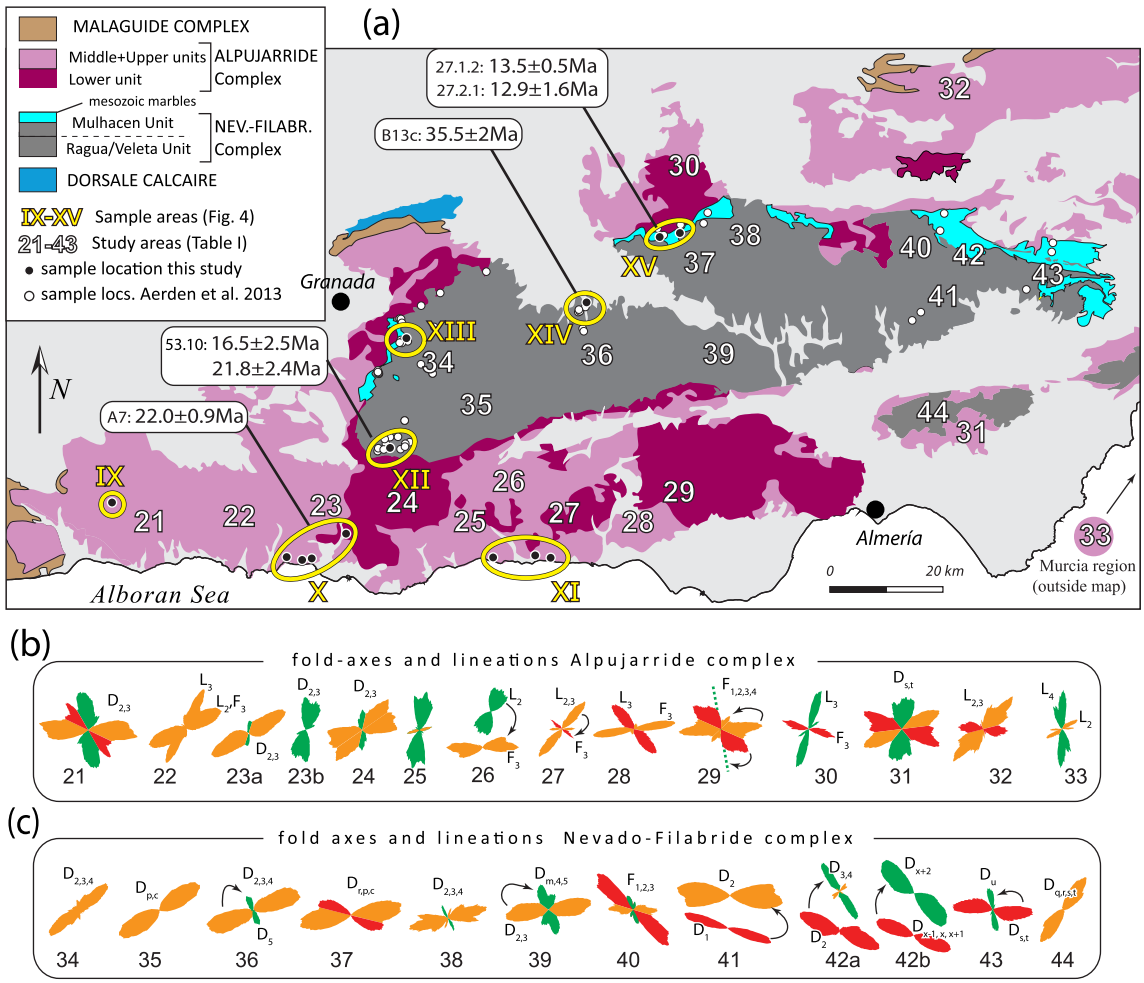

Figure 3. (a) Map of the Internal Zones in the central and eastern Betics with indication of our sample areas (XI–XV), approximate location of study areas of the works listed in Table 1, and new Sm-Nd garnet ages. The map location is shown in Figure 1. (b and c) Rose diagrams for lineation- and fold-axes from the works listed in Table 1. Black arrow point from older structural trends to younger ones as interpreted by the original workers. The original nomenclature of different structural elements is also indicated: "F" for fold axes, "L" for lineations, and "D" for both.

Samples were collected in 15 areas given roman numbering in Figures 2a, 2b and 3a. Areas I to V lie in the Filali schists (Lower Sebtide unit) above the Beni-Bousera peridotites. Area-VI (northwest of Ceuta) is a restricted outcrop of Paleozoic schists (Benzu schists) at the base of the Federico unit for which Bouybaouene et al. (1999) derived conditions of 12 kbar/500°C. Areas VII and VIII lie in the Jubrique schists above the Bermeja Massif (Ronda peridotites) and areas IX–XI pertain to the upper Alpujarride unit of the Central Betics (Figure 3a). The seven Mulhacen-unit samples come from the western Sierra Nevada (XII–XIII) and western Sierra de los Filabres (XV).

3.2. Measuring Strikes of Inclusion Trails

The strikes of relatively straight inclusion-trails of individual porphyroblasts were measured in precisely oriented horizontal thin sections (i.e., cut parallel to the horizontal plane) and horizontal X-ray micro-tomographic slices. A total of 1,760 measurements were made and plotted in moving-average rose diagrams using the program "MARD" of Munro and Blenkinsop (2012). As pointed out by these authors, such rose diagrams are more adequate for identifying modal maxima in sets of continuous directional data (0–360°) than traditional binned rose diagrams, because the latter are significantly influenced by the choice of bin boundaries and bin widths. A counting window of 21° was used except where specified otherwise and non equal-area plotting was selected. This data is shown in column A of Figure 4 for garnet, plagioclase, staurolite, and/or andalusite porphyroblasts.

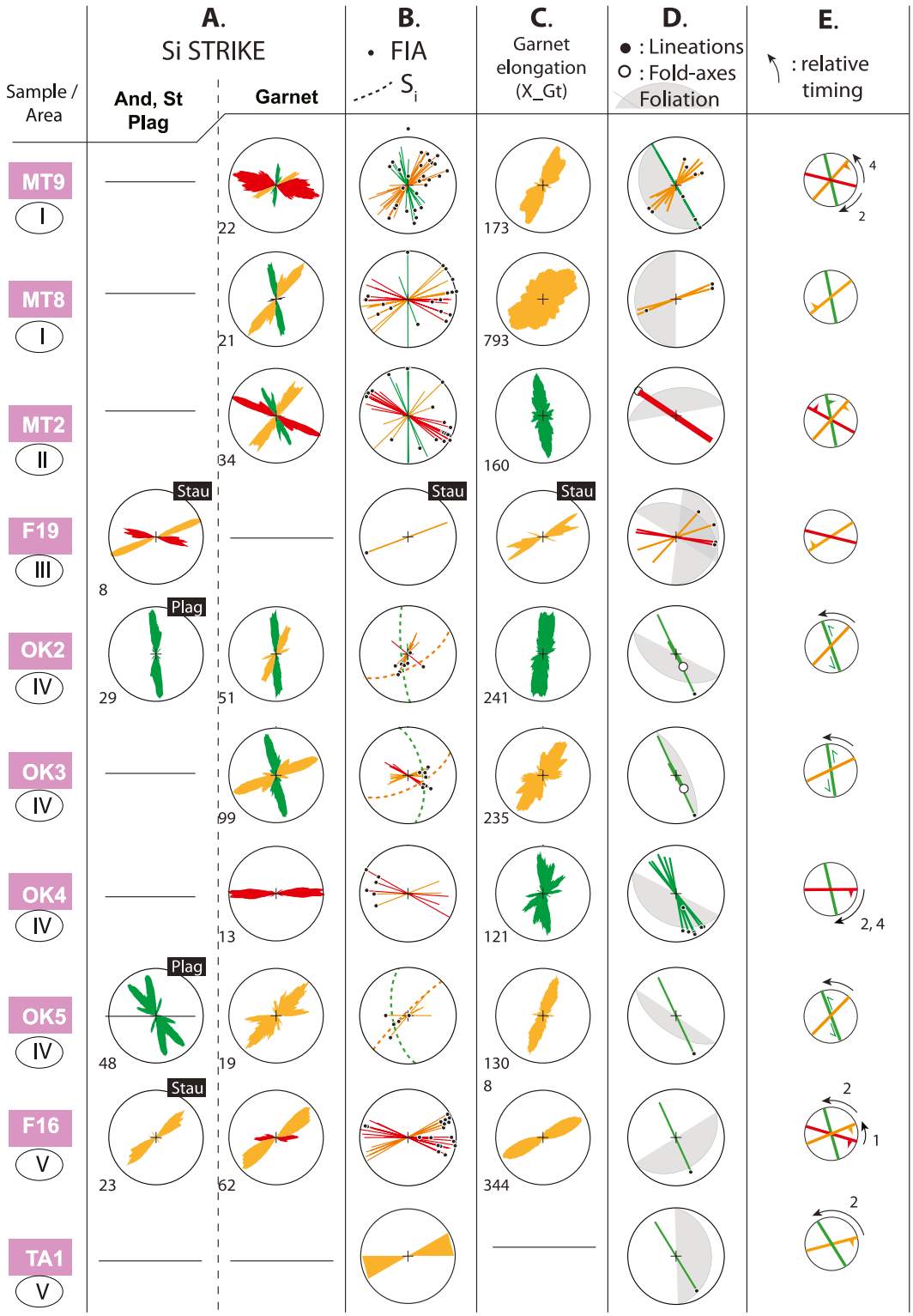

Figure 4.

3.3. Measuring Average FIA Trends Using Sets of Radial Thin Sections

"FIA" is an acronym of Foliation Inflexion/Intersection. It refers to the axes of inclusion-trail curvature, or what has traditionally been assumed to be the porphyroblast-rotation axes. Spiral-shaped inclusion trails typically exhibit internal discontinuities or truncations (e.g., Hayward, 1992) where the trails of more inward zones are intersected by those of more outward zones, hence the name Foliation Inflexion *or Intersection* Axes. According to the "non-rotational" model, such truncations represent cleavage planes that intensified against porphyroblast margins before being included in a new growth zone (Figure 5a; see also Figure 3 of D. Aerden and Sayab (2008)). Hayward (1990) devised a method for measuring the average orientation of FIAs in a rock specimen by cutting multiple vertical thin sections in a radial pattern around the compass and recording the dominant (S or Z) asymmetry of inclusion trails in each section. An average FIA trend can then be constrained between two sub-sets of thin sections exhibiting opposite inclusion-trail asymmetries for a constant viewing direction. We applied this method to 31 samples by cutting six vertical thin sections of each one with 30° spacing. Unambiguous results were only obtained for 10 samples apparently containing a single FIA population with a normal distribution of their trends ("von Mises" distribution). These 10 average FIAs are represented with bow-chart symbols in column B of Figure 4. In other samples, no clear switch in dominant inclusion-trail asymmetry could be identified because, as later tomographic analysis showed, these samples contain mixed FIA populations with different average trends, and in some cases FIAs with very steep plunges that render Hayward's (1990) method less applicable.

3.4. Measuring Internal Foliation Planes and Individual FIAs Using X-Ray Tomography

X-ray computed micro-tomography (XCT) was applied to thin-section blocks of 26 samples. The blocks were scanned at resolutions of 10–30 μm with an Xradia 510 (Versa Zeiss) microtomographer at the University of Granada using 140 kV voltage and 2,500–3,200 projections. Orientation arrows made of metal wire were previously stuck on the blocks to aid reorientation of the generated Tiff image-stacks in such a way that East, North and the vertical coincide with the *X*, *Y*, and *Z* axes of the image stacks, respectively. Image stacks were processed and analyzed with the open-source software package Fiji (Schindelin et al., 2012). Orientations of relatively planar internal foliations present in 16 samples were determined by measuring their strike and pitch on *XY*, *YZ*, and *XZ* slices of tomographic image stacks, and fitting these angles to great circles on a stereonet. Full results for individual sample are given in separate stereoplots that can be found in Supporting Information S2. The data are plotted collectively in Figures 6a and 6c and will be interpreted in Section 4.

Individual porphyroblast FIAs defined by sigmoidal or spiral inclusion trails were measured in an analogous fashion as Hayward's (1990) method, but now counting with an unlimited number of virtual slices of any desired orientation (D. G. A. M. Aerden & Ruiz-Fuentes, 2020; Huddlestone-Holmes & Ketcham, 2010). FIA trends were constrained by first interactively rotating a vertical slice through the porphyroblast center about a vertical axes and recording the orientation where the inclusion-trail asymmetry flips. Then, a new slice was rotated about a horizontal axes oriented normal to the FIA trend to determine the FIA plunge and plunge direction. Error ranges associated with this procedure are estimated as ±5° to ±15° depending on the size and definition of inclusion trails. Quartz-rich inclusion trails proved ideal because of the high X-ray attenuation contrast with garnet, but unfortunately, many of our ASC samples contain inclusion trails composed of very fine-grained graphite that are poorly visible or not visible in the scans. A total of 346 garnet FIAs could still be measured, which are plotted in the stereograms of column B of Figure 4 for separate samples. Great-circles in some of these stereoplots represent the average orientation of inclusion-trail planes whose intersections produce the FIAs. FIAs are also plotted collectively for all samples in Figure 6b, to be discussed in Section 4.

Figure 4. Chart with microstructural data for 44 studied samples from 15 areas (I–XV) shown on the maps of Figures 2a and 2b and 3a. Sample numbers have background colors and ornament patterns matching those of the corresponding tectonic units in the maps. (Column A) Strike of inclusion trails in staurolite, andalusite, plagioclase (left) and garnet porphyroblasts (right). (Column B) Bow-tie symbols: average Foliation Inflexion/Intersection Axes (FIAs) determined with radial sets of thin sections. Black dots with colored trend lines: individual porphyroblast FIAs measured with X-ray tomography. Great circles: representative orientation of internal foliation planes. (Column C) Moving-average rose diagrams for garnet long-axes (X_{GRT}). (Column D): Black dots: matrix lineations. Large white dots: fold axes. (Column E) Trend bars summarizing the main microstructural trends apparent from the data in columns A–D. Black arrows point from older to younger microstructural trends and small numbers indicate which of the four criteria were used (see Section 4.2). Small arrowheads drawn orthogonal to trend bars indicate the dominant sense of inclusion trail curvature as explained in Section 3.7.

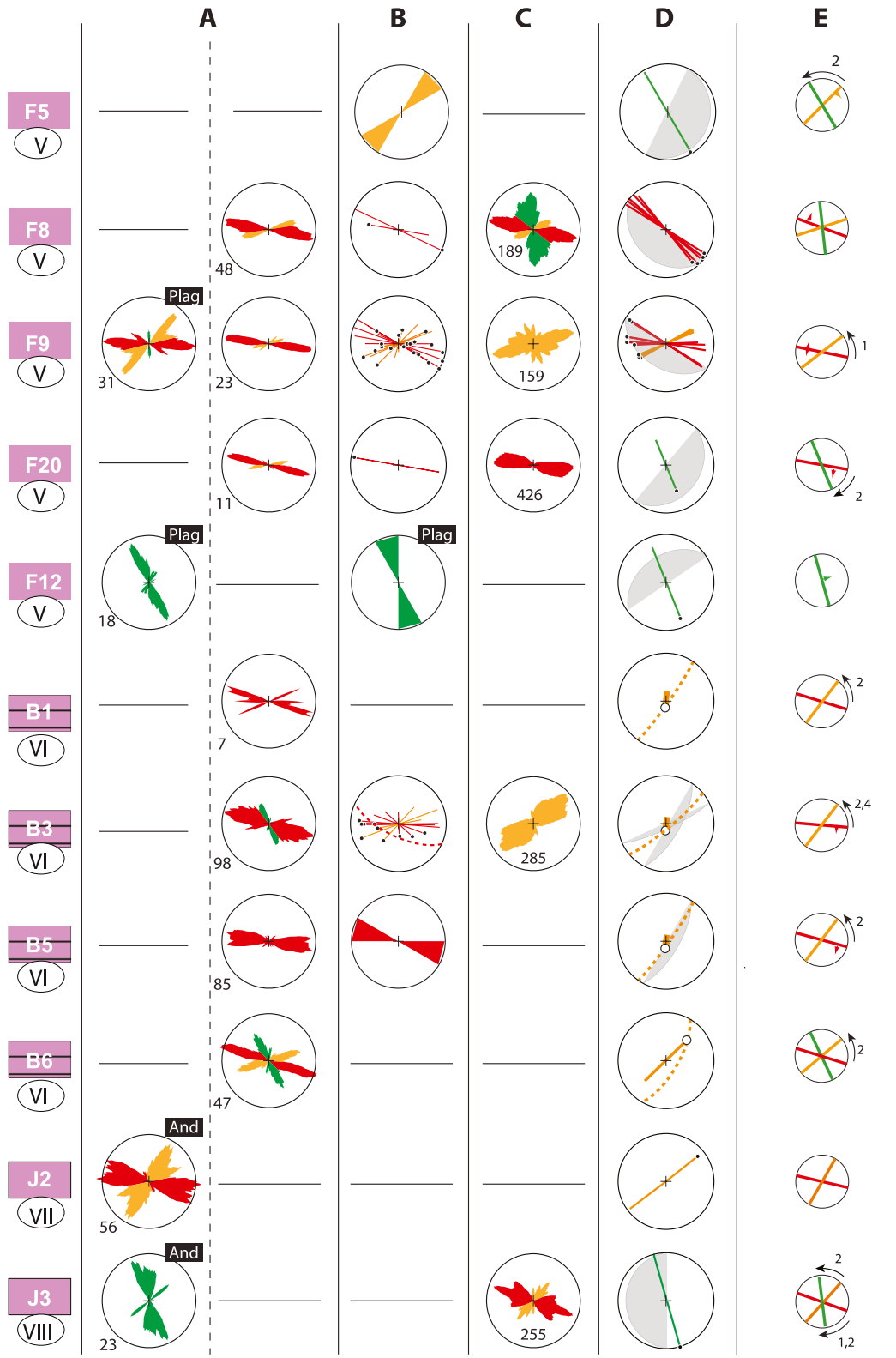

Figure 4. (Continued)

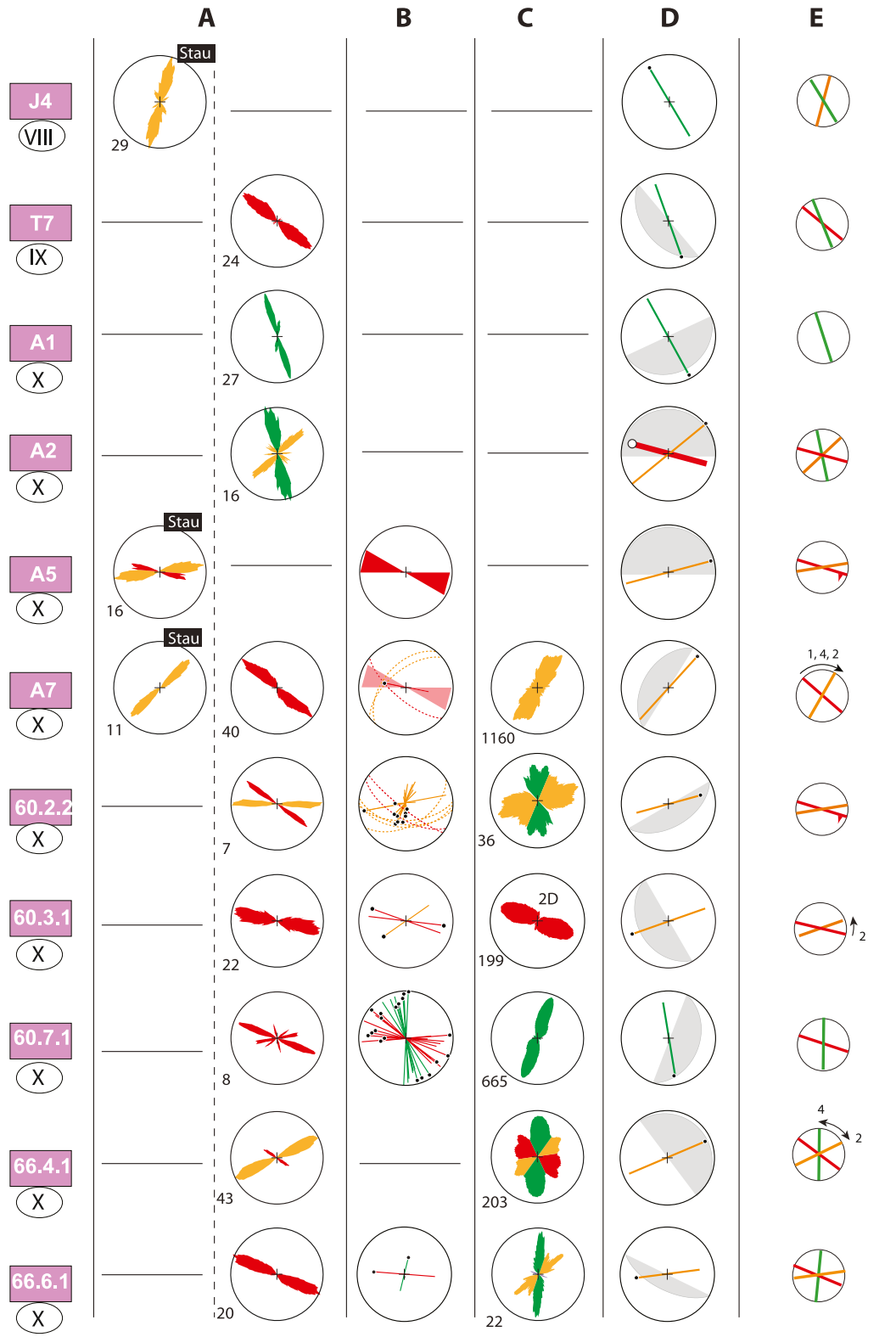

Figure 4. (Continued)

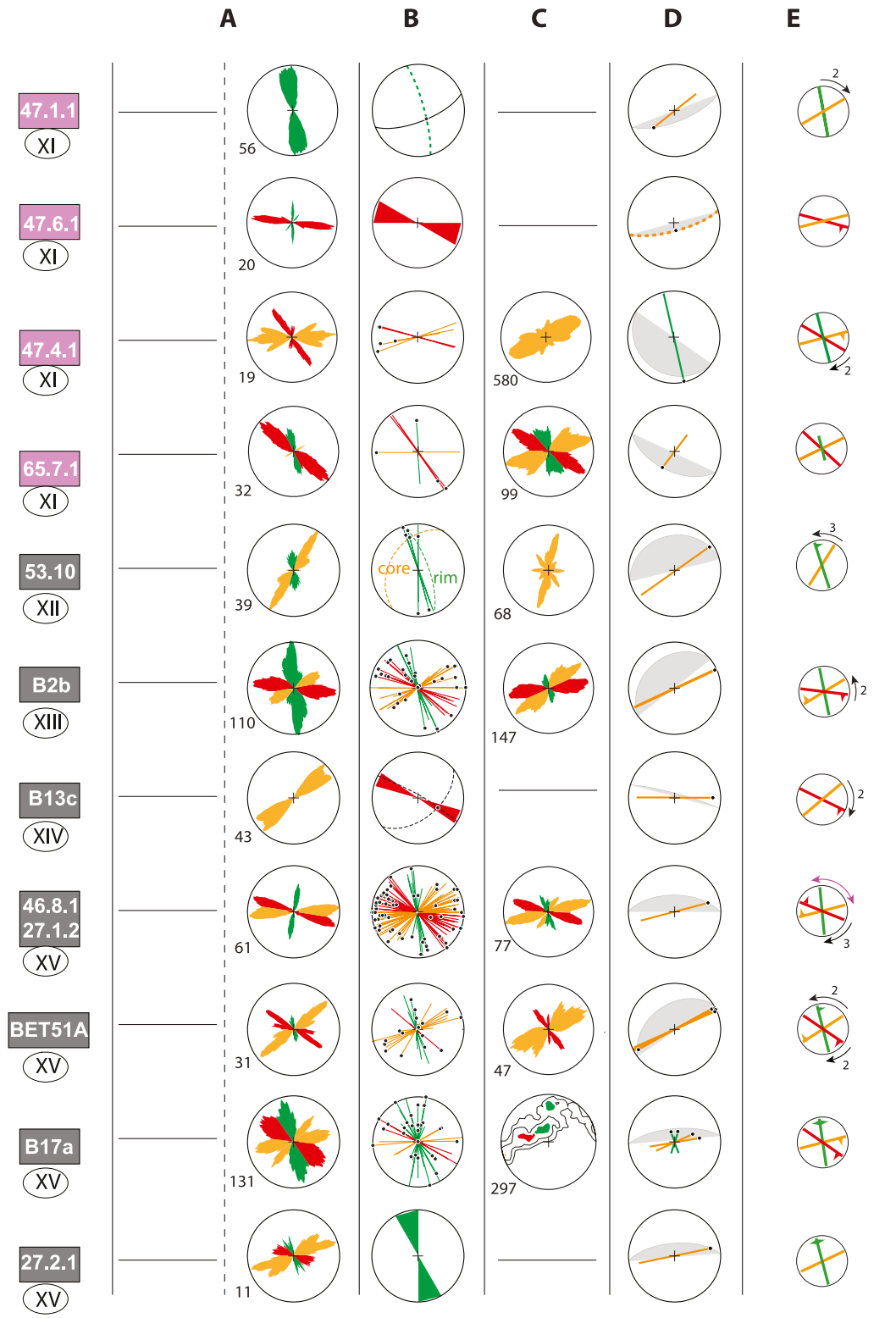

Figure 4. (Continued)

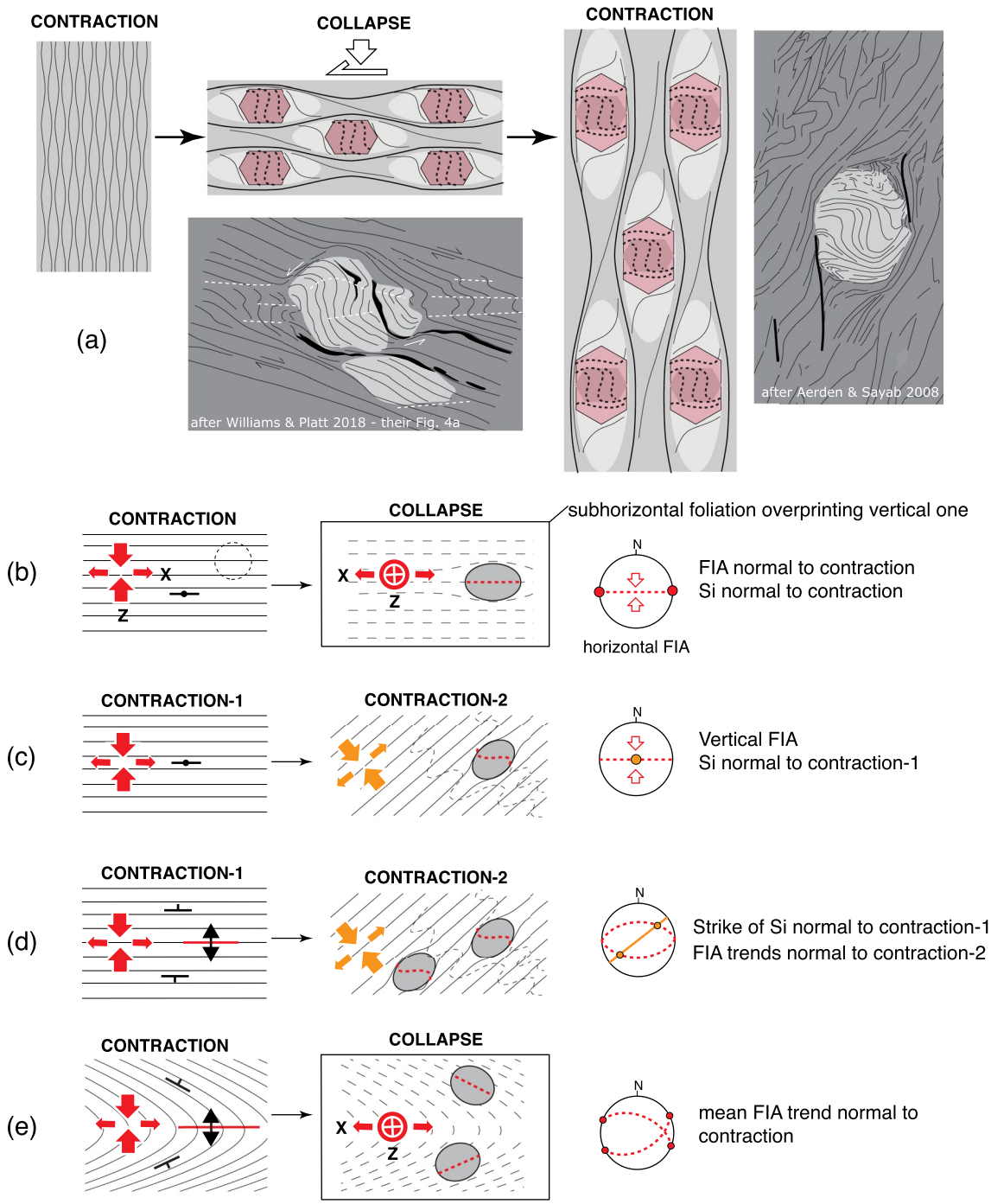

Figure 5. (a) Conceptual sketch showing how sigmoidal and spiral-shape inclusion trails may form by overgrowth of 1 or 2 successive crenulation cleavages without porphyroblast rotation. Real examples are shown next to each deformation and growth stage. In the example Williams & Platt (2018), note that internal axial-planes (white dashes) are parallel to matrix crenulations. Thin black and white arrows depict antithetic and synthetic shearing on new and pre-existing foliation, respectivey. (b) Conceptual model for horizontal Foliation Inflexion/Intersection Axes (FIAs) forming by contraction followed by gravitational collapse with a constant stretching direction. (c) Formation of a vertical FIA via a superposition of two crustal shortening directions. Inclusion trails strike orthogonal to the older shortening direction. Porphyroblast elongation directions are controlled by the younger shortening direction. Panel (d) similar as panel (c), but with a pre-existing anticline causing variable FIA plunges with similar trend. Panel (e) similar as panel (b), but with a pre-existing plunging fold causing simultaneous development of FIAs with variable trends, but with the mean FIA still normal to the shortening direction.

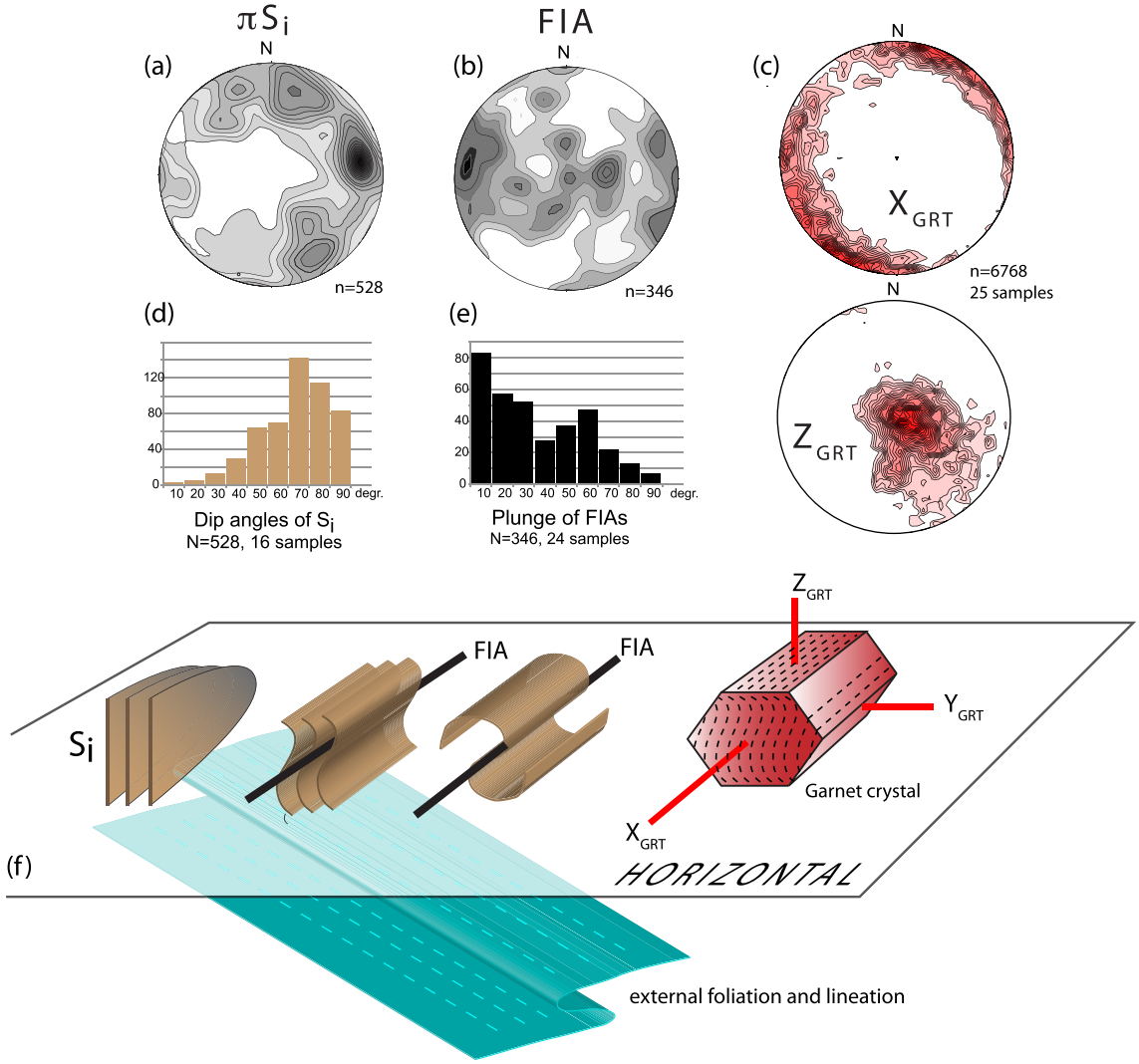

Figure 6. (a) Poles of all simple inclusion-trail planes measured for this study. (b) All measured Foliation Inflexion/Intersection Axes (FIAs). (c) All garnet porphyroblast long axes (X_{GRT}) and short axes (Z_{GRT}). (d) Histogram for the dip angle of simple internal foliations demonstrating their preference for steep. (e) Histogram for FIA plunges showing their preference for horizontal plus a weaker preference for ~60°. (f) Schematic representation of the measured microstructures commonly lacking any direct relationships with the external foliation and lineation (see Figure 8).

3.5. Garnet Porphyroblast Shapes

Previous 3D studies of spiral garnets have found that these are commonly elongated either parallel or perpendicular to their FIAs owing to anisotropic growth controlled by the included foliation and/or the overprinting crenulation cleavage that triggered porphyroblast growth (D. G. A. M. Aerden & Ruiz-Fuentes, 2020; Robyr et al., 2007; Sayab et al., 2021). Thus, we analyzed the shape and shape orientation of all garnet porphyroblasts present in XCT scans as a potentially valuable extra information regarding the orientation and timing of FIAs. The "BoneJ" plugin of Fiji (Doube et al., 2010) was used for this purpose. This tool enables rapid calculation of best-fit ellipsoids for a large number of objects present in a binary image stack. To implement this, our image stacks were first thresholded (setting all voxel values outside the range of garnet to zero), then binarized (setting all remaining voxels to 1) and size-filtered to eliminate small particles. In some cases, the "dilate" tool was still applied to re-join fragments of single garnets separated by fractures and associated alteration.

Well developed preferred shape orientations of garnet crystals were found in all samples with typical X_{GRT}/Z_{GRT} aspect ratios of about 2.0. The complete data including X_{GRT}, Y_{GRT}, and Z_{GRT} best-fit ellipsoid axes are included in the aforementioned collection of stereoplots with microstructural data of Supporting Information S2. Figure 6c

plots garnet long-axes (X_{GRT}) and short-axes (Z_{GRT}) collectively and highlights their preferred horizontal and vertical orientations, respectively. In column-C of Figure 4, the trends of garnet long-axes are plotted in rose diagrams and confirm, with few exceptions, that these are generally subparallel to FIAs in the same sample or a particular subset of FIAs. However, in sample OK4, FIAs align with Y_{GRT} axes and hence sub-perpendicular to X_{GRT}. In sample A7, long-axes are subparallel to crenulation axes in the matrix.

3.6. Lineations and Fold Axes Data

The exact nature of tectonic lineations cannot always be ascertained in the field. In some cases they are clearly defined by crenulation axes, whereas in others they are more finely spaced and may correspond to intersecting cleavage planes and/or mineral elongation. Study of thin sections and XCT scans showed that mineral lineations are systematically associated with variably spaced crenulation axes or intersecting foliation planes although these were not always perceived in the field. Two of our Nevado-Filabride samples (53.10 and BET51A) containing relatively large and abundant opaque minerals in the matrix provided an opportunity to quantitatively characterize the shape and shape orientations of these grains using the BoneJ plugin (Figures 7b and 7d). This confirmed a strong alignment parallel to crenulation axes in both samples and associated outcrop-scale folds. These findings are in accordance with many reports in the literature of fold axes being generally parallel to stretching lineations in medium to high-grade rocks of the Betic-Rif orogen. Lineations and fold axes measurements are given in column D of Figure 4 for each sample. Part of this data was measured within XCT image stacks by recording the *X*, *Y*, and *Z* coordinates of different points located on individual crenulation axes followed through the scans and applying simple trigonometry.

3.7. Curvature Sense of Inclusion Trails

Column E of Figure 4 summarizes the main microstructural trends apparent from the data in columns A–D. Small arrowheads drawn perpendicular to these bars indicate the curvature sense of sigmoidal or spiral inclusion trails when viewed from above looking down on the FIA axes. That is, an E-W bar with a north pointing arrowhead stands for inclusion trails that curve clockwise in a N-S sections when viewed in westward direction. Similarly, a N-S trending bar with an east pointing arrowhead corresponds to inclusion trails curving clockwise when viewed northward in an E-W section. The sense of inclusion-trail curvature is highly consistent within individual samples except in F9, which contains roughly equal proportions of opposite inclusion trails probably as a consequence of coaxial deformation.

4. Microstructural Interpretation

4.1. Preferred Orientations and Their Genetic Implications

Several studies in the Betic Cordillera already concluded to a lack of porphyroblast rotation based on (a) consistent orientations of inclusion-trail orientations in individual samples uninfluenced by folding and shearing (Bell & Forde, 1995; D. G. A. M. Aerden et al., 2010), (b) subvertical and subhorizontal preferred orientations of inclusion trails (D. G. A. M. Aerden et al., 2013; D. G. A. M. Aerden & Ruiz-Fuentes, 2020), and (c) regionally consistent trends of FIAs and strikes of inclusion-trails measured in 85 samples of the NFC (D. G. A. M. Aerden et al., 2013). These and similar observations in other metamorphic belts (cited in Section 1) have been interpreted to witness an alternation of crustal shortening and gravitational collapse phases, and we note that Balanya et al. (1997) and Azañon et al. (1997) already independently reached this conclusion based on conventional structural and metamorphic evidence. FIAs forming during compression-collapse cycles should form normal to the shortening direction with subhorizontal plunges as shown in Figures 5a and 5b. This has been confirmed in 36 samples of the Alps (Bell & Wang, 1999) and 30 samples of NW-Iberia (D. G. A. M. Aerden, 2004) D. G. A. M. Aerden et al. (2021) recently reported FIAs having mainly moderate to steep plunges in Variscan blueschists of southern Brittany. They showed that these FIAs correspond to the intersections of two steeply dipping foliations with different strikes (Figures 5c and 5d). In this case, the FIA does not provide information on the shortening directions, but the strike of the inclusion-trails still does.

Several additional complications need to be considered that potentially contribute to scattering inclusion-trail orientations. (a) Where porphyroblasts nucleate in response to deformation that has already caused a certain

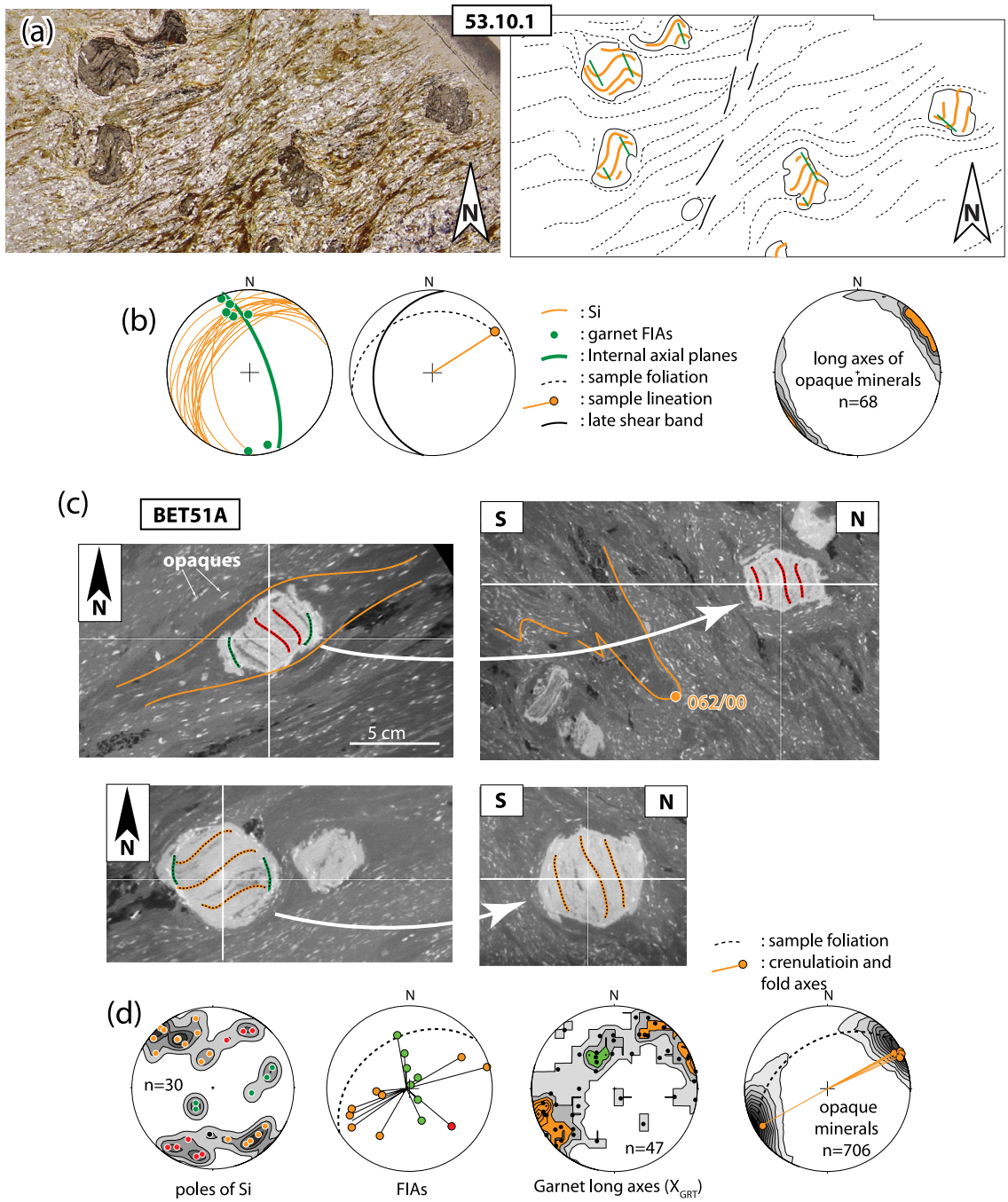

Figure 7. (a) Microphotograph and line diagram of garnets in sample 53.10.1 preserving NE-SW striking inclusion trails deflected in outer porphyroblast zones toward a subvertical NNW-SSE striking orientation. (b) Orientation data with colors matching the microstructures shown in panel (a). (c) Tomographic slices of sample BET51A showing N-S striking inclusion trails in porphyroblast rims (green) truncating subvertical inclusion trails with NE-SW strike (orange) or NW-SE strike (red) in porphyroblast cores. (d) Orientation data with colors matching microstructures shown in panel (c). Note similar orientations of FIAs and X_{GRT} axes, and the mutual parallelism of elongate opaque minerals, crenulation axes, and fold axes.

amount of reorientation and folding of the pre-existing foliation, these porphyroblasts will not preserve the original orientation of that foliation but the orientation as it was at the time of overgrowth. (b) The orientation of FIAs is conceivably influenced by preexisting folds. For example, where gravitational collapse triggers a first phase of porphyroblast growth in pre-existing folds with inclined axes, FIAs will form with different trends in opposite fold limbs (Figure 5e), although the average FIA trend still lies normal to the shortening direction. FIAs

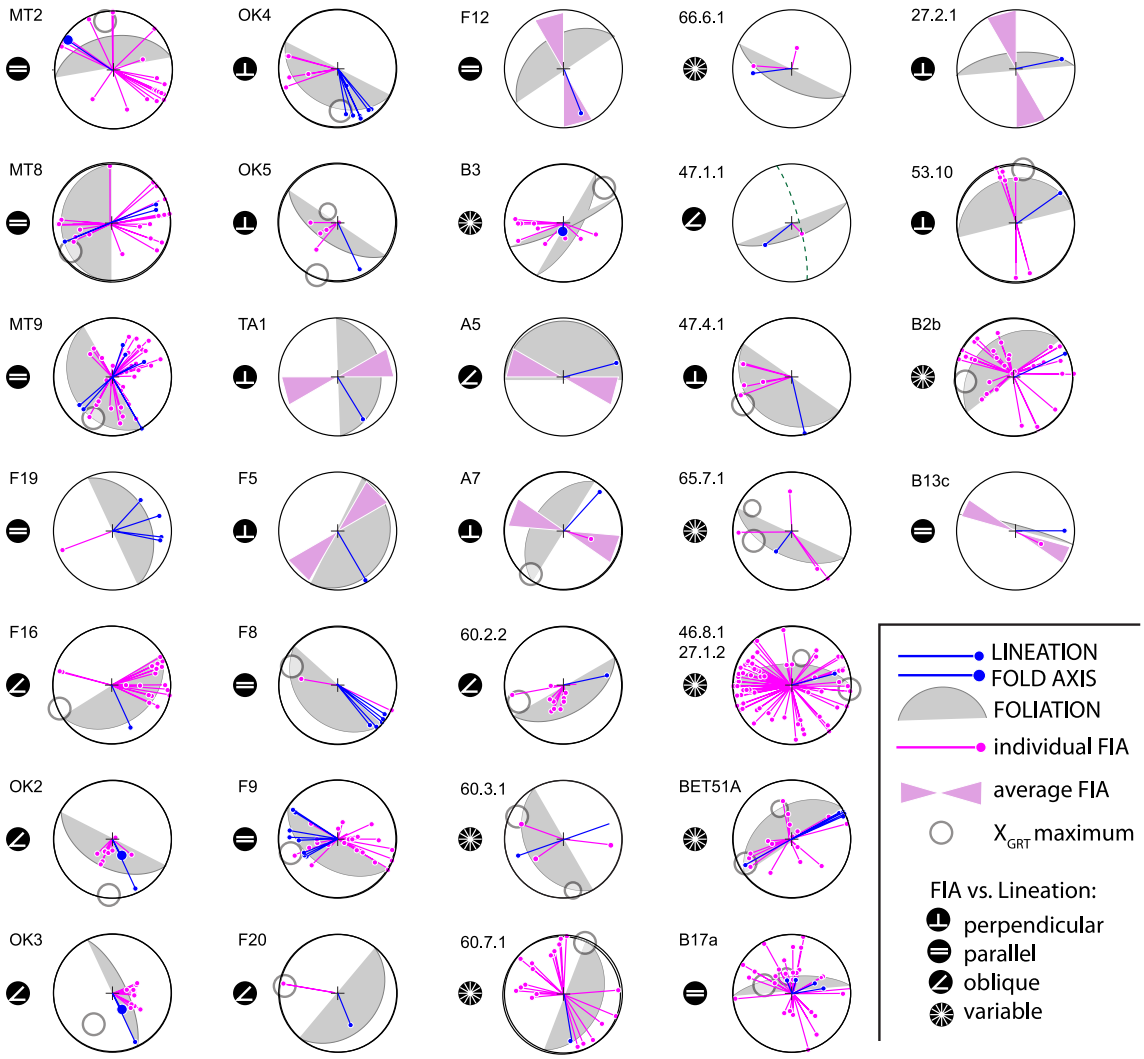

Figure 8. Orientation of Foliation Inflexion/Intersection Axes (FIAs), compared with that of the matrix lineation and foliation in 32 samples. Note the lack of a systematic relationship between internal and external fabrics as one would expect if porphyroblasts were rotated by shear on the main foliation. Also note the predominantly gentle to subhorizontal plunges of FIAs and X_{GRT} axes regardless the orientation of matrix fabrics.

developing during second and subsequent growth stages of porphyroblasts should be less affected by previous or synchronous folding because these FIA form by overgrowth of cleavage planes that intensified against porphyroblast margins subparallel of the axial planes of synchronous folds (Figure 5a). (c) Finally, porphyroblast orientations have been shown to be potentially affected by differential rotations related to boudinage, fracturing and faulting (D. Aerden & Sayab, 2017; D. G. A. M. Aerden, 1995; D. G. A. M. Aerden et al., 2010; Johnson, 2009).

Despite these and other complicating factors, inclusion trails in our samples still preserve well developed orientations as follows:

1. The total of 528 simple inclusion trails measured in 16 samples exhibit a strong preference for steep (70°–80°) dip angles (Figures 5a and 5d), consistent with a widely accepted contractional origin but implying limited porphyroblast rotation thereafter.
2. The total of 345 FIAs measured in 24 samples exhibit a strong preference for subhorizontal plunges plus a weaker preference for 50°–60° (Figure 6e). Garnet long-axes (X_{GRT}) and short-axes (Z_{GRT}) are preferentially subhorizontal and subvertical, respectively (Figure 6c). Note that these patterns are as predicted by the FIA model of Figures 5a–5c, but find no explanation within the classic "rotational" model. Note further that the lack of any systematic relationship between internal and external fabrics demonstrated in Figure 8, refutes an interpretation of FIAs in terms of porphyroblast rotation induced by shearing along the foliation parallel to

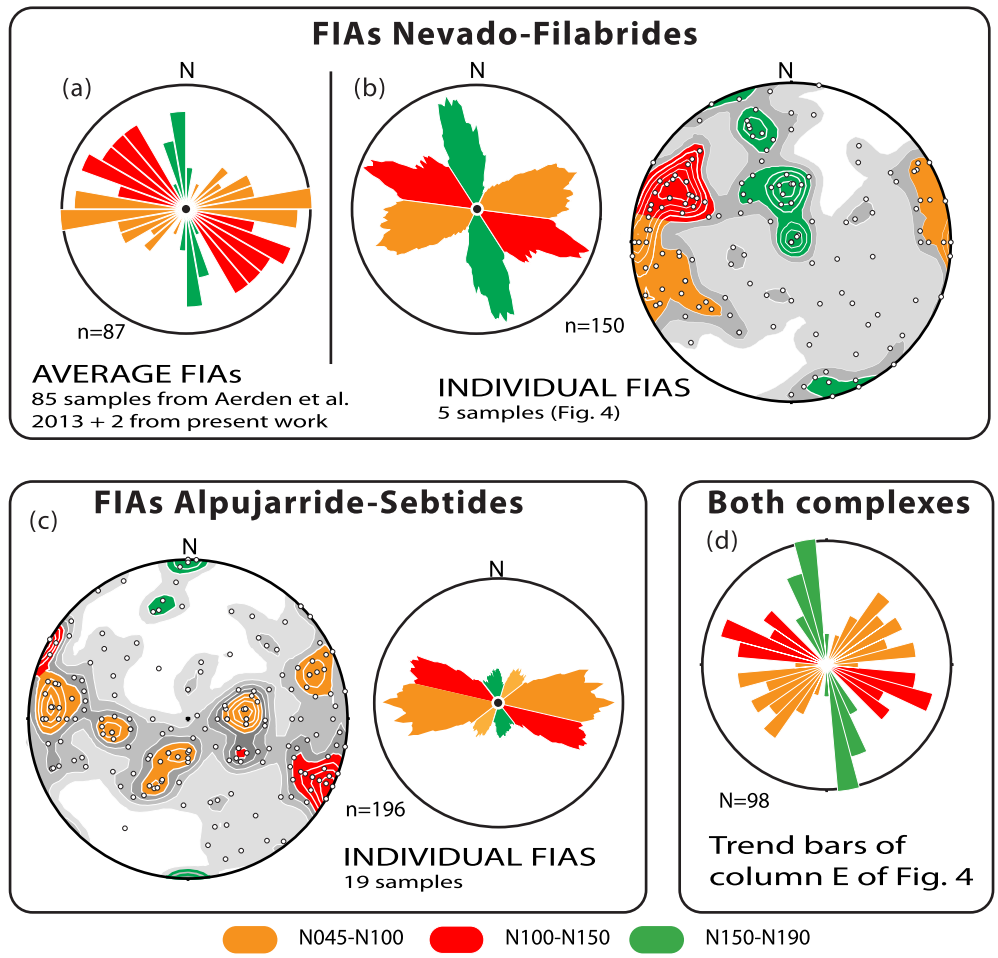

Figure 9. (a) Average Foliation Inflexion/Intersection Axes (FIAs) mainly determined by D. G. A. M. Aerden et al. (2013) through study of multiple thin sections of each sample. (b) Individual garnet FIAs newly measured in Nevado-Filabride samples and corresponding moving-average rose diagram. (c) Individual garnet FIAs measured in Alpujarride-Sebtide samples and corresponding moving-average rose diagram. (d) Rose diagrams for all microstructural trend bars in column E of Figure 4. Red, orange, and green colors are used to highlight the clustering of all data in three distinct trend ranges.

the lineation. This points instead to a superposition of different kinematic frames responsible for internal and external fabrics.

3. A total of 150 individual garnet FIAs measured in five Nevado-Filabride samples exhibit a similar distribution of their trends as the 87 average FIAs that were measured earlier by D. G. A. M. Aerden et al. (2013) using sets of radial thin-sections (Figure 9a). The trends of 196 FIAs measured in ASC samples are still sufficiently similar to those of the NFC to suggest a shared tectono-metamorphic evolution (Figure 9c). This is further confirmed by the rose diagram of Figure 9d, which collects all trend bars of column E of Figure 4. The similar orientations of modal maxima and minima observed in all rose diagrams shown in Figure 9 is suggestive of a mixture of three FIA sets with trend ranges of N030-N090, N090-N150, and N150-N180, and corresponding modal maxima at N070, N110, and N165. We have highlighted these trend ranges with orange, red and green colors and explore their geological significance in the following sections. For ease of discussion, we will further simply refer to "orange," "red," and "green" FIAs without always stating the corresponding trend ranges.

4.2. Relative Timing Criteria for FIAs

After having justified a "non-rotational" approach to porphyroblast microstructures in the previous section, four relative-timing criteria can be defined for FIAs with different trends.

Criterion 1: Early burial metamorphism in the ASC was accompanied by growth of chloritoid, garnet, and kyanite, followed by a progressive increase in temperature and decrease in pressure that produced garnet, staurolite and plagioclase, and eventually plagioclase, andalusite and sillimanite (e.g., Azañón et al., 1997; Balanya et al., 1997; Gueydan et al., 2015). An example of an early garnet next to a younger andalusite is shown in Figure 10e. Therefore, inclusion trails in garnet porphyroblasts should always predate those of andalusite porphyroblasts, but may overlap in time with those of staurolite and plagioclase porphyroblasts.

Criterion 2: FIAs oriented parallel to crenulation and fold axes in the matrix may be considered to have formed by overgrowth of those crenulations as, for example, in sample MT2 or F8 (Figure 4). On the contrary, FIAs oriented oblique or orthogonal to matrix crenulations are interpreted as older crenulation axes fixed in porphyroblasts (e.g., samples OK4 or F16).

Criterion 3: Some samples contain porphyroblasts with differently oriented inclusion trails in cores versus rims and thereby directly establishing the relative timing of two trends as shown in Figure 7.

Criterion 4: In most samples, FIA and X_{GRT} trends (columns B and C in Figure 4) broadly align with each other and also with the mean strike of inclusion trails (column A). This is as expected given the preference of FIAs for subhorizontal or gentle plunges in our samples. A few samples, though, contain a high proportion of steeply plunging FIAs resulting in oblique or orthogonal relationships between inclusion-trails strikes on the one hand and FIA plus X_{GRT} axes on the other (Figure 4—MT9, OK4, B3, A7, 27.2.1, B13c, 66.6.1). In such cases, the strike of inclusion trails corresponds to the overgrown foliation, and the FIAs and X_{GRT} trends correspond to the overprinting crenulation cleavage (Figure 5d).

Relative timing relationships exhibited by differently oriented microstructures in our samples are summarized in column E of Figure 4 with black arrows pointing from older to younger trends. Small numbers written next to these arrows refer to the four criteria listed in the previous section. In the next two sections we describe and discuss this evidence first for our Alpujarride-Sebtide samples and then for the Nevado-Filabride samples.

4.3. FIA Sequence in the Studied Alpujarride-Sebtide Samples

Sample F12 (Area-V) contains relatively large (2–3 mm) plagioclase porphyroblasts with weakly sigmoidal inclusion trails. A "green" average FIA (N165 ± 15) parallel to the matrix lineation was determined for these crystals using the radial thin-section technique. Some plagioclase crystals include tiny garnets suggesting that garnet FIAs in other samples from the same area are older (criterion 1). This is supported further by the fact that "red" and "orange" garnet FIAs in TA1, F5, and F20 are surrounded by a "green" matrix lineation (Criterion 2).

Samples OK5, F9, and A7 host garnet, plagioclase and/or staurolite porphyroblasts. Assuming that garnet nucleated earlier, the different inclusion-trail strikes in these minerals indicate that "red" FIAs formed first, followed by "orange" and then "green" FIAs (criterion 1; Figures 10a and 10d). This is corroborated by "orange" X_{GRT} axes versus "red" inclusion-trail strikes in A7 (criterion 4).

Samples B1, B5, B6, and A5 host garnets with "red" FIAs and/or inclusion-trail strikes wrapped by a (younger) subvertical crenulation cleavage with "orange" strike (criterion 2). Orange X_{GRT} axes in garnets of B3 postdate "red" strikes of inclusion trails according to criterion 4. Although no FIAs were measured in J3 owing to very small garnet sizes (<0.5 mm), X_{GRT} axes define a strong "red" maximum that can be assumed as a proxy for a "red" FIA. Younger andalusite porphyroblasts in the same sample have inclusion-trails with "green" strikes parallel to the matrix lineation (Criterion 2) and a similar relationship is observed between "red" X_{GRT} axes in samples F20 surrounded by "green" crenulation axes in the matrix.

Samples OK2, OK3, OK4, and OK5 were collected within 150 m of each other along the northern bank of Oued Kanar. OK5 contains plagioclase porphyroblasts with "green" strikes plus garnets with (older) "orange" strikes (criterion 1). Garnets in OK3 preserve inclusion trails with orange strikes in their cores versus "green" inclusion trail strikes in rims continuous with the matrix foliation (Figure 10c; criterion 3). Garnets in sample OK4 have "green" X_{GRT} axes oblique to internal foliations with "red" strikes (criterion 3).

Samples MT9, B3, F9, and A7 contain garnets with "orange" X_{GRT} maxima versus "red" inclusion trail strikes indicating an older age of the "red" trend (criterion 4). MT9 contains a "green" matrix lineation versus "orange" and "red" internal fabrics (criterion 2). Sample 60.3.1 hosts garnets with "red" X_{GRT} axes subparallel to the mean

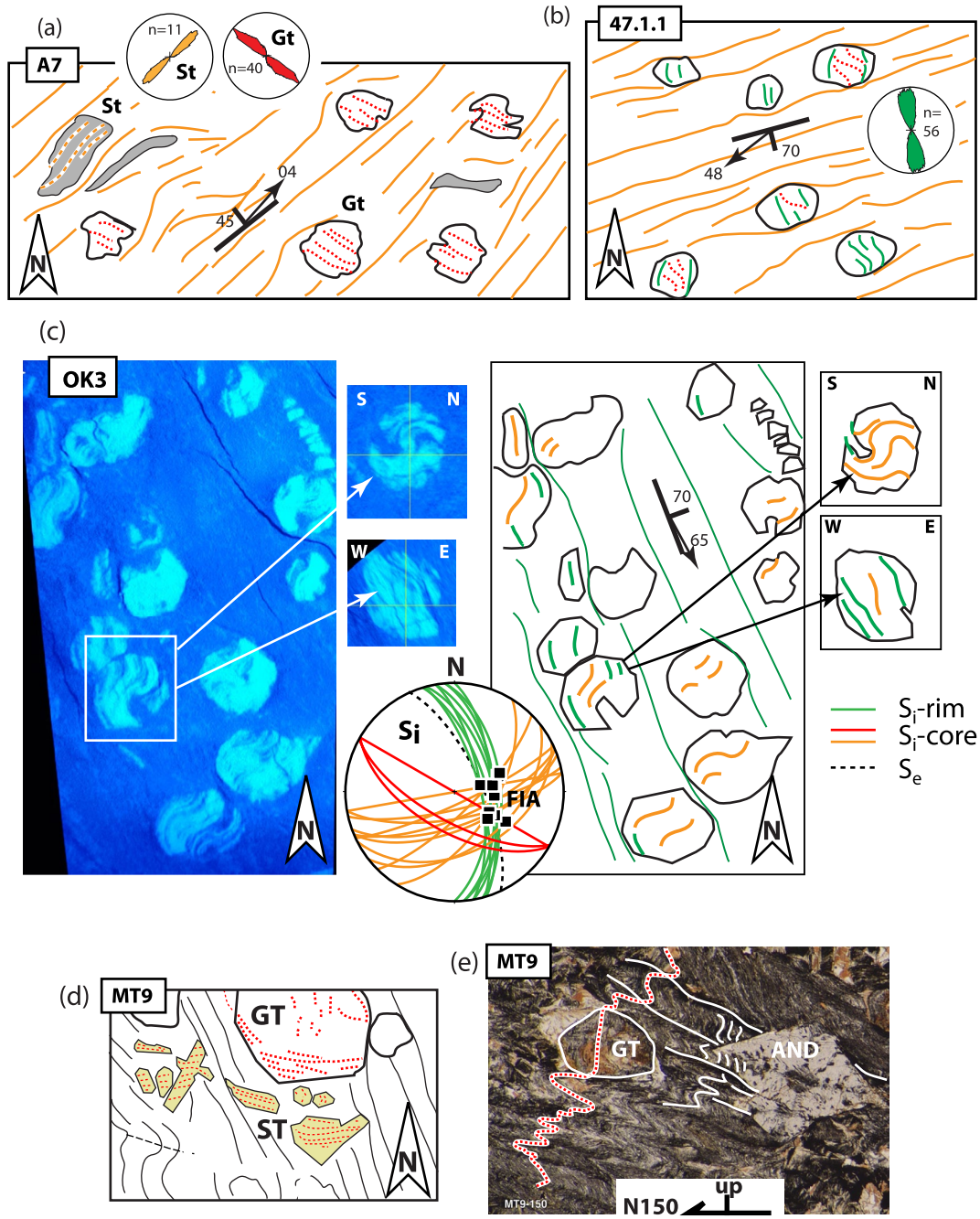

Figure 10. (a) Sketch of garnet and staurolite porphyroblasts in sample A7 with differently striking inclusion-trails indicating earlier garnet growth. (b) NNW-SSE striking internal foliation (green) in garnets of sample 47.1.1 surrounded by a ENE-WSW trending (orange) matrix foliation. (c) Horizontal and vertical tomographic slices and corresponding line drawings of garnets in sample OK3. Note the steep dips of internal foliations and resultant steep Foliation Inflexion/Intersection Axis (FIA) plunges (black squares). (d) Several small staurolite crystals with remarkably constant Si despite variable shapes of the crystals. (e) Vertical thin section striking N150-N330 showing a garnet that grew pre- or early-syn crenulation cleavage, and an andalusite porphyroblast that grew post crenulation cleavage.

strike of inclusion-trails, and surrounded by an "orange" crenulation lineation (criterion 2). Garnets with both "orange" and "red" FIAs in 47.4.1 are surrounded by a "green" matrix lineation.

Eighteen individual garnet FIAs measured by XCT in sample F16 define two FIA subsets with "red" and "orange" trends surrounded by a "green" matrix lineation (criterion 2). But, X_{GRT} axes only exhibit a single "orange" maximum suggesting that "red" FIAs represent a minority that, for some reason, is over-represented in the 18 manually measured FIAs. This may be probably due our selective measurement of the most strongly curved (spiral) inclusion trails, which are ideal for the FIA technique, where most garnets have straight or weakly curved trails. A similar selection bias explains the non-coincident trends of FIAs and X_{GRT} in samples OK4, B3, and A7.

So far, the described microstructural evidence coherently points to a succession of "red," "orange," and "green" FIAs in the ASC, but some data do not so readily fit this picture. Sample J2 (Area-VII; Jubrique unit) hosts small andalusite porphyroblasts whose inclusion trails exhibit bimodal "red" and "orange" strikes closely mimicking X_{GRT} trends in nearby sample J3. In particular, the "red" strike is not expected in andalusite as this mineral grew after most if not all garnet porphyroblasts in these rocks. Considering that andalusite probably grew during gravitational collapse (e.g., Williams & Platt, 2018), we suggest that the strike of their inclusion trails is inherited from pre-existing folds as drawn schematically in Figure 5e. The data for samples 47.1.1. and A2 are also paradoxical by showing garnets with "green" internal fabrics surrounded by "orange" matrix lineations, hence indicating an opposite relative timing of these trends as concluded from other samples (Figure 10b). A possible explanation will emerge from evidence presented below indicating either alternate or synchronous development of "orange" and "green" FIAs in the NFC during the Miocene, after garnet growth in the Alpujarride Complex had already ceased.

4.4. FIA Sequence in the Studied Nevado-Filabride Samples

Samples 27.1.2 and 46.8.1 were collected within a few meters distance from each other in the western Sierra de los Filabres (Figure 3a, Area-XV). Both are light-gray quartz-rich schists containing numerous and variably sized garnets (2–12 mm) with well-developed spiral-shaped inclusion trails. An average FIA trend of N075 ± 15 ("orange") was initially determined for the larger garnets (>5 mm) in sample 27.1.2 by studying inclusion trails with a hand lens on differently oriented polished slabs. Subsequent X-ray tomography of sample 46.8.1 (D. G. A. M. Aerden & Ruiz-Fuentes, 2020) revealed the presence of two additional FIA sets with "green" and "red" trends, which are exclusively hosted in smaller garnets (<5 mm). This mixture of three FIA sets is also reflected in the tri-modal trend distribution of inclusion-trail strikes (Figure 4). Relative timing evidence for the three FIA sets presented by D. G. A. M. Aerden and Ruiz-Fuentes (2020), however, remained limited to a single porphyroblast apparently preserving an orange FIA in the core and a green FIA in the rim (Criterion 3). Yet, the matrix foliation is subparallel to the "orange" FIA.

Garnets in samples BET51A preserve inclusion-trails with "orange" or "red" strikes in their cores truncated by inclusion trails with "green" strikes in narrow rims surrounded by an "orange" matrix lineation (Figures 7b and 7c). Garnets in samples 53.10 (Area-XII; Figures 7a and 7b) and sample 27.2.1 yielded "green" average FIAs (N165 ± 15) in both cases surrounded by an "orange" matrix lineation.

Ruiz-Fuentes and Aerden (2018—their Figure 9b) reported a sample containing small plagioclase crystals whose "orange" FIAs are parallel to and genetically related with a regionally dominant crenulation lineation post-dating garnet growth. D. G. A. M. Aerden et al. (2013—their Figure 3b) reported in four of their samples (all from Areas XII and XIII) late plagioclase porphyroblasts with "orange" or "green" FIAs coexisting with older garnet porphyroblasts with "red" FIAs.

The above microstructural timing criteria found in Nevado-Filabride samples are consistent with "red" FIAs having formed first, followed by "orange" FIAs and then "green" FIAs. Nevertheless, all samples contain "orange" (E-W to NE-SW) crenulation- or mineral lineations, which suggests that "orange" fabrics not only formed before but also after "green" ones. Our garnet ages for some of these samples will shed more light on this question.

Sample B13c is anomalous insofar it contains "red" FIAs caused by the intersection of SE dipping inclusion trails with "orange" strikes and a subvertical crenulation cleavage with "red" strike. An explanation for the opposite timing of "red" versus "orange" microstructures as in other samples will be discussed later in view of a particularly old garnet age we obtained for this rock.

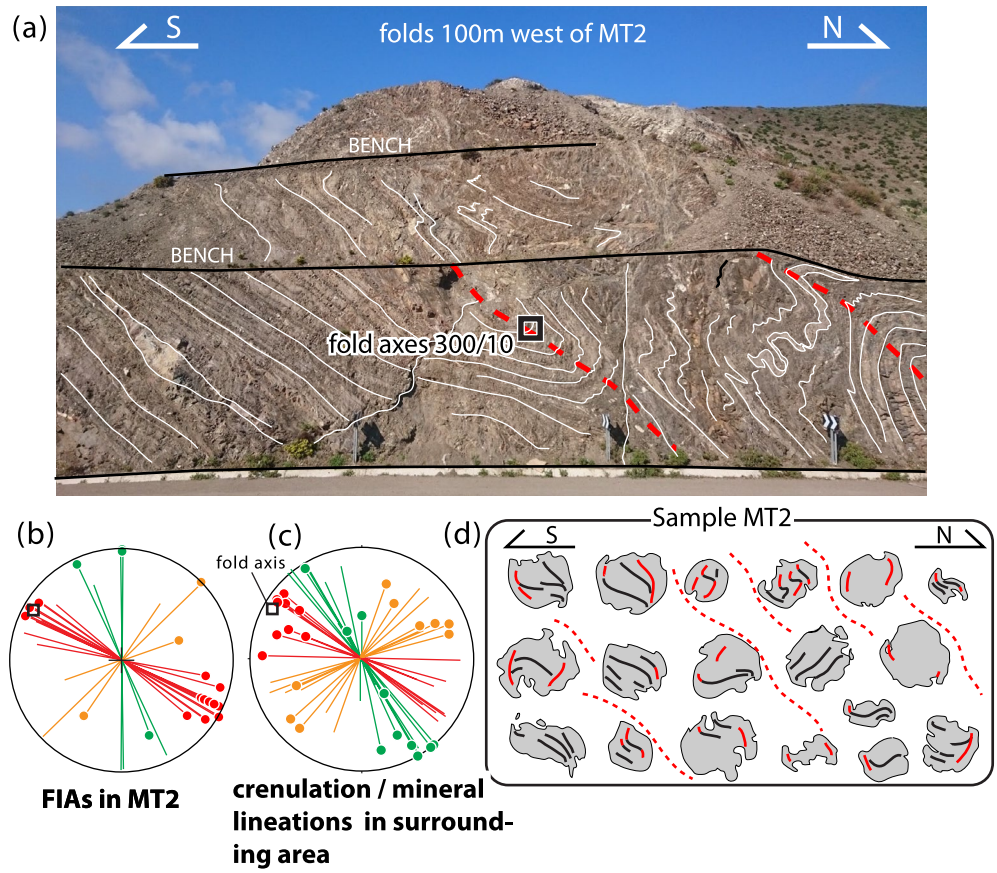

Figure 11. (a) Decameter-scale folds in a road outcrop 100m west of the sample location of MT2 (Beni-Bousera massif). The measured fold axis is parallel to a main group of "red" Foliation Inflexion/Intersection Axes (FIAs) measured in MT2. (b) FIAs measured in MT2. (c) Crenulation or mineral lineations measured within 10 km distance of the outcrop. (d) Line drawings of representative inclusion trails in MT2 viewed in a vertical N-S striking thin section. Inclusion trails are interpreted as relics of a subvertical crenulation cleavage originally parallel to the axial planes of the macroscopic folds, before being rotated toward a north-dipping position.

5. Relationships Between FIAs and Folding

5.1. Genetic Relationships Between FIA and Outcrop-Scale Folds

The relationships between FIAs and macroscopic folds were studied in three outcrops of the Sebtide Complex. The first is a road outcrop near M'ter (Area-II) where MT2 was collected. Decameter-scale folds at this location have WNW-ESE trending axes that are conspicuously parallel to a main group of "red" FIAs identified in MT2 hence suggesting a genetic relationship (Figure 11). Some additional FIAs with different directions were also found and match "orange" and "green" crenulation- and fold axes sets measured in the surrounding area (Figures 11b and 11c). Based on relative timing criteria described in Section 4.3, these extra FIAs probably formed after the "red" FIAs without causing significant modification of the pre-existing macrostructures. This is not unexpected considering that FIAs have been shown to develop during incipient stages of crenulation-cleavage development and hence do not imply deformation continuing to large finite strains after cessation of porphyroblast growth (Adshead-Bell & Bell, 1999; Bell & Hayward, 1991). The detailed geometry of inclusion trails in MT2 (Figure 11d) allows them to be interpreted as relics of a subvertical crenulation cleavage. This implies that the macroscopic folds originated in an upright position during crustal shortening and were later rotated toward an inclined position by synorogenic gravitational spreading (i.e., thrusting) or post-orogenic extensional collapse.

At the beach of Targha, well developed cm- to m-scale folds can be observed in two large outcrops of finely layered dark-gray schists from where samples F8, F9, and F20 were taken. Again, the FIAs of these samples have very similar orientations as mesoscopic fold axes and crenulation lineations measured in both outcrops and the

surrounding area (Figure 12a). The field data, however, show a significantly larger spread and include NW-SE to NNW-SSE trends that are absent from the FIA data. We interpret this difference to reflect variable clockwise reorientations of fold axes, originally all parallel to "red" FIAs, toward a younger "green" (N165) folding direction. This interpretation is consistent with N-S deflections of the matrix against porphyroblasts in sample F9 (Figures 12a and 12b). Internal foliations in all three samples consistently dip steeply to subvertical with E-W strikes. They are continuous with a penetrative matrix schistosity tightly crenulated and folded (Figure 12c) with gently SW dipping axial planes. Consequently, we interpret that the main foliation was formed subvertical by N-S shortening, and was later folded and rotated to a flat lying position by deformation(s) involving a component of gravity-induced (vertical) shortening.

About 4 km northwest of Ceuta, immediately east of the village of Benzu, cm to m-scale folds with steeply south-plunging axes are present well outlined by thin quartz veins in finely laminated Pre-Permian black schists pertaining to the lowermost part of the Federico unit (Figure 13). Garnets in four samples from this outcrop (B1, B3, B5, and B6) preserve a steeply south-west dipping internal foliation that is continuous with the principal matrix schistosity. The latter is tightly folded with steeply dipping axes and vertical axial planes striking NE-SW ("orange" strike). D. G. A. M. Aerden et al. (2010) already studied another sample from this outcrop (their "sample A") in which they demonstrated a rapid pulse of garnet growth during incipient folding stages followed by progressive fold tightening without causing significant porphyroblast rotation. X_{GRT} axes measured in sample B3 trend parallel to the axial planes of the folds as predicted by the conceptual model of Figure 5c. The 10 FIAs measured in the sample correspond to garnets with relatively rare sigmoidal- to spiral-shaped trails as most garnets have straight inclusion trails. We interpret these FIAs as a mixture of "red" and "orange" ones. The strong "orange" X_{GRT} maximum corresponding to a total of 285 garnets suggests that the large majority grew during the "orange" FIA event.

5.2. Regional Fold and Lineation Patterns

The relationships between FIAs, fold axes and lineations were examined further through compilation of over 15,000 field data from the 47 works listed in Table 1 (including about 500 own field data). This data is represented in moving-average rose diagrams for 44 study areas (Figures 2c, 2d, and 3c) and is also provided in full detail as a collection of interactive stereoplots that can be found in Supporting Information S3. These stereoplots allow separate evaluation of different types of structures or different generations of the same type of structure distinguished by the original authors. The rose diagrams (Figures 2c, 2d, and 3c) plot lineations and fold axes jointly justified by the fact that these elements are generally subparallel. Rose diagrams showing a single modal maximum in some cases correspond to two or more generations of homo-axial folds and lineations associated with type-3 fold-interference patterns (e.g., Areas 9, 23a,b, 34, 35, 38, and 44). Rose diagrams with two or three modal maxima in most cases correspond to different generations or types of structures with specific orientations. The originally interpreted relative timing of different structural trends is then indicated with black arrows. In some areas, however, multi-modal rose diagrams cannot be clearly correlated with different sets of structures, either because they were not discriminated by the original workers (Area-17) or because the orientations of different structures are fully intermixed (Areas 7, 21, 24, and 31).

The structural sequences interpreted by different authors and their nomenclature are highly variable and partially conflicting. For example, the bimodal rose diagram for Area-29 corresponds to four fold generations according to Orozco (1971), whereas a very similar rose diagram for neighboring Area-28 was interpreted as representing a single fold set (F_3) and associated (L_3) stretching lineation (Orozco et al., 1998). Similar bimodal rose diagrams for Areas-16 and 17 represent two lineations according to Tubía et al. (1993) and Tubía (1994), but a single lineation according to Williams and Platt (2018). Despite these and other inconsistencies, the originally interpreted relative timing of differently trending structures is still surprisingly consistent with that deduced herein for three FIA set. Thus, Mazzoli et al. (2013; Figure 2a—Area-11a) distinguished an early "red" lineation and associated isoclinal folds overprinted by more open "orange" folds. Tubía (1994; Figure 2—Area-16) recognized an early "red" lineation (interpreted as transtensional) overprinted by a younger "orange" one (interpreted as transpressional). Kornprobst (1974; Areas 1 and 8) and Balanya et al. (1997; Area-10) recognized "orange" folds and/or lineations overprinted by "green" folds in the Beni-Bousera and Bermeja massifs, but Argles et al. (1999) interpreted an opposite timing in the Carratraca massif (Area-18). Sanz-de-Galdeano and Andreo (1995; Area-14b) proposed a broadly synchronous origin of E-W and N-S trending folds during progressive development of the

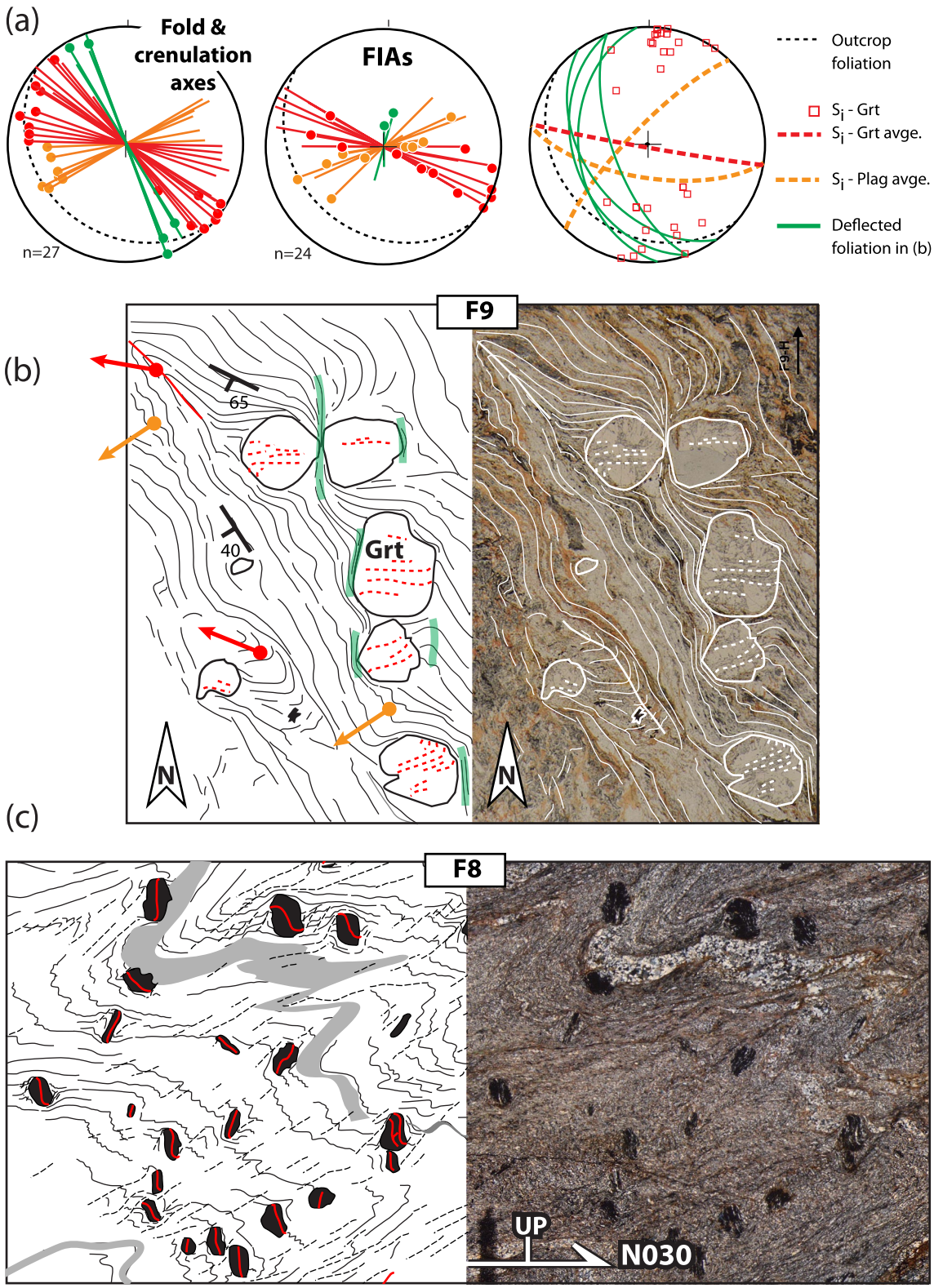

Figure 12. (a) Orientations of Foliation Inflexion/Intersection Axes (FIAs), crenulation axes, fold axes, and internal foliation planes measured in samples F8, F9, and F20 all taken at Targha beach within 500 m from each other. (b) Horizontal thin section of F9 showing consistently E-W striking inclusion trails in garnets despite complex folding in the matrix. Early isoclinal microfolds (small red arrows) are overprinted by weaker NW-SW trending crenulations (orange). Cleavage is deflected into a N-S direction against porphyroblast margins. (c) Vertical thin section striking N030 containing steeply dipping inclusion trails showing relatively minor variation despite intense folding in the matrix.

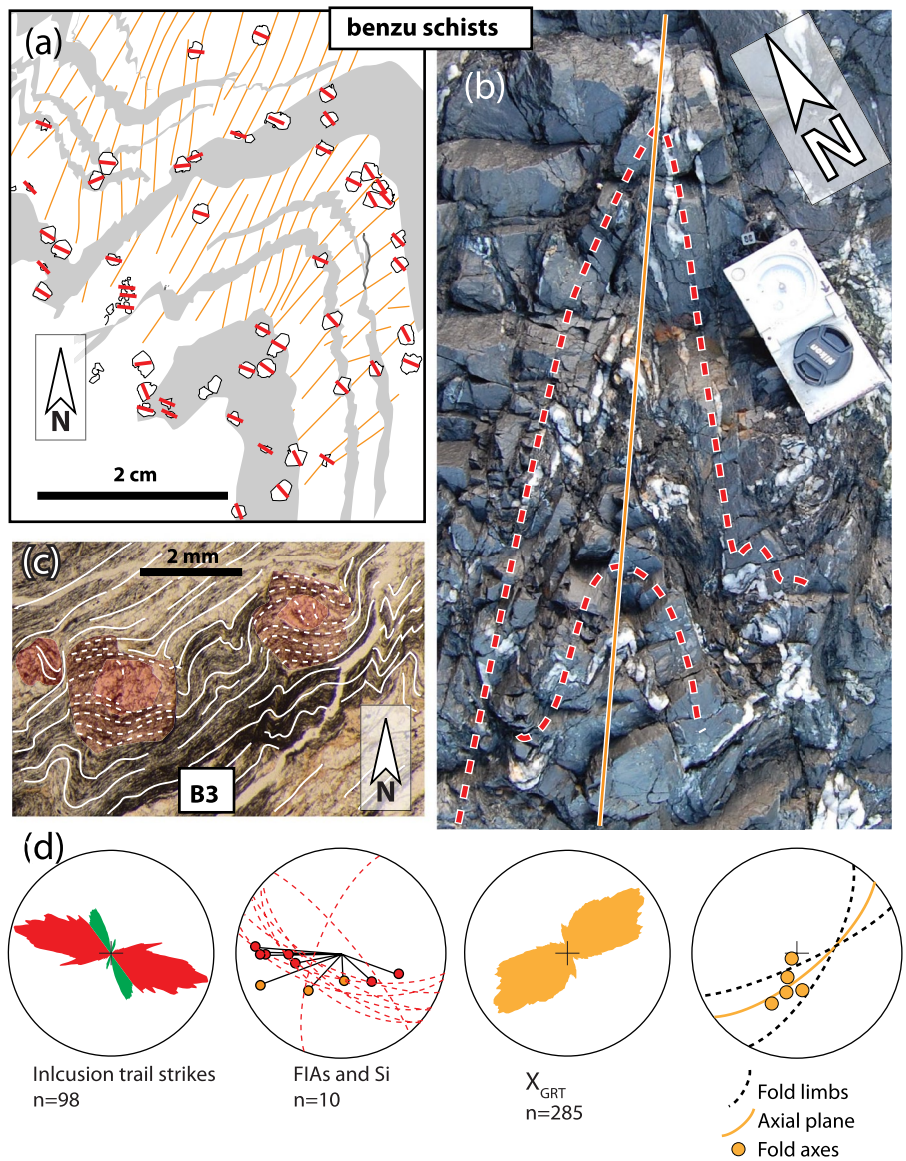

Figure 13. Observations at different scales in rocks of the outcrop (samples B1, B3, B5, and B6). (a) Line drawing of a horizontal thin section studied by D. G. A. M. Aerden et al. (2010) showing inclusion trail in small garnets consistently striking WNW-ESE, despite intense later folding in the matrix. (b) Outcrop-scale folds with steeply SW plunging axis at the spot where sample B3 was taken. (c) Plane polarized microscope image of two garnets (highlighted red) seen in a horizontal thin section of B3 preserving E-W striking inclusion trails ("red") surrounded by crenulations with "orange" axial planes. (d) Microstructural data from sample B3 showing inclusion trails striking oblique to the principal garnet elongation trends (X_{GRT}) as explained conceptually in Figure 5c.

Gibraltar Arc. In the Dorsale Calcaire, using stratigraphic criteria, Vitale et al. (2014, 2015; Areas 3 and 4) deduced an alternation of "orange" and "green" fold trends during the Miocene and interpreted this in terms of a dynamic interference between NW-SE shortening driven by Iberia-Africa convergence and suborthogonal WSW-ENE shortening induced by independent westward motion of the Alboran Domain. Orozco (1971) and Orozco et al. (2004) interpreted N-S trending folds in Areas 29 and 25, respectively, as post-dating ENE-WSW ("orange") and NW-SE ("red") ones. Williams and Platt (2018) grouped lineations across the entire Alpujarride Complex in two main sets with "orange" and "green" trends. They envisaged synchronous development of both sets in deeper and shallower crustal levels, respectively, so that rocks crossing the transition zone between both domains during their exhumation first developed "orange" lineations and then "green" ones.

Table 1
List of Authors Whose Field Data Are Represented by the Rose Diagrams in Figures 2c, 2d, and 3c

Field area	Authors	*N*
1.	Kornprobst (1974, Figure 48)	98
2.	Afiri et al. (2011)	106
2.	El Maz and Guiraud (2001)	50
2.	This study	122
3.	Vitale et al. (2015)	551
4.	Vitale et al. (2014)	394
5.	Chalouan and Michard (1990)	197
5.	Chalouan and Michard (1985)	25
6.	Kornprobst (1974, Figures 4 and 67)	29
6.	Romagny (2014, Figure 44)	18
6.	This study (Cabo Negro)	12
7.	Kornprobst (1974)	16
7.	Romagny (2014, Figure 35)	11
7.	Homonnay et al. (2018)	27
7.	Homonnay (2019)	74
7.	This study	31
8.	Kornprobst (1971, 1974)	51
9.	Précigout et al. (2013)	66
10.	Balanya (1997) / Loomis (1972)	124
11a.	Mazzoli et al. (2013)	92
11b.	Bessière, Jolivet, et al. (2021)	92
12.	Tubía et al. (2013, Figure 6)	130
13.	Tubía et al. (2013, Figure 6)	41
14.	Orozco and Alonso-Chaves (2012)	122
14.	Sanz de Galdeano and Andreo (1995)	49
15.	Tubía et al. (1997)	75
16.	Tubía et al. (1993) and Tubía (1994)	30
17.	Williams and Platt (2018, Figure 8L)	30
18.	Argles et al. (1999)	1,014
19.	Tubía et al. (2004)	67
20.	Cuevas et al. (2001)	33
21.	Alonso Chaves and Orozco (2012)	468
22.	Williams and Platt (2017)	429
23a.	Rossetti et al. (2005) L+M Alpuj.	513
23a.	Rossetti et al. (2005) U Alpuj.	96
24.	Simancas (2018, Figure 1d)	521
25.	Orozco et al. (2004, Figure 5-1)	117
26.	Azañon et al. (1997)	273
27.	Tubía et al. (1992, Figure 4)	53
28.	Orozco et al. (1998)	153
29.	Orozco (1971)	624
30.	Williams and Platt (2018, Figure 8r)	32

Rose diagrams summarizing structural data for the NFC (Figure 3b) are rather similar to those for adjacent Alpujarride areas (Figure 3a), although "green" modal maxima appear rotated toward NW-SE making their distinction with "red" modal maxima less clear. De Jong (1991, Area-41) and Langenberg (1972, Area-42) distinguished an early WNW-ESE trending L_1 ("red") overprinted by E-W to ENE-WSW trending ("orange") L_2 and associated F_2 folds, still overprinted by F_3 and F_4 folds with NNE-SSW ("green") axes. Martínez Martínez (1986a, 1986b; Area-39) described an earlier "orange" lineation (N080 trend; L_2) and younger "green" one (N150; his L_3 and L_m). Lozano-Rodríguez (2019) interpreted regional-scale fold-interference involving N-S and ENE-WSW trending folds but did not interpret their relative timing. Although the deformation history of the Malaguide-Ghomaride complex falls outside the scope of this study, we nevertheless point out that fold trends measured in this complex by Chalouan and Michard (1985, 1990; Area-5) and Cuevas et al. (2001; Area-20) remarkably match those of adjacent Sebtide areas and thus call for careful re-evaluation of a Variscan origin of these folds interpreted by these workers.

Figure 14 highlights the coincident directions of linear field structures and FIAs, allowing to extrapolate the genetic relationships between FIAs and folds established in selected outcrops (Section 5.1.) to the whole of the Betic-Rif belt. Significantly, similar relationships between FIAs, fold axes and lineations have been previously documented in other metamorphic belts as well, including the Iberian and Armorican massifs (D. G. A. M. Aerden, 2004; D. G. A. M. Aerden et al., 2021), the Proterozoic Mount Isa inlier (Sayab, 2005), or the northern Appalachians (Bell & Sanislav, 2011).

6. Sm-Nd Dating of Garnet Porphyroblasts

6.1. Dating Method

Bulk Sm-Nd garnet geochronology (i.e., work on a bulk garnet separate from a single hand specimen) follows the general approach reviewed in Baxter and Scherer (2013) and Baxter et al. (2017). The samples chosen for bulk Sm-Nd garnet geochronology were crushed to a fine gravel using a large tungsten-carbide mortar and pestle. Approximately 20%–25%, representing a homogeneous whole rock fraction was set aside for isotopic analysis with care taken not to fractionate based on grain-size. This whole rock separate was powdered in an agate mortar and pestle and sieved to $a \lesssim 75$ μm grain-size. The remaining sample material (approximately 75%–80%) was processed to obtain a representative bulk garnet separate. The extraction of garnets from the surrounding matrix was accomplished through an iterative combination of crushing, sieving, magnetic Franz separation, and hand-picking. Once approximately 100 mg of visibly clean garnet was obtained, it was crushed using a small tungsten-carbide mortar and pestle and sieved to a grain size between 75 and 150 μm; anything finer than 75 μm was collected as a "garnet powder" separate. The 75–150 μm grain-size was determined by Pollington and Baxter (2011) to be the ideal grain-size to maximize exposure of inclusion phases while minimizing sample loss during the partial dissolution step. To further cleanse the garnet of its contaminating mineral inclusions, both garnet and garnet powder separates were put through a rigorous partial dissolution procedure described below.

Failure to remove contaminating mineral inclusions within garnet can lead to imprecise ages or—if the inclusions are inherited—inaccurate ages. Generally, pure garnet will yield $^{147}Sm/^{144}Nd$ above 1.0 (e.g., Baxter et al., 2017).

Table 1
Continued

Field area	Authors	*N*
31.	Platt et al. (1983)/Williams and Platt (2018)	343
31.	Williams and Platt (2018, Figure 8s)	102
32.	Williams and Platt (2018, Figure 8s)	102
33.	Tubía et al. (1992, Figure 3)	23
34.	Ruiz-Fuentes and Aerden (2018)	291
35.	Galindo-Zaldivar (1993)	3,526
36.	This study	101
37.	Jabaloy-Sánchez (1993)	581
38.	D. G. A. M. Aerden et al. (2013)	63
39.	Martínez-Martínez (1986a)	705
40.	Vissers (1981)	394
41.	De Jong (1991)	549
42a.	Langenberg (1972)	509
42b.	Bakker et al. (1989)	238
43.	Soto (1991)	407
44.	Platt and Behrmann (1986)	445
	Total	15,435

Note. The data can be examined in more detail in Supporting Information S2 (stereoplot collection).

In the clean lab, the separates were put through a partial dissolution procedure consisting of alternating 7 normal (N) nitric acid (HNO_3) and dilute hydrofluoric (HF) acid steps in an enclosed 7 mL TeflonTM beaker for 2 hr at 120°C for each step. The separates were first put in 2 mL of 7N nitric to dissolve any exposed non-silicate inclusions. Next, separates were put in anywhere from 10 to 100 μL of concentrated HF and 1 mL Milli-Q H_2O partially dissolving the sample to further access inclusions, and to dissolve any silicate inclusions present. The separates were then put back in 7N HNO_3 to remove any secondary fluorides that accumulated during the HF step. These alternating steps were continued until there had been approximately 75%–95% mass of sample loss. Following partial dissolution, each separate was fully dissolved. All whole rock separates were fully dissolved using the same procedure as garnet and garnet powder separates. After full dissolution samples were stored in an 8:1 aqua regia solution. Prior to column chromatography, sample aliquots were spiked with a mixed $^{150}Nd/^{147}Sm$ spike for isotope dilution TIMS (ID-TIMS) analysis.

For many of the garnet and garnet powder separates, a "leachate," representing a single combined HF + nitric step was collected during the partial dissolution process. Each leachate collected represents a different stage of sample loss during partial dissolution, and thus represents an intermediate step between the cleaned and uncleaned separate. If the garnet and inclusion phases grew in isotopic equilibrium the leachates should lie along the isochron between pure garnet and whole rock, however if the inclusions have an inherited isotopic signature then the leachate will lie off the isochron.

The isolation of Sm and Nd was accomplished using the three-column procedure described in Harvey and Baxter (2009). The procedure consists of an iron clean-up column using AG50w-X4 resin, rinsed with 1.5 N HCl to remove iron and sample eluted with 6N HCl, a TRU-spec resin column, rinsed with 2N HNO_3 to remove major cations and REEs eluted with 0.05 N HNO_3, and a 2-methyl-lactic acid (MLA) column using AG50w-X4 resin conditioned with 10 mL of 0.2 M MLA. This final column was used to separate Sm from Nd and remove isobaric interferences, predominately Pr on Nd and Gd on Sm.

For the majority of samples, Sm and Nd isotopic ratios were analyzed on an Isotopx Phoenix Thermal Ionization Mass Spectrometer at Boston College following the loading methods of Harvey and Baxter (2009). Nd isotopes were loaded with 2 μL of 2N nitric onto Re filaments with 2 μL of tantalum oxide (Ta_2O_5) activator slurry added to facilitate greater sample ionization. Samples were run in multi-dynamic mode as the oxide species (NdO+). Instrument-induced mass fractionation was normalized to $^{146}Nd/^{144}Nd = 0.7219$ using an exponential correction factor. Sm isotopes were loaded with 2 μL of 2N nitric onto Ta filaments and run in static mode as metal species (Sm+). Instrumentational inducted mass fractionation was normalized to $^{149}Sm/^{152}Sm = 0.516860$ using an exponential correction factor. Both Sm and Nd samples, as well as standards were loaded using parafilmTM dams to decrease sample spread across the filament. Two 4 ng loads of an in-house Ames NdO standards were run with every barrel to track the external reproducibility. Over the period of analysis, the $^{143}Nd/^{144}Nd$ long-term value from the Boston College Phoenix was 0.512152 ± 13.25 ppm 2σ (standard deviation; $n = 32$) and $^{147}Sm/^{144}Nd$ external reproducibility is 0.054% based on repeat analysis of a gravimetrically calibrated mixed Sm–Nd solution. One sample (B13c) was analyzed on the Boston University Thermo Triton TIMS also following Harvey and Baxter (2009); these analyses were performed in static mode with amplifier rotation. The Sm run on the Triton was loaded on zone-refined Re filaments. The $^{143}Nd/^{144}Nd$ long-term value from the Boston University Triton during the period of analysis was 0.512120 ± 17.9 ppm 2σ ($n = 67$) and $^{147}Sm/^{144}Nd$ external reproducibility is 0.023%. In isochron error propagation, the larger (poorer) of the external precision or internal analytical precision (Table 2) was used.

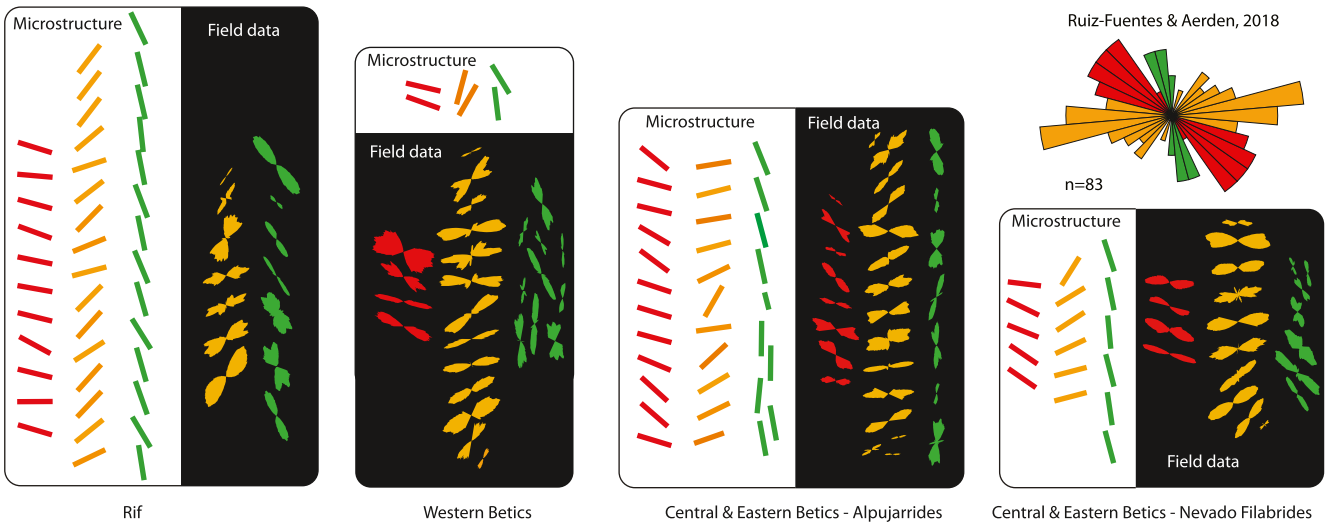

Figure 14. Overview of microstructural trends represented in column E of Figure 4 and of all rose-diagram maxima defined by the ca. 15,000 linear field data represented in Figures 2 and 3. The large rose diagram represents 82 average Foliation Inflexion/Intersection Axes measured by D. G. A. M. Aerden et al. (2013) in the Nevado-Filabride complex. The similar multimodal distributions of the microstructures and regional strongly suggests a genetic link.

6.2. Age Results

All samples yielded one or more garnet analysis with $^{147}Sm/^{144}Nd$ above 1.0 (Table 2). This is a strong indication that efforts to cleanse garnets of contaminant inclusions were successful, thus producing accurate garnet growth ages. Isochron diagrams and resulting age interpretations are shown in Figure 15. Figure 16 presents an overview of the range of garnet ages associated with each FIA sets compared with earlier published geochronological results.

Sample B5 (Benzu schists), F16 and MT8 (Filali schists) produced very similar bulk garnet ages of 26.2 ± 2.5, 24.95 ± 0.61, and 26.9 ± 1.5 Ma, respectively, which agree well with monazite and xenotime ages in the range 21–28 Ma obtained in higher-grade metapelite and orthogneisses near Ceuta (Homonnay et al., 2018) and Ar-Ar ages on micas from lower-grade Sebtide rocks (Marrone, Monié, Rossetti, Lucci, et al., 2021; Michard et al., 2006). Since samples F16 and MT8 have well defined "orange" X_{GRT} maxima representative of the bulk garnet content, their isochrons can be interpreted as dating the "orange" FIA-forming event. As for B5, this sample was taken next to B3, whose garnets were already shown in Section 4.3 to have formed during the "orange" FIA event. The "red" average FIA determined for this sample using six vertical thin sections corresponds to a few garnets with spiral inclusion trails, which probably grew earlier than the vast majority of garnets with simple E-W striking inclusion simple trails similar as observed in B3 (Figure 13).

Sample F8 (Filali schist) exhibits potential age zonation with a four-point isochron corresponding to a low-magnetic garnet fraction giving an age of 26.1 ± 1.4 Ma, and a two-point age of 35.6 ± 2.8 Ma for a high-magnetic garnet fraction presumably richer in Fe-rich inclusions such as magnetite, rutile or ilmenite. Since the presence of two FIA sets with older "red" and younger "orange" trends was already interpreted in samples F8, F9, and F20 (Figure 12), the two ages can be tentatively correlated with these two FIA sets. Note, however, that some degree of mixing between the two garnet fractions is likely so these ages should be considered as a minimum for the old component and a maximum age for the younger component.

The 21.98 ± 0.86 Ma age obtained for A7 corresponds to garnets that overgrew a subvertical foliation with "red" strike during the development of an "orange" cleavage (Figure 10a). The "red" average FIA determined for this sample plunges steeply being controlled by the intersection of two steeply dipping foliations.

Sm-Nd garnet ages obtained in four samples of the Mulhacen unit are all Miocene (22–13 Ma; Figure 15). The youngest age of 12.9 ± 1.6 Ma corresponds to 3–4 mm sized garnets in 27.2.1 with "green" FIAs. Detailed age results for core-, median- and rim zones of three large garnets with spectacular spiral inclusion trails of sample 27.1.2 are reported separately in Farrell (2019) and will be published in a soon forthcoming paper. Here it is sufficient to consider the average age of 13.4 ± 0.4 Ma, which is for "orange" FIAs (~N070).

Table 2
Principal Sm-Nd Geochronological Data

Sample name	Material	ng Nd loaded	Nd ppm	Sm ppm	$^{147}Sm/^{147}Nd$	±2 SE	$^{143}Nd/^{144}Nd$	±2 SE
A7	Whole rock	9.6	31.39	5.882	0.113362	0.00001	0.5120169	0.0000026
	Garnet powder	2.5	0.51	2.297	2.72516	0.00044	0.512414	0.000022
	Garnet powder leachate	2.6	0.819	2.251	1.66311	0.00021	0.512246	0.000013
	Garnet	5.3	1.026	3.209	1.89252	0.00073	0.512237	0.000013
	Garnet leachate	12	1.749	2.621	0.90628	0.00025	0.512141	0.000028
B5	Whole rock	63	45.13	8.636	0.115771	0.000015	0.5120061	0.0000043
	Garnet	0.7	0.215	0.771	2.17416	0.00049	0.512344	0.000039
	Garnet powder	1.9	0.731	0.741	0.612982	0.000064	0.5121	0.000014
B13c	Whole rock	67	27.4	5.35	0.117679	0.000036	0.5119587	0.0000086
	Garnet	1.9	0.12	0.52	2.68096	0.00062	0.512558	0.000035
	Garnet	3.1	0.17	0.39	1.42211	0.0006	0.512212	0.000086
F8	Whole rock	50	35.59	6.8	0.116307	0.000014	0.5119347	0.0000053
	Garnet	1.3	0.151	0.377	1.5128	0.0049	0.51226	0.000025
	Garnet	0.4	0.132	0.398	1.823	0.00019	0.512243	0.000042
	Garnet	3.5	0.199	0.427	1.2962	0.00022	0.512137	0.000009
	Garnet leachate	0.8	0.197	0.362	1.11068	0.00019	0.512088	0.000021
F16	Whole rock	9.6	37.4	7.387	0.119471	0.000013	0.5120028	0.0000054
	Garnet	0.8	1.103	2.812	1.54368	0.00078	0.512269	0.000071
	Garnet leachate	2.1	0.529	1.752	2.00517	0.00023	0.512322	0.000011
	Garnet powder	2.7	0.59	2.049	2.1019	0.003	0.5123224	0.0000079
	Garnet powder leachate	5.2	0.893	2.035	1.37893	0.00017	0.512204	0.00001
MT8	Whole rock	16	3.123	0.802	0.15542	0.000018	0.511993	0.0000047
	Garnet powder	2	0.177	0.402	1.37712	0.00024	0.51221	0.00001
	Garnet	1.8	0.341	0.539	0.95548	0.00015	0.512139	0.000021
	Garnet	11	0.439	0.77	1.06126	0.00051	0.512151	0.000012
	Garnet powder	8.3	0.526	0.713	0.82038	0.00028	0.512104	0.000006
	Garnet leachate	5.6	0.799	0.984	0.7445	0.00013	0.5120981	0.0000078
27.1.2	Whole rock	10	34.17	6.57	0.116316	0.000088	0.511997	0.000021
	Garnet	6.7	1.267	4.43	2.1148	0.00056	0.512193	0.0000066
	Garnet	11	1.089	2.631	1.4616	0.0018	0.512131	0.000009
	Garnet powder	2.2	0.419	0.232	0.33562	0.000049	0.512035	0.000005
27.2.1	Whole rock	61	42.09	8.197	0.117807	0.000015	0.5120168	0.0000032
	Whole rock	59	45.47	8.828	0.117443	0.000017	0.5120086	0.0000044
	Garnet	6.5	1.032	2.559	1.49932	0.00053	0.512118	0.000017
	Garnet	6.3	0.854	2.261	1.60073	0.0007	0.512127	0.000008
	Garnet leachate	2.5	0.462	1.599	2.10295	0.00033	0.512191	0.000012
	Garnet powder	37	5.758	2.854	0.299869	0.000065	0.512027	0.000007
	Garnet leachate	166	21.64	5.595	0.15639	0.0001	0.512009	0.000011
53.10.1	Whole rock	57	41.02	8.152	0.120213	0.000014	0.5120053	0.0000078
	Garnet	10	1.22	1.181	0.58554	0.00014	0.5120741	0.0000059
	Garnet	11	1.109	1.16	0.632932	0.000059	0.5120807	0.0000052

Table 2
Continued

Sample name	Material	ng Nd loaded	Nd ppm	Sm ppm	$^{147}Sm/^{147}Nd$	±2 SE	$^{143}Nd/^{144}Nd$	±2 SE
	Garnet	5.1	1.256	1.55	0.74641	0.00014	0.512079	0.00001
	Garnet powder	2.5	0.631	1.245	1.19346	0.00043	0.512107	0.000023
	Garnet powder	2.3	0.738	1.125	0.92255	0.00014	0.512116	0.000012

A six-point regression containing all analyses for sample 53.10 (south-western Sierra Nevada) gives an imprecise age of 16.3 ± 8.4 Ma for garnets with sigmoidal to spiral-shaped inclusion trails defining "green" FIAs. Considering the high scatter in the data it may be meaningful to consider the possibility of (at least) two age domains. This results in an older four-point isochron age of 21.8 ± 2.4 Ma (MSWD = 0.49) and a younger three-point isochron age of 16.5 ± 2.5 Ma (MSWD = 2.29). Both ages include garnet points with relatively high $^{147}Sm/^{144}Nd$ ratios of 0.923 and 1.193, respectively. Therefore, we expect that both age are reliable and not significantly affected by contamination of inherited inclusions, although they must be considered minimum and maximum ages for garnet growth owing to inevitable partial mixing of both components in the dated garnet fractions.

A three-point isochron age of 35.5 ± 2.0 Ma was obtained for sample B13c from the Veleta Unit hosting numerous small (1–2 mm) garnets in a matrix composed of quartz, chlorite and phengite. A detailed microstructural description and strain analysis of this sample can be found in D. G. A. M. Aerden et al. (2010; their "sample B").

7. Discussion

7.1. Implications for the Metamorphic Evolution of the Internal Zone

Published P-T-t paths for the NFC differ considerably (see Bessière, Jolivet, et al., 2021 for a review) partially reflecting real differences between samples and partially different methods and their intrinsic uncertainties (cf., Massonne, 2014; Platt et al., 2013). Agreement exists, though, regarding early glaucophane- to eclogite conditions reached in the complex reequilibrated in the Upper Greenschist- to Amphibolite facies. In this section, we will consider the two most recent P-T-t reconstructions by Li and Massonne (2018) and Santamaría-López et al. (2019).

Li and Massonne (2018) studied two graphitic schist samples of the Ragua- and Calar-Alto units, although this attribution is somewhat uncertain for the Ragua sample whose geographic coordinates fall exactly on the line drawn by Martínez-Martínez et al. (2002) between both units, which is supposed to represent a ca. 500m wide shear zone in a monotonous sequence of dark schists. In any event, both samples yielded similar P-T-t trajectories featuring two prograde-retrograde cycles, the first reaching higher pressures at lower temperature (Figure 17b). The timing of these events was deduced from two chemically distinct populations of monazite grains giving mean U-Pb ages of 40 Ma, and 24 Ma. The authors complemented their data with P-T path segments constructed by D. G. A. M. Aerden et al. (2013) using the garnet-isopleth method for one light-gray schist of the Ophiolitic subunit (sample B26, Area-XIV) and one dark schist of the Veleta unit (B13a—Area-XIV). Since sample B13a was collected at less than 1m of sample B13c and is petrologically identical, the metamorphic path of this sample can be linked to the ∼35 Ma garnet age obtained for B13c. This path is unusual insofar it combines a pressure increase from 6 to 11 kbar with slight cooling. Such paths have been recently argued to be probable artifacts of the garnet-isopleth method where applied to garnets that grew under isobaric and isothermal conditions after significantly overstepping the garnet-producing reaction (Spear & Wolfe, 2021; Wolfe & Spear, 2018). In such cases, only the garnet rim composition reflects the true (constant) growth conditions. Applied to B13c this means that its garnets grew at 11 kbar/500°C around 35 Ma. Figure 17b shows that this P-T-t point is consistent with the first metamorphic cycle of Li and Massonne (2018). D. G. A. M. Aerden et al.'s (2013) sample B26 was taken from the same outcrop as samples 27.1.2 and 46.8. All three are light-gray garnet schists containing variably sized garnets (2–12 mm). As already stated in Section 6.2, an age of 13.4 ± 0.4 Ma was obtained by Farrell (2019) for three large garnets containing "orange" FIAs in sample 27.1.2. This age coincides with the younger limit of the monazite age range (33–13 Ma; 24 Ma weighted mean) that was assigned by Li and Massonne (2018) to their second metamorphic cycle. Since the peak metamorphic conditions of this cycle coincide with those estimated

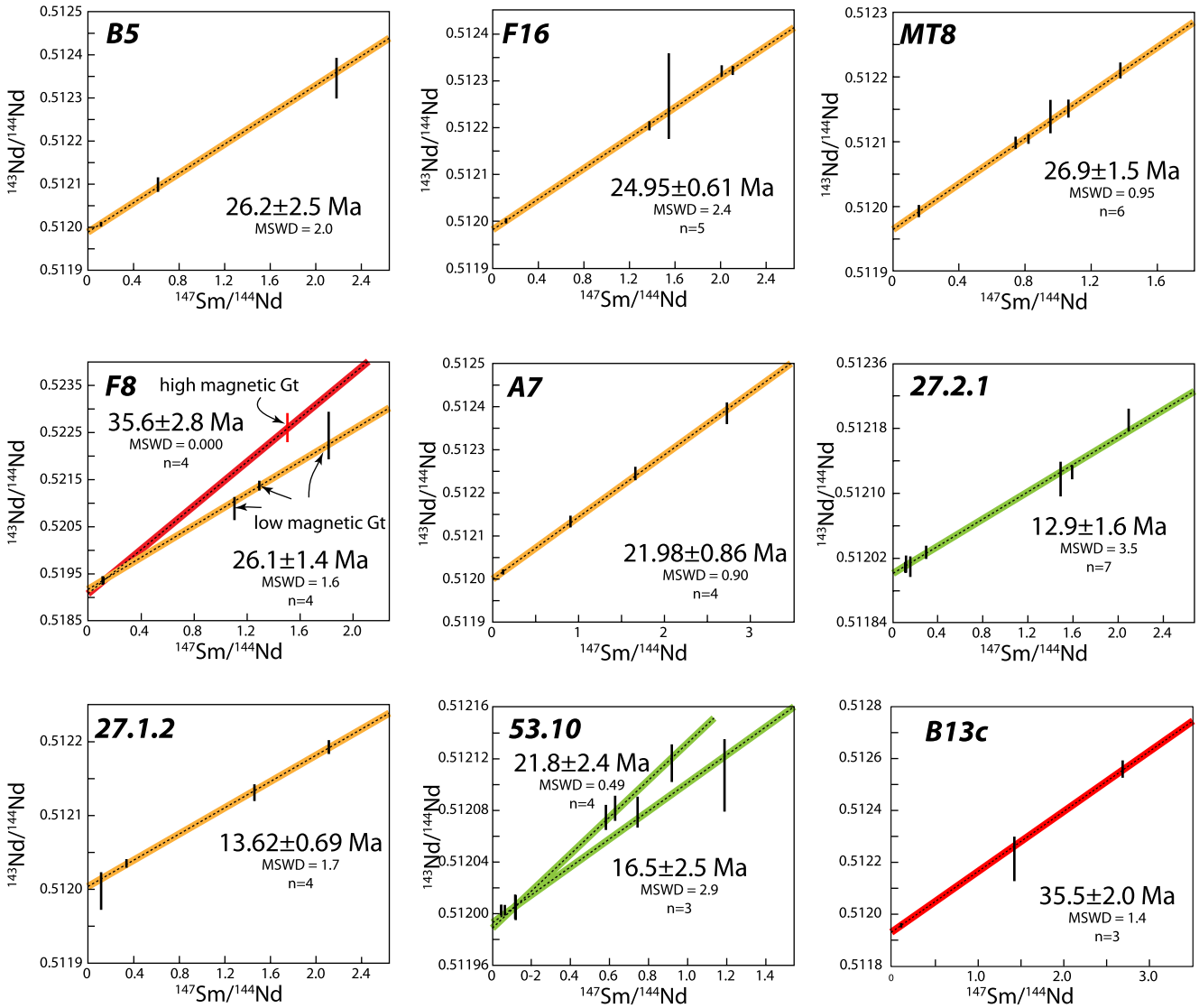

Figure 15. Isochron diagrams discussed in Section 6.2.

by D. G. A. M. Aerden et al. (2013) for sample B26, we interpret that monazite mainly grew during prograde metamorphism (Figure 17b).

Still unexplained is why so far only Miocene garnet ages (21–12 Ma) have been obtained in the Mulhacen unit, assuming that this unit was deformed and metamorphosed synchronously with the Veleta unit. The answer to this question may be related to fact that the Mulhacen unit experienced stronger heating (600°C–650°C) during the Miocene accompanied by more extensive garnet growth. Indeed, if the small garnets (1–2 mm) of B13c could be dated as Late-Eocene, this is only thanks to the absence of younger garnet generations in this sample. Thus, we suggest that garnets of similar age and size are also present in the Mulhacen unit where they occur mixed with much younger and larger garnets that have skewed bulk-garnet ages toward them. Significantly, D. G. A. M. Aerden and Ruiz-Fuentes (2020) demonstrated a mixture of three FIA sets preserved in sample 46.8 that can be correlated with different garnet-size fractions. The larger garnets (5–12 mm fraction) dated 13.4 Ma exclusively contain "orange" FIAs, whereas smaller garnets (<5 mm) also comprises "red" and "green" FIAs. Chemical profiles of selected garnets representative of the three sets shown in Figure 17c demonstrate significant compositional differences supporting growth under different PT conditions.

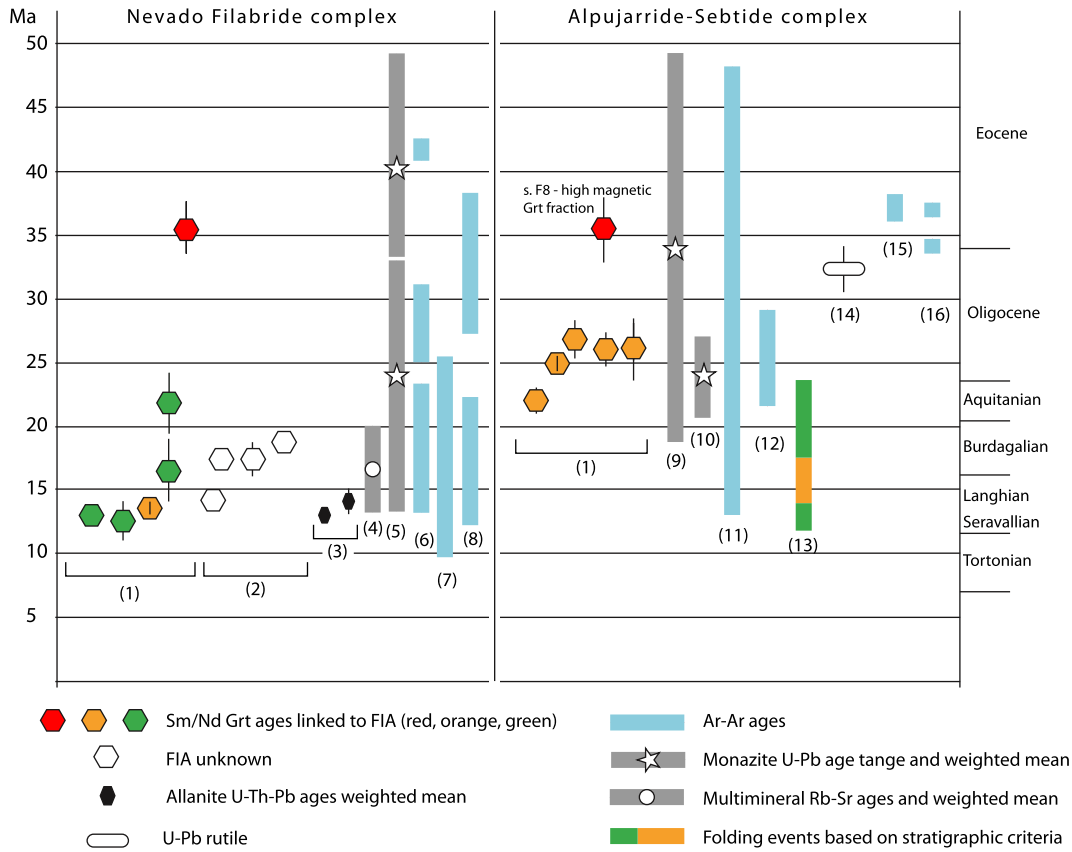

Figure 16. Earlier geochronological evidence relevant to this study. 1: This study, 2: Platt et al. (2006), 3: Santamaría-López et al. (2019), 4: Kirchner et al. (2016), 5: Li and Massonne (2018), 6: Augier et al. (2005), 7: Behr and Platt (2012), 8: Porkoláb et al. (2022); 9: Massonne (2014), 10: Gueydan et al. (2015), 11: Platt et al. (2005), 12: Marrone, Monié, Rossetti, Lucci, et al. (2021), 13: Vitale et al. (2014, 2015), 14: Bruguier et al. (2017; Edough Massif), 15: Bessière, Jolivet, et al. (2021), 16: Marrone, Monié, Rossetti, Aldega, et al. (2021).

Santamaría-López et al. (2019) did not find evidence for two Alpine metamorphic cycles in their study of four micaschist samples of the Mulhacen unit plus one of the Veleta unit, but reconstructed similar decompression paths for both units from ca. 20–22 kbar/475°C down to 6 kbar accompanied by heating to 530°C in the Veleta unit and to 600°C in the Mulhacen unit (Figure 17). The stronger heating in the Mulhacen unit was interpreted to record the passage of overlying hot Alpujarride rocks. U-Th-Pb ages for allanite grains included in narrow garnet rims and in the matrix allowed them to constrain the timing of the latest garnet growth to ~13 Ma at 6 kbar/~550°C, while earlier garnet growth stages at pressures from 18 kbar downwards remained undated. Although the P-T condition of sample B13c are, in principle, compatible with the metamorphic path of the Veleta unit propose by these workers, the Late-Eocene garnet age we have obtained for this rock favors the prograde trajectory of Li and Massonne (2018) because of independent evidence for crustal thickening at this time in the Betic-Rif orogen.

In the ASC no major conflicts exist between P-T trajectories of different workers, but the timing (Variscan or Alpine) of a HP/HT event recorded in the migmatitic gneisses above the Beni-Bousera and Ronda peridotites is debated. This event has been associated with intense deformation at the peridotite-crust contact, so its age is relevant to the history of emplacement and exhumation of the peridotites from an original depth of 85 km (Garrido et al., 2011). Two anatectic events of Late Carboniferous-Permian and Oligocene-Early Miocene age have been demonstrated in the migmatitic gneisses by zircon and monazite dating (e.g., Acosta-Vigil et al., 2014; Massonne, 2014; Rossetti et al., 2010, 2020; Ruiz-Cruz & Sanz-de-Galdeano, 2014; Sánchez-Navas et al., 2014), but the depths at which these events took place are less certain. Massonne (2014) identified a Variscan monazite population included in low-Ca garnets and a late-Eocene population (~34 Ma) included in high-Ca garnets. Metamorphic conditions were estimates as 7 kbar/800°C (granulite facies) for the Variscan event and 13 kbar/650°

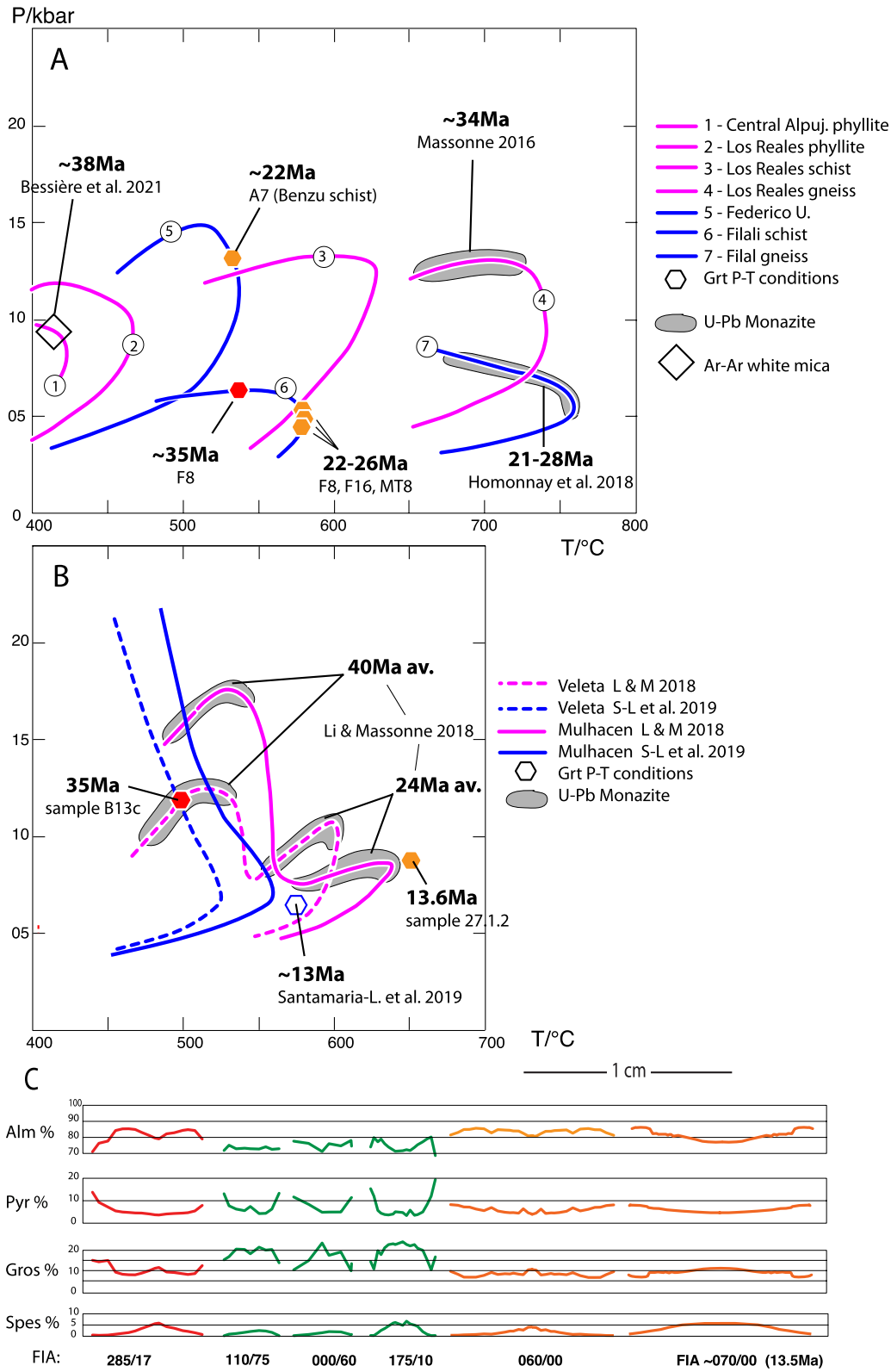

Figure 17.

(Barrovian facies) for the Alpine event. This polycyclic history is consistent with reported Variscan andalusite crystals transformed to kyanite during the Alpine orogeny (Sánchez-Navas et al., 2012) and 28 Ma Monazite and Xenotime ages linked to HP/HT conditions in the Lower Sebtides (Homonnay et al., 2018).

However, Bouybaouene et al. (1998), Montel et al. (2000), Gueydan et al. (2015) and Rossetti et al. (2020) have interpreted Variscan HP/HT conditions in the Lower Sebtide complex based on pre-Alpine monazite inclusions hosted in garnets versus Alpine (<30 Ma) monazite grains in the matrix. Particularly relevant here is Gueydan et al.'s (2015) petrological study of three Filali-schist samples from our Area-V that were collected at about 1 km distance from our samples F8 and F16. These authors derived conditions of 6–8 kbar/520°C–620°C for "S1" inclusion trails of synkinematic garnets and 4–7 kbar/620°C–660°C for the principal matrix foliation ("S2"). They inferred that the first (Barrovian) metamorphic event is Variscan based on variably reset pre-Alpine ages (250–170 Ma) of monazite inclusions preserved within garnets of another migmatitic-gneiss sample located much closer to the peridotites. However, our Oligocene ages for "syn-D1" garnets in samples F8, F16, and MT8 clearly demonstrate an Alpine origin of the inclusion trails and hence of the Barrovian conditions deduced from them. The pre-Alpine monazite grains present in some garnets at deeper and higher-grade levels must either have grow syngenetic with an earlier (Variscan) generation of garnets or represent inherited grains overgrown by Alpine garnets.

7.2. Kinematic Significance of FIAs and Lineations

Deformation sequences reconstructed by different workers in the NFC and their tectonic interpretation have differed dramatically over the years. Vissers (1981) interpreted four fold generations, which he related to northward and southward thrusting events. Platt and Behrmann (1986) distinguished five foliations, which were attributed to progressive top-to-the-NNE thrusting. Bakker et al. (1989) and De Jong (1993) also recognized five foliations but interpreted NW-directed thrusting, followed by SE-directed extension, followed by NNE- and SSW-directed thrusting. Jabaloy et al. (1993) described four foliations and proposed progressive top-to-the-W extensional shearing. Booth-Rea et al. (2015) distinguished two foliations supposedly formed during westward thrusting. D. G. A. M. Aerden et al. (2013) and Ruiz-Fuentes and Aerden (2018) distinguished four matrix foliations plus additional ones preserved inside porphyroblasts and interpreted an alternation of crustal shortening and gravitational collapse phases.

In the ASC, three foliations have been traditionally distinguished corresponding to relics of an "S1," the main matrix foliation (S2), and a younger crenulation cleavage (S3). However, this is necessarily a simplified scheme as some authors have documented two crenulation cleavages both overprinting the main foliation (Orozco et al., 1998; Platt et al., 1983) and we have also observed this in several Alpujarride outcrops (this will be shown in detail in a separate paper in preparation by Aerden and Ruiz-Fuentes). Moreover, "S1" has been shown herein to encompass multiple foliations. Tectonic interpretations of the traditional D2 and D3 events range from (a) NE-SW extension in lower crustal levels (D2) synchronous with N-S extension (D3) at higher levels (Williams & Platt, 2018), (b) NE-SW oriented transpression in lower crustal levels (D2) synchronous with N-S gravitational spreading at higher levels (Tubía et al., 1997, 2013), (c) NE-SW extension followed by N-S contraction (Azañón et al., 1997; Balanya et al., 1997; Rossetti et al., 2005), or (d) top-to-the NE thrusting followed by crustal extension in opposite direction (Homonnay et al., 2018).

The disparity of tectonic models reflects three fundamental problems: (a) a lack of constraints on the original orientations of fabrics and subsequent changes thereof, (b) the lack of a structural reference frame allowing reliable orogen-wide correlation of fabrics, and (c) uncertainty regarding the kinematic significance of lineations and folds in general. Our study exemplifies again how the first two knowledge gaps can be filled by integrating porphyroblast inclusion-trail data in tectonic studies. However, such data also bear important implications for the general tectonic significance of foliations and lineations by implying major coaxial components of deformation associated with distributed crustal shortening, tectonic escape and gravitational spreading (Figure 5). In spite of sub-coaxial deformation having been frequently inferred from inconsistent shear-sense indicators and

Figure 17. (a) P-T-t paths and garnet-growth conditions for Alpujarride-Sebtide units based on: 1. Azañon et al. (1997); 2. and 3. Balanya et al. (1997); 4. Massonne (2014); 5. Bouybaouene et al. (1999) and Michard et al. (2006); 6. Gueydan et al. (2015); 7. Homonnay et al. (2018). (b) P-T-t trajectories for the Veleta and Mulhacen units of the Nevado-Filabride complex according to Li and Massonne (2018) and Santamaría-López et al. (2019). (c) Compositional profiles of five garnets with "green," "orange," or "red" Foliation Inflexion/Intersection Axes (FIAs) present in the same thin section of Mulhacen sample 46.8.1. Significant compositional differences support different timing and P-T-X conditions of different FIA sets.

strain analysis in the Betic-Rif orogen (e.g., Azañon et al., 1997; Galindo-Zaldivar et al., 1989; Platt & Behrmann, 1986; Précigout et al., 2013; Reuber et al., 1982; Tubía et al., 2013; Vissers, 1981), tectonic models are still commonly based on the assumption of tectonic transport associated with simple shear parallel to lineations. This view forces the further assumption of very large shear strains, sufficient to have caused pervasive reorientation of fold axes parallel to the stretching lineation and to have generated sheath folds. This model faces two major problems, which are not exclusive to the Betic-Rif orogen (cf., D. G. A. M. Aerden et al., 2021). First, sheath folds are quite rare compared to cylindrical ones and many can be alternatively explained as fold-interference structures. A pluri-kilometric sheath fold proposed by Orozco et al. (2004, 2017) in the Sierra de Lujar was recently reinterpreted as a fold-interference structure by Simancas (2018) who showed the limited curvature of the fold axes, ubiquitous evidence for meso-scale fold interference and relatively low strains. Major sheath-folds interpreted in the Sierra Blanca and Sierra de la Contraviesa (Orozco & Alonso-Chaves, 2012; Orozco et al., 2017) can probably be reinterpreted in a similar fashion considering evidence presented by these workers for two major folding events in this region. Eye-shaped outcrop patterns on a mountain slope in the central Betics interpreted as sheath folds by Williams and Platt (2018, their Figure 3a), on inspection in Google Earth (Lat. 36.897° and Long. −4.02°), appear to be topographic cut effects where an E-W trending anticline is transected by perpendicular mountain valleys. The second problem is that quantitative strain analyses have only yielded moderate strain values (Vissers, 1981: 70%; Jabaloy & González Lodeiro, 1988: 72%; D. G. A. M. Aerden et al., 2010: 115%; Borrodaile, 1976: 150%; Soto, 1991: 150%), which are an order of magnitude lower than required to rotate fold axes subparallel to the shearing direction in analogue experiments. Recognizing this problem, Zevenhuizen (1989) and Soto (1991) already realized that the sheath-fold like structures they observed in the eastern NFC must have formed by deformation of pre-existing folds whose axes happened to be sub-parallel to the future stretching/shearing direction. Galindo-Zaldivar (1993) suggested the analogy of an elastic sheet progressively developing folds while being stretched parallel to the fold axes. Note the close affinities of these models with the conceptual FIA mechanisms sketched in Figures 5e and 5b, respectively. These models predict fold-axes parallel stretching as a consequence of the original orientation of foliations close to the *XZ* plane of superposed deformations causing folding (e.g., Grujic & Mancktelow, 1995). Strongly non-cylindrical folds (i.e., sheath folds) can still form in such a context where the axes of pre-existing folds lie oblique to the *XY* plane of the superposed deformation, for example, where gravitational collapse is superposed on upright folds with gently to steeply plunging fold axes (Figure 5d; Figure 12 of D. G. A. M. Aerden et al., 2021).

7.3. Paleogeographic Implications

Following up on the above discussion, we interpret the WNW-ESE trend of our "red" FIA set to record orthogonal NNE-SSW crustal shortening in the Late Eocene to Early Oligocene. In the NFC, this time frame is indicated by our new ∼35 Ma garnet age for sample B13c, in accordance with Ar-Ar ages for relic "S1" (Augier et al., 2005; Porkoláb et al., 2022), a mean U-Pb age of ∼40 Ma for high-Y monazite grains (Li & Massonne, 2018), and Eocene U-Pb ages for zircon rims (Poulaki et al., 2020). In the Alpujarride Complex, a similar timing of burial metamorphism is indicated by the 35 Ma Sm-Nd age obtained for high-magnetic garnet in sample F8, in agreement with a mean age of ∼34 Ma for high-Y monazite grains in the Los Reales unit (Massonne, 2014), 34–38 Ma white-mica (Ar-Ar) ages associated with HP/HT assemblages (Bessière, Jolivet, et al., 2021; Marrone, Monié, Rossetti, Aldega, et al., 2021), and a 32.4 ± 3.3 Ma U-Pb age of rutile inclusions in garnets from high-pressure rocks in the Kabylias (Bruguier et al., 2017). Garnets preserving "orange" FIAs in the ASC have yielded Oligocene to Early Miocene (27–22 Ma) ages implying a major change in shortening direction from NNE-SSW to NW-SE. "Green" FIAs in the same complex began to form shortly after 22 Ma according to our age data, followed by rapid exhumation and heating.

In the NFC, garnets with "orange" or "green" FIAs have yielded Miocene ages (21–13 Ma) without showing consistent relative- or absolute age relationships between both FIA sets. This suggests that both sets formed in alternation or perhaps simultaneously at different locations due to deformation partitioning (Figure 16). Significantly, alternating WSW-ESE and NW-SE contraction in the Miocene was earlier proposed by Vitale et al. (2014, 2015) in the Dorsale Calcaire and External Zone of the Rif based on detailed structural analysis of multiple fold and thrusts generations with sub-orthogonal vergences. They attributed this to dynamic interference between NW-SE Africa-Iberia convergence and suborthogonal westward motion of the Alboran Domain. The same explanation can be envisaged for the generation of two suborthogonal FIA sets in the NFC.

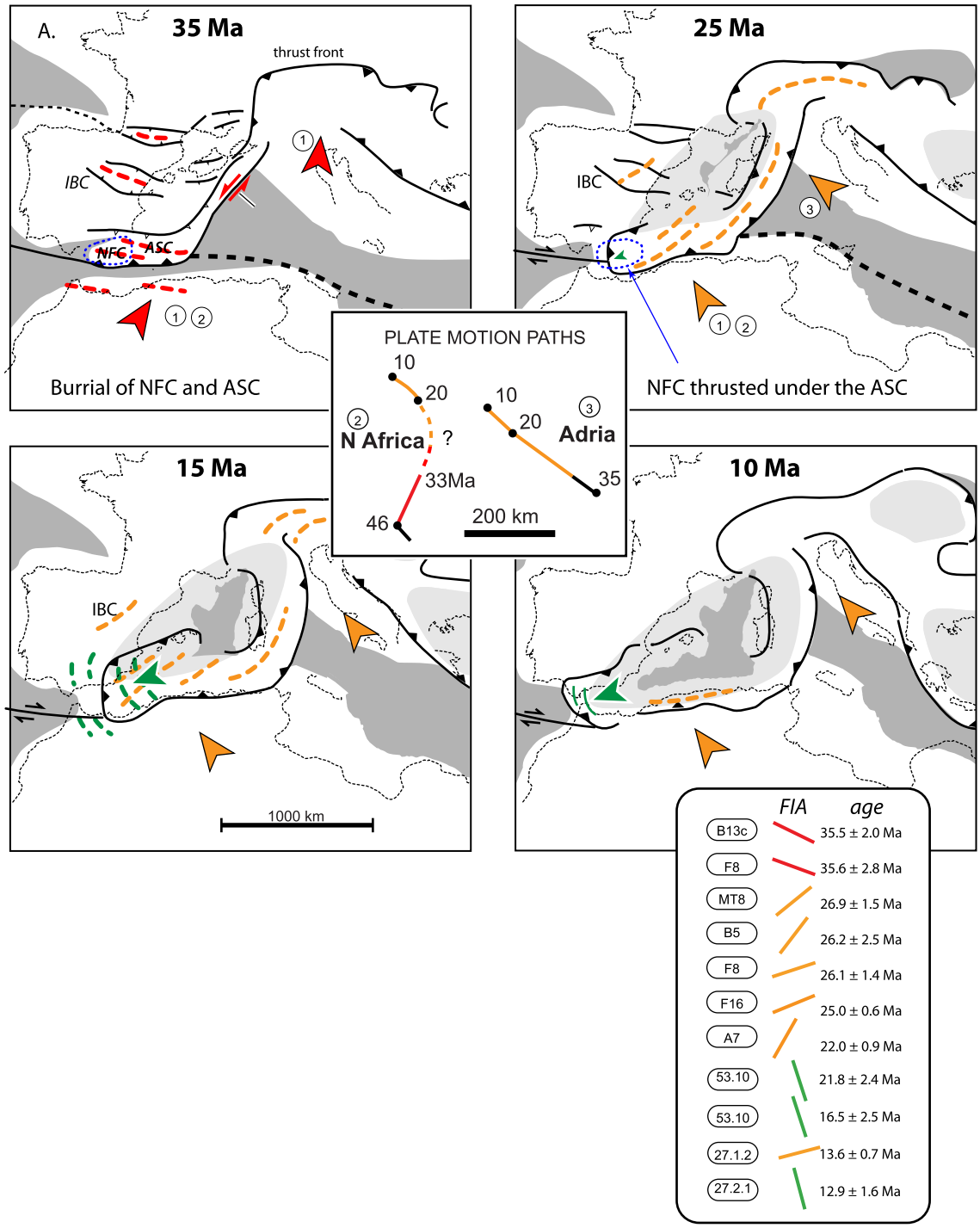

Figure 18. Paleogeographic sketches modified after Faccenna et al. (2014) with plate motion vectors relative to Eurasia taken from (1) Rosenbaum et al. (2002), (2) DeMets et al. (2015), and (3) Handy et al. (2010). See Section 7.3 for detailed explanation. The central inset shows the plate motion path followed by Africa relative to Iberia including the change from NNE to NW directed. Foliation Inflexion/Intersection Axis (FIA) trends and corresponding Sm-Nd ages are summarized below the maps for comparison. Note that these FIA lie normal to plate convergence vectors for the same age.

Figure 18 illustrates how the above described sequence of crustal shortening directions may be related to the paleogeographic evolution of the western Mediterranean Alpine belt and to relative plate-motion vectors after Rosenbaum et al. (2002), DeMets et al. (2015), and Handy et al. (2015). NNE-SSW shortening in the Late Eocene—Oligocene as recorded by "red" FIAs agrees remarkably well with a NNE directed motion of Africa

relative to Eurasia in this period. Note that this convergence direction is difficult to reconcile with a commonly assumed NE-SW trending orogenic trend (e.g., Faccenna et al., 2014; Frizon de Lamotte et al., 2011; Stampfli & Hochard, 2009) because of the low angle with the plate-convergence vector. We therefore favor a more E-W trending orogen as depicted in paleogeographic reconstructions by Dercourt et al. (1986), Bouillin (1986), Stampfli et al. (1998), Jolivet and Faccenna (2000), or Guerrera et al. (2012). Further north, in the eastern Pyrenees, Southern France, Sardinia and Corsica, an important sinistral strike-slip component is expected, evidence for which has been presented by Lacombe and Jolivet (2005) and Marroni et al. (2019).

The "orange" FIA set (Oligocene and Miocene ages) can be linked to a new "Apenninic" subduction direction following an anticlockwise rotation of the plate motion vector for Africa relative to Iberia from NNE to NW. The exact timing and duration of this change has remained poorly constrained between 33 and 20 Ma owing to a lack of magnetic anomalies for this period (DeMets et al., 2015; Jolivet & Faccenna, 2000). Our FIA ages constrain this shift to 35–27 Ma (Rupelian). A change in subduction direction provides an explanation for the fact that Late Oligocene back-arc basins opened oblique to a pre-existing Betic front (Doglioni et al., 1997), and for re-burial of the NFC (Li & Massonne, 2018) below a now westward moving ASC undergoing gravitational collapse (cf., Platt et al., 1983, their Figure 18). The NNW-SSE trend of "green" FIAs can, in turn, be related to independent westward motion of the Alboran Domain driven by some combination of subduction roll-back and lateral extrusion between the Iberian and African plates.

The geodynamic model sketched in Figure 18 is akin to that proposed by Porkoláb et al. (2022) by considering (a) that the NFC and ASC occupied laterally equivalent positions and were simultaneous undergoing burial metamorphism during the Eocene-Oligocene, (b) a northward subduction polarity (see next section), and (c) tectonic differentiation of both complexes in the Late-Oligocene/Early Miocene when the NFC is overthrusted by the ASC in NW- to SW direction.

Also noteworthy is that the sequence of crustal shortening directions deduced herein from FIAs is similar to that reconstructed by Liesa and Simón (2009) from paleostress data in the Iberian Chain, a zone of intraplate deformation in central-eastern Spain (Figure 18). These authors distinguished a Middle Eocene to Late Oligocene NE–SW compression phase (their "Iberian" phase), followed by Late Oligocene to Early Miocene NW–SE compression (their "Betic" phase), followed by Miocene "Guadarrama"- and "Pyrenean" compressions oriented NNW–SSE and NNE-SSW, respectively. The "Iberian" and "Betic" phases can be correlated with our "red" and "orange" FIA sets, respectively, whereas the "Guadarrama" compression may be linked to the Middle-Miocene "orange" FIAs of the NFC.

7.4. Subduction Polarity

Bell and Johnson (1989, their Figure 25) argued that the curvature sense of sigmoidal or spiral-shaped inclusion trails in metamorphic belts should reflect the vergence of thrusting or the polarity of subduction. Our "red" FIA set is defined by inclusion trails curving anticlockwise in 12 samples (eight of the Alpujarride-Sebtides and four of the Nevado-Filabrides), clockwise in three samples (two Alpujarride-Sebtides; one Nevado-Filabrides), and show inconsistent asymmetries in one sample (F9; Sebtides), all viewed in westward direction. The predominant anticlockwise asymmetry implies southward thrusting or northward subduction as envisaged, amongst others, by Dercourt et al. (1986), Stampfli et al. (1998), Jolivet and Faccenna (2000), Lacombe and Jolivet (2005) or Platt et al. (2013). The sense of inclusion-trail curvature associated with "orange" FIAs was determined in seven samples (all from the Sebtide complex) and is predominantly anticlockwise when viewed toward the SW (5–2 ratio). This is consistent with unanimously accepted NW directed subduction of Africa/Adria below Iberia in the Oligocene. Significantly, the same prevalent asymmetries associated with "orange" FIA set has been found in about 40 Alpujarride samples studied by Ruiz-Fuentes and the first author that will be soon published in a separate article.

Although the number of Nevado-Filabride samples studied by us is insufficient to draw firm conclusions from inclusion-trail curvature senses, we note that "orange" FIAs in our samples, presumably of Miocene age, mostly curve clockwise (five to one ratio) when viewed to the SE. This is, in principle, consistent with SE-directed underthrusting of the complex during the Miocene below the Alboran Domain (cf., Platt et al., 2006).

7.5. Implications for the Mechanism of the Gibraltar Arc

Didon et al. (1973) and Kornprobst (1971) already recognized the same two fold sets with NE-SW and NW-SE trend in peridotites of the Beni-Bousera massif, in Ceuta, and in the Bermeja Massif of the western Betics. They concluded from this that the Gibraltar Arc could not have formed by bending of an originally straight belt. Our microstructural data and compilation of regional fold trends extend this homology of structural directions to the entire Internal zone (Figure 14) and thereby refute major rigid-body rotations within the Alboran Domain. Consequently, rotations previously inferred from remnant magnetization directions in the Internal zone (e.g., Berndt et al., 2015 and references cite therein) are probably related to heterogeneous ductile strain and foliation development (e.g., Borradaile, 1997). Paleomagnetic data from the External Zone indicate predominantly clockwise rotations in southern Spain and anticlockwise ones in the Rif, consistent with westward motion of the Alboran domain having driven these rotations (Platt et al., 2013). However, the data are problematic in detail (Platt et al., 2013; van Hinsbergen et al., 2020) and are probably also influenced by strain.

We interpret the Gibraltar Arc as a polyphase structure formed by the interplay of two sub-orthogonal shortening and folding directions (related to "green" and "orange" FIAs) caused by NNW motion of Africa and simultaneous WSW motion of the Alboran domain relative to stable Iberia. N-S trending fold axes ("green") appear concentrated in the frontal part of the Arc, whereas "orange" fold trends dominate further east normal to the Iberia-Africa convergence direction. These features plus evidence for synchronous radial thrusting in the External Zone (Balanya et al., 2007; Platt et al., 2003) are highly suggestive of the channeled extrusion analogue models of Gilbert and Merle (1987) and Cruden et al. (2006; their Figure 10).

8. Conclusions

The integration of high-resolution microstructural analysis using X-ray microtomography, Sm-Nd garnet dating and field data has allowed us to reveal close links between structures ranging from the micro-tectonic to plate-tectonic scale in the Betic-Rif orogen. Inclusion trails of garnet-, staurolite-, plagioclase-, and andalusite porphyroblasts in the Internal zone of this belt have been shown to pertain to different age groups, whose specific orientations are maintained around the Gibraltar Arc from the Beni-Bousera massif to the eastern Betics. The different timing of these groups is demonstrated by microstructural and petrologic criteria and 10 new Sm-Nd garnet ages.

Inclusion-trail curvature axes or "FIA" (Foliation Inflexion/Intersection Axis) in the Betic-Rif orogen represent multiple generations of "fossilized" crenulation axes. This explains similar multi-modal trends exhibited by FIAs, folds and lineations shown in this work. The regional consistency of FIA orientations confirms the control of deformation partitioning on porphyroblast growth and its role in suppressing porphyroblast rotation during ductile deformation (e.g., Bell, 1985; Fay et al., 2008).

Preferred subvertical and subhorizontal (bimodal) orientations of inclusion trails and of porphyroblast shape axes confirm a history of alternating crustal shortening and synorogenic gravitational collapse, as previously recognized form field-data and petrological evidence (Azañon et al., 1997; Balanya et al., 1997). Stretching lineations parallel to fold axes in this context are best interpreted in terms of lateral extrusion or "tectonic escape" normal to plate-convergence directions.

The occurrence of similar FIA sequences in the NFC and ASC implies a largely shared tectonometamorphic evolution. The earliest two FIA sets (WNW-ESE and NE-SW) can be matched to ca. 60° anticlockwise rotation of the plate-motion vector of Africa relative to Iberia from NNE- to NW independently deduced from kinematic modeling of magnetic seafloor anomalies (e.g., DeMets et al., 2015). The prevalent curvature sense of rotational inclusion trails (anticlockwise when viewed in westward direction) indicates a northward changing to north-westward subduction direction of the African plate below the south-Iberian margin itself or Alkapeca crustal fragment. The youngest N165 trending FIA set started to develop in the Early Miocene and can be linked to compression generated by the westward migration of the Alboran Domain creating the Gibraltar Arc.

The range of garnet ages of 35–13 Ma obtained in the NFC coupled to previous estimates of P-T conditions during garnet growth support two Alpine cycles separated by partial exhumation of the complex (cf., Puga et al., 2002; Li & Massonne, 2018). The first cycle was shared with the ASC and reached peak-pressures of ~15 to 20 kbar around 35 Ma. The second cycle (~8– to 10 kbar) can be attributed to re-burial of the NFC below the ASC,

probably related to a change in relative plate motion (Figure 18). The range of ages (22–27 Ma) obtained for garnets of the ASC that grew under Barrovian metamorphic conditions (Gueydan et al., 2015), strongly suggest that higher-grade (HT-HP) Barrovian assemblages preserved near the crust-peridotite contact are also Alpine.

Data Availability Statement

All data used for this paper have been provided in paper figures and/or in three sets of Supporting Information (Supporting Information S1, Supporting Information S2, and Supporting Information S3) that can be found at the Mendeley Data repository (https://data.mendeley.com/). Supporting Information S1 is a sample list with petrological descriptions and location coordinates (https://doi.org/10.17632/67d697k38y.1). Supporting Information S2 is a collection of 33 stereoplots with microstructural data obtained by X-ray microtomography (https://doi.org/10.17632/2pjj9k3m9d.1). Supporting Information S3 is a collection of 46 stereoplots with field data compiled from the literature (https://doi.org/10.17632/9gnbx8s4r3.1). All stereoplots were made with the program "Stereonet" (v. 11.3.1) by Rick Allmendinger, available at https://www.rickallmendinger.net/stereonet.

Acknowledgments
The authors would like to thank Ángel Perandrés-Villegas for preparing the thin sections used for this study, Fátima Linares Ordóñez for X-ray computed micro-tomography scanning, Mike Tappa for assistance with thermal ionization mass spectrometry analysis, Francisco Alonso-Chaves and Fernando Simancas for sending structural data, Whitney Behr, Johannes Glodny, Sean Mulcahy, and an anonymous reviewer for providing helpful reports, and editors Laurent Jolivet and Federico Rossetti for additional comments that helped improve two earlier manuscript versions. EFB gratefully acknowledges support from the NSF Grants EAR-1250497 and PIRE-1545903 as well as start up funds from the Boston College. DA and ARF gratefully acknowledge financial support through Spanish project "DAMAGE" (CGL2016-80687-R AEI/FEDER), and Junta de Andalucía project RNM148, both directed by Jesús Galindo Zaldivar. ARF acknowledges an PhD Grant (FPU) from the Spanish government. Open access fees have been funded by Universidad de Granada /CBU.

References

Acosta-Vigil, A., Rubatto, D., Bartoli, O., Cesare, B., Meli, S., Pedrera, A., et al. (2014). Age of anatexis in the crustal footwall of the Ronda peridotites, S Spain. *Lithos*, *210–211*, 147–167. https://doi.org/10.1016/j.lithos.2014.08.018

Adshead-Bell, N. S., & Bell, T. H. (1999). The progressive development of a macroscopic upright fold pair during five near-orthogonal foliation-producing events: Complex microstructures versus a simple macrostructure. *Tectonophysics*, *306*(2), 121–147. https://doi.org/10.1016/s0040-1951(99)00055-4

Aerden, D., & Sayab, M. (2008). From Adria- to Africa-driven orogenesis: Evidence from porphyroblasts in the Betic Cordillera, Spain. *Journal of Structural Geology*, *30*(10), 1272–1287. https://doi.org/10.1016/j.jsg.2008.06.009

Aerden, D. G. A. M. (1994). Kinematics of orogenic collapse in the Variscan Pyrenees deduced from microstructures in porphyroblastic rocks from the Lys-Caillaouas massif. *Tectonophysics*, *238*(1–4), 139–160. https://doi.org/10.1016/0040-1951(94)90053-1

Aerden, D. G. A. M. (1995). Porphyroblast non-rotation during crustal extension in the Variscan Lys-Caillaouas Massif, Pyrenees. *Journal of Structural Geology*, *17*(5), 709–725. https://doi.org/10.1016/0191-8141(94)00090-M

Aerden, D. G. A. M. (1998). Tectonic evolution of the Montagne Noire and a possible orogenic model for syncollisional exhumation of deep rocks, Variscan belt, France. *Tectonics*, *17*(1), 62–79. https://doi.org/10.1029/97tc02342

Aerden, D. G. A. M. (2004). Correlating deformation in Variscan NW-Iberia using porphyroblasts; implications for the Ibero-Armorican Arc. *Journal of Structural Geology*, *26*(1), 177–196. https://doi.org/10.1016/S0191-8141(03)00070-1

Aerden, D. G. A. M., Bell, T. H., Puga, E., Sayab, M., Lozano, J. A., & Diaz de Federico, A. (2013). Multi-stage mountain building vs. relative plate motions in the Betic Cordillera deduced from integrated microstructural and petrological analysis of porphyroblast inclusion trails. *Tectonophysics*, *587*, 188–206. https://doi.org/10.1016/j.tecto.2012.11.025

Aerden, D. G. A. M., & Ruiz-Fuentes, A. (2020). X-ray computed microtomography of spiral garnets: A new test of how they form. *Journal of Structural Geology*, *136*, 104054. https://doi.org/10.1016/j.jsg.2020.104054

Aerden, D. G. A. M., Ruiz-Fuentes, A., Sayab, M., & Forde, A. (2021). Kinematics of subduction in the Ibero-Armorican arc constrained by 3D microstructural analysis of garnet and pseudomorphed lawsonite porphyroblasts from Île de Groix (Variscan belt). *Solid Earth*, *12*(4), 971–992. https://doi.org/10.5194/se-12-971-2021

Aerden, D. G. A. M., & Sayab, M. (2017). Probing the prodigious strain fringes from Lourdes. *Journal of Structural Geology*, *105*, 88–106. https://doi.org/10.1016/j.jsg.2017.11.001

Aerden, D. G. A. M., Sayab, M., & Bouybaouene, M. L. (2010). Conjugate-shear folding: A model for the relationships between foliations, folds and shear zones. *Journal of Structural Geology*, *32*(8), 1030–1045. https://doi.org/10.1016/j.jsg.2010.06.010

Afiri, A., Gueydan, F., Pitra, P., Essaifi, A., & Précigout, J. (2011). Oligo-Miocene exhumation of the Beni-Bousera peridotite through a lithosphere-scale extensional shear zone. *Geodinamica Acta*, *24*(1), 49–60. https://doi.org/10.3166/ga.24.49-60

Ali, A. (2010). The tectono-metamorphic evolution of the Balcooma Metamorphic Group, north-eastern Australia: A multidisciplinary approach. *Journal of Metamorphic Geology*, *28*(4), 397–422. https://doi.org/10.1111/j.1525-1314.2010.00871.x

Ali, A., Yar, M., Khan, M. A., & Faisal, S. (2016). Interrelationships between deformation and metamorphic events across the western hinterland zone, NW Pakistan. *Journal of Earth Sciences*, *27*(4), 584–598. https://doi.org/10.1007/s12583-016-0717-1

Alonso Chaves, F. M., & Orozco, M. (2012). El Complejo Alpujárride de La Axarquía: Zonas de cizalla dúctiles a escala cortical y pliegues recumbentes asociados. *Geogaceta*, *52*, 5–8.

Argles, T. W., Platt, J. P., & Waters, D. J. (1999). Attenuation and excision of a crustal section during extensional exhumation: The Carratraca Massif, Betic Cordillera, southern Spain. *Journal of the Geological Society*, *156*(1), 149–162. https://doi.org/10.1144/gsjgs.156.1.0149

Augier, R., Agard, P., Monie, P., Jolivet, L., Robin, C., & Booth-Rea, G. (2005). Exhumation, doming and slab retreat in the Betic Cordillera (SE Spain): In situ $^{40}Ar/^{39}Ar$ ages and *P-T-d-t* paths for the Nevado-Filabride complex. *Journal of Metamorphic Geology*, *23*(5), 357–381. https://doi.org/10.1111/j.1525-1314.2005.00581.x

Azañón, J. M., & Crespo-Blanc, A. (2000). Exhumation during a continental collision inferred from the tectonometamorphic evolution of the Alpujárride complex in the central Betics (Alboran domain, SE Spain). *Tectonics*, *19*(3), 549–565. https://doi.org/10.1029/2000tc900005

Azañon, J. M., Crespo-Blanc, A., & García-Dueñas, V. (1997). Continental collision crustal thinning and nappe forming during the pre-Miocene evolution of the Alpujarride Complex (Alboran Domain, Betics). *Journal of Structural Geology*, *19*(8), 1055–1071. https://doi.org/10.1016/s0191-8141(97)00031-x

Bakker, H. E., de Jong, K., Helmers, H., & Biermann, C. (1989). The geodynamic evolution of the internal Zone of the Betic Cordilleras (SE Spain): A model based on structural analysis and geothermobarometry. *Journal of Metamorphic Geology*, *7*(3), 359–381. https://doi.org/10.1111/j.1525-1314.1989.tb00603.x

Balanya, J. C., Crespo-Blanc, A., Díaz Azpiroz, M., Expósito, I., & Luján, M. (2007). Structural trend line pattern and strain partitioning around the Gibraltar Arc accretionary wedge: Insights as to the mode of orogenic arc building. *Tectonics*, *26*(2), TC2005. https://doi.org/10.1029/2005TC001932

Balanya, J. C., Garcia-Dueñas, V., Azañón, J. M., & Sanchez-Gomez, M. (1997). Alternating contractional and extensional events in the Alpujarride Nappes of the Alboran domain (Betics, Gibraltar Arc). *Tectonics*, *16*(2), 226–238. https://doi.org/10.1029/96TC03871

Baxter, E. F., Caddick, M. J., & Dragovic, B. (2017). Garnet: A rock-forming mineral petrochronometer. *Book Series Reviews in Mineralogy & Geochemistry*, *83*(1), 469–533. https://doi.org/10.2138/rmg.2017.83.15

Baxter, E. F., & Scherer, E. E. (2013). Garnet: Timekeeper of tectonometamorphic evolution. *Elements*, *9*(6), 433–438. https://doi.org/10.2113/gselements.9.6.433

Behr, W. M., & Platt, J. P. (2012). Kinematic and thermal evolution during two-stage exhumation of a Mediterranean subduction complex. *Tectonics*, *31*(4), TC4025. https://doi.org/10.1029/2012TC003121

Bell, T. H. (1985). Deformation partitioning and porphyroblast rotation in metamorphic rocks: A radical reinterpretation. *Journal of Metamorphic Geology*, *3*(2), 109–118. https://doi.org/10.1111/j.1525-1314.1985.tb00309.x

Bell, T. H., & Forde, A. (1995). On the significance of foliation patterns preserved around folds by mineral overgrowth. *Tectonophysics*, *246*(1–3), 171–181. https://doi.org/10.1016/0040-1951(94)00263-9

Bell, T. H., Forde, A., & Wang, J. (1995). A new indicator of movement direction during orogenesis – Measurement technique and application to the Alps. *Terra Nova*, *7*(5), 500–508. https://doi.org/10.1111/j.1365-3121.1995.tb00551.x

Bell, T. H., & Hayward, N. (1991). Episodic metamorphic reactions during orogenesis: The control of deformation partitioning on reaction sites and reaction duration. *Journal of Metamorphic Geology*, *9*(5), 619–640. https://doi.org/10.1111/j.1525-1314.1991.tb00552.x

Bell, T. H., Hickey, K. A., & Upton, G. J. G. (1998). Distinguishing and correlating multiple phases of metamorphism across a multiply deformed region using the axes of spiral, staircase, and sigmoidally curved inclusion trails in garnet. *Journal of Metamorphic Geology*, *16*(6), 767–794. https://doi.org/10.1111/j.1525-1314.1998.00170.x

Bell, T. H., & Johnson, S. E. (1989). Porphyroblast inclusion trails: The key to orogenesis. *Journal of Metamorphic Geology*, *7*(3), 279–310. https://doi.org/10.1111/j.1525-1314.1989.tb00598.x

Bell, T. H., Johnson, S. E., Davis, B., Forde, A., Hayward, N., & Wilkins, C. (1992). Porphyroblast inclusion-trail orientation data: *Eppure non son girate*! *Journal of Metamorphic Geology*, *10*(3), 295–307. https://doi.org/10.1111/j.1525-1314.1992.tb00084.x

Bell, T. H., & Mares, V. M. (1999). Correlating deformation and metamorphism around arcs in orogens. *American Mineralogist*, *84*(11–12), 1727–1740. https://doi.org/10.2138/am-1999-11-1203

Bell, T. H., Rubenach, M. J., & Fleming, P. D. (1986). Porphyroblast nucleation, growth and dissolution in regional metamorphic rocks as a function of deformation partitioning during foliation development. *Journal of Metamorphic Geology*, *4*(1), 37–67. https://doi.org/10.1111/j.1525-1314.1986.tb00337.x

Bell, T. H., & Sanislav, I. V. (2011). A deformation partitioning approach to resolving the sequence of fold events and the orientations in which they formed across multiply deformed large-scale regions. *Journal of Structural Geology*, *33*(7), 1206–1217. https://doi.org/10.1016/j.jsg.2011.03.014

Bell, T. H., & Sapkota, J. (2012). Episodic gravitational collapse and migration of the mountain chain during orogenic roll-on in the Himalayas. *Journal of Metamorphic Geology*, *30*, 651–666. https://doi.org/10.1111/j.1365-3121.1995.tb00551.x

Bell, T. H., & Wang, J. (1999). Linear indicators of movement direction versus foliation intersection axes in porphyroblasts (FIAs) and their relationship to directions of relative plate motion. *Earth Science Frontiers*, *6*, 31–46.

Berndt, T., Ruiz-Martinez, V. C., & Chalouan, A. (2015). New constraints on the evolution of the Gibraltar Arc from palaeomagnetic data of the Ceuta and Beni Bousera peridotites (Rif, northern Africa). *Journal of Geodynamics*, *84*, 19–39. https://doi.org/10.1016/j.jog.2014.09.014

Bessière, E., Augier, R., Jolivet, L., Precigout, J., & Romagny, A. (2021). Exhumation of the Ronda peridotite during hyper-extension: New structural and thermal constraints from the Nieves Unit (western Betic Cordillera, Spain). *Tectonics*, *40*(10), 2020TC006271. https://doi.org/10.1029/2020TC006271

Bessière, E., Jolivet, L., Augier, R., Scaillet, S., Precigout, J., Azanon, J. M., et al. (2021). Lateral variations of pressure-temperature evolution in non-cylindrical orogens and 3-D subduction dynamics: The Betic-Rif Cordillera example. *BSGF – Earth Sciences Bulletin*, *192*(1), 8. https://doi.org/10.1051/bsgf/2021007

Bons, P. D., Jessell, M. W., Griera, A., Fay, C., Bell, T., & Hobbs, B. (2009). Porphyroblast rotation versus nonrotation: Conflict resolution! COMMENT. *Geology*, *37*(2), e188. https://doi.org/10.1130/g25131c.1

Booth-Rea, G., Martínez-Martínez, J. M., & Giaconia, F. (2015). Continental subduction, intracrustal shortening, and coeval upper-crustal extension: P-T evolution of subducted south Iberian paleomargin metapelites (Betics, SE Spain). *Tectonophysics*, *663*, 122–139. https://doi.org/10.1016/j.tecto.2015.08.036

Borradaile, G. J. (1976). A strain study of a granite-granite gneiss transition and accompanying schistosity formation in the Betic orogenic zone, SE. Spain. *Journal of the Geological Society*, *132*(4), 417–428. https://doi.org/10.1144/gsjgs.132.4.0417

Borradaile, G. J. (1997). Deformation and paleomagnetism. *Surveys in Geophysics*, *18*(4), 405–435. https://doi.org/10.1023/a:1006555906559

Bouillin, J. P. (1986). Le bassin Maghrébin: Une ancienne limite entre l'Europe et l'Afrique à l'ouest des Alpes. *Bulletin de la Société géologique de France*, *8*(4), 547–558. https://doi.org/10.2113/gssgfbull.ii.4.547

Bouybaouene, M. L., Alami, R., Azañon-Hernandez, J. M., & Goffe, B. (1999). HP-LT metamorphism of the Filali-Benzou schists (Sebtides, Morocco). *Chlortoid-Garnet-Phengite Therrnobarometry*. Geogaceta 26.

Bouybaouene, M. L., Michard, A., & Goffé, B. (1998). High-pressure granulites on top of the Beni Bousera peridotites, Rif Belt, Morocco: A record of an ancient thickened crust in the Alboran Domain. *Bulletin de la Societe Geologique de France*, *2*, 153–162.

Bruguier, O., Bosch, D., Caby, R., Vitale-Brovarone, A., Fernandez, L., Hammor, D., et al. (2017). Age of UHP metamorphism in the Western Mediterranean: Insight from rutile and minute zircon inclusions in a diamond-bearing garnet megacryst (Edough Massif, NE Algeria). *Earth and Planetary Science Letters*, *474*, 215–225. https://doi.org/10.1016/j.epsl.2017.06.043

Calvert, A., Sandvol, E., Seber, D., Barazangi, M., Roecker, S., Mourabit, T., et al. (2000). Geodynamic evolution of the lithosphere and upper mantle beneath the Alboran region of the western Mediterranean: Constraints from travel time tomography. *Journal of Geophysical Research*, *105*(B5), 10871–10898. https://doi.org/10.1029/2000jb900024

Chalouan, A., & Michard, A. (1985). Pre-Visean age of the main Variscan folding in the Ghomarides nappes, inner Rif, Morocco. *Sciences Géologiques, bulletins et mémoires*, *38*(2), 165–174. https://doi.org/10.3406/sgeol.1985.1704

Chalouan, A., & Michard, A. (1990). The Ghomarides nappes, Rif coastal range, Morocco – A variscan chip in the Alpine belt. *Tectonics*, *9*(6), 1565–1583. https://doi.org/10.1029/TC009i006p01565

Cruden, A. R., Nasseri, M. H. B., & Pysklywec, R. (2006). Surface topography and internal strain variation in wide hot orogens from three-dimensional analogue and two-dimensional numerical vice models. In S. J. H. Buiter & G. Schreurs (Eds.), *Analogue and numerical modelling of crustal-scale processes* (Vol. 253, pp. 79–104). Geological Society Publishing House. https://doi.org/10.1144/gsl.sp.2006.253.01.04

Cuevas, J., Navarro-Vila, F., & Tubía, J. M. (2001). Evolución estructural poliorogénica del Complejo Maláguide (Cordilleras Béticas). *Boletin Geologico y Minero*, *112*(3), 47–58.

De Jong, K. (1991). *Tectonometamorphic studies and radiometric dating in the Betic Zone (SE Spain) with implications for the dynamics of extension and compression in the western Mediterranean area* (PhD thesis, pp. 204). Vrije UNiversiteit.

De Jong, K. (1993). Redefinition of the deformation scheme of the Mulhacen Complex and implications for the relative timing of the overthrusting of the Alpujarride Complex in the Betic Zone (SE Spain). *Geologie en Mijnbouw*, *71*, 317–326.

DeMets, C., Iaffaldano, G., & Merkouriev, S. (2015). High-resolution Neogene and Quaternary estimates of Nubia-Eurasia-North America Plate motion. *Geophysical Journal International*, *203*(1), 416–427. https://doi.org/10.1093/gji/ggv277

Dercourt, J., Zonenshain, L. P., Ricou, L. E., Kazmin, V. G., Lepichon, X., Knipper, A. L., et al. (1986). Geological evolution of the Tethys belt from the Atlantic to the Pamirs since the Lias. *Tectonophysics*, *123*(1–4), 241–315. https://doi.org/10.1016/0040-1951(86)90199-X

Didon, J., Durand-Delga, ' M., & Kornprobst, J. (1973). Homologies geologiques entre les deux rives du detroit de Gibraltar. *Bulletin de la Societe Geologique de France*, *7*, 79–105. https://doi.org/10.2113/gssgfbull.S7-XV.2.77

Doglioni, C., Gueguen, E., Sabat, F., & Fernandez, M. (1997). The Western Mediterranean extensional basins and the Alpine orogen. *Terra Nova*, *9*(3), 109–112. https://doi.org/10.1046/j.1365-3121.1997.d01-18.x

Doube, M., Kłosowski, M. M., Arganda-Carreras, I., Cordeliéres, F., Dougherty, R. P., Jackson, J., et al. (2010). BoneJ: Free and extensible bone image analysis in ImageJ. *Bone*, *47*(6), 1076–1079. https://doi.org/10.1016/j.bone.2010.08.023

El Maz, A., & Guiraud, M. (2001). Paragenèse a faible variance dans les metapelites de la serie de Filali (Rif interne marocain); description, interpretation et consequence geodynamique. *Bulletin de la Societe Geologique de France*, *172*(4), 469–485. https://doi.org/10.2113/172.4.469

Evins, P. M. (2005). A 3D study of aligned porphyroblast inclusion trails across shear zones and folds. *Journal of Structural Geology*, *27*(7), 1300–1314. https://doi.org/10.1016/j.jsg.2004.08.003

Faccenna, C., Becker, T. W., Auer, L., Billi, A., Boschi, L., Brun, J. P., et al. (2014). Mantle dynamics in the Mediterranean. *Reviews of Geophysics*, *52*(3), 283–332. https://doi.org/10.1002/2013RG000444

Farrell, T. P. (2019). *Investigating the Tectonic Significance of Spiral Garnets from the Betic-Rif Arc of Southern Spain and Northern Morocco Using Sm-Nd Garnet Geochronology* (MSc thesis, pp. 234). Boston College. Retrieved from https://dlib.bc.edu/islandora/object/bc-ir:108592

Fay, C., Bell, T. H., & Hobbs, B. E. (2008). Porphyroblast rotation versus nonrotation: Conflict resolution! *Geology*, *36*(4), 307–310. https://doi.org/10.1130/G24499A.1

Fay, C., Bell, T. H., & Hobbs, B. E. (2009). Porphyroblast rotation versus nonrotation: Conflict resolution!: Reply. *Geology*, *37*(2), E188. https://doi.org/10.1130/G25630Y.1

Frizon de Lamotte, D., Raulin, C., Mouchot, N., Wrobel-Daveau, J.-C., Blanpied, C., & Ringenbach, J.-C. (2011). The southernmost margin of the Tethys realm during the Mesozoic and Cenozoic: Initial geometry and timing of the inversion processes. *Tectonics*, *30*(3), TC3002. https://doi.org/10.1029/2010TC002691

Fyson, W. K. (1980). Fold fabrics and emplacement of an Archean granitoid pluton, Cleft Lake, Northwest Territories. *Canadian Journal of Earth Sciences*, *17*(3), 325–332. https://doi.org/10.1139/e80-032

Galindo-Zaldivar, J. (1993). *Geometría de las deformaciones Neógenas en Sierra Nevada (Cordilleras Beticas)* (PhD thesis, pp. 249). Universidad de Granada.

Galindo-Zaldivar, J., Gonzalez-Lodeiro, F., & Jabaloy, A. (1989). Progressive extensional shear structures in a detachment contact in the Western Sierra Nevada (Betic Cordilleras, Spain). *Geodinamica Acta*, *3*(1), 73–85. https://doi.org/10.1080/09853111.1989.11105175

García-Dueñas, V., Martínez-Martínez, J. M., Orozco, M., & Soto, J. I. (1988). Plis nappes, cisaillements syn-à post-métamorphiques et cisaillements ductiles-fragiles en distension dans les Névado-Filabrides (Cordillères bétiques, Espagne). *Comptes Rendus de l'Académie des Sciences*, *2*(307), 1389–1395.

Gardner, J., & Wheeler, J. (2021). The influence of large second phase grains on microstructural evolution during diffusion creep. *Journal of Structural Geology*, *148*, 104371. https://doi.org/10.1016/j.jsg.2021.104371

Garrido, C. J., Gueydan, F., Booth-Rea, G., Precigout, J., Hidas, K., Padrón-Navarta, J. A., & Marchesi, C. (2011). Garnet lherzolite and garnet-spinel mylonite in the Ronda peridotite: Vestiges of Oligocene backarc mantle lithospheric extension in the western Mediterranean. *Geology*, *39*(10), 927–930. https://doi.org/10.1130/g31760.1

Gilbert, E., & Merle, O. (1987). Extrusion and radial spreading beyond a closing channel. *Journal of Structural Geology*, *9*(4), 481–490. https://doi.org/10.1016/0191-8141(87)90123-4

Griera, A., Llorens, M. G., Gomez-Rivas, E., Bons, P. D., Jessel, M. W., Evans, L. A., & Lebensohn, R. (2013). Numerical modelling of porphyroclast and porphyroblast rotation in anisotropic rocks. *Tectonophysics*, *587*, 4–29. https://doi.org/10.1016/j.tecto.2012.10.008

Grujic, D., & Mancktelow, N. S. (1995). Folds with axes parallel to the extension direction. *Journal of Structural Geology*, *17*(2), 279–291. https://doi.org/10.1016/0191-8141(94)E0048-4

Guerrera, F., Martín-Algarra, A., & Martín-Martín, M. (2012). Tectono-sedimentary evolution of the "Numidian Formation" and Lateral Facies (southern branch of the western Tethys): Constraints for central-western Mediterranean geodynamics. *Terra Nova*, *24*(1), 34–41. https://doi.org/10.1111/j.1365-3121.2011.01034.x

Guerrera, F., Martín-Algarra, A., & Perrone, V. (1993). Late Oligocene-Miocene syn- late-orogenic successions in western and central Mediterranean chains from the Betic Cordillera to the southern Apennines. *Terra Nova*, *5*(6), 525–544. https://doi.org/10.1111/j.1365-3121.1993.tb00302.x

Gueydan, F., Pitra, P., Afiri, A., Poujol, M., Essaifi, A., & Paquette, J.-L. (2015). Oligo-Miocene thinning of the Beni Bousera peridotites and their Variscan crustal host rocks, Internal Rif, Morocco. *Tectonics*, *34*(6), 1244–1268. https://doi.org/10.1002/2014TC003769

Handy, M. R., Schmid, S. M., Bousquet, R., Kissling, E., & Bernoulli, D. (2010). Reconciling plate-tectonic reconstructions of Alpine Tethys with the geological-geophysical record of spreading and subduction in the Alps. *Earth-Science Reviews*, *102*(3–4), 121–158. https://doi.org/10.1016/j.earscirev.2010.06.002

Handy, M. R., Ustaszewski, K., & Kissling, E. (2015). Reconstructing the Alpse-Carpathianse-Dinarides as a key to understanding switches in subduction polarity, slab gaps and surface motion. *International Journal of Earth Sciences*, *104*(1), 1–26. https://doi.org/10.1007/s00531-014-1060-3

Harvey, J., & Baxter, E. F. (2009). An improved method for TIMS high precision neodymium isotope analysis of very small aliquots (1 – 10 ng). *Chemical Geology*, *258*(3–4), 251–257. https://doi.org/10.1016/j.chemgeo.2008.10.024

Hayward, N. (1990). Determination of early fold axis orientations in multiply deformed rocks using porphyroblast inclusion trails. *Tectonophysics*, *179*(3–4), 353–369. https://doi.org/10.1016/0040-1951(90)90301-N

Hayward, N. (1992). Microstructural analysis of the classical spiral garnet porphyroblasts of south-east Vermont – Evidence for non-rotation. *Journal of Metamorphic Geology*, *10*(4), 567–587. https://doi.org/10.1111/j.1525-1314.1992.tb00106.x

Hickey, K. A., & Bell, T. H. (1999). Behaviour of rigid objects during deformation and metamorphism: A test using schists from the Bolton syncline, Connecticut, USA. *Journal of Metamorphic Geology*, *17*(2), 211–228. https://doi.org/10.1046/j.1525-1314.1999.00192.x

Homonnay, E. (2019). *Évolution tectono-métamorphique et chronologie de mise en place des unités métamorphiques du Rifinterne (Maroc)* (PhD thesis, pp. 305). Université Côte d'Azur. Retrieved from https://tel.archives-ouvertes.fr/tel-02887924

Homonnay, E., Corsini, M., Lardeaux, J.-M., Romagny, A., Munch, P., Bosch, D., et al. (2018). Miocene crustal extension following thrust tectonic in the Lower Sebtides units (internal Rif, Ceuta Peninsula, Spain): Implication for the geodynamic evolution of the Alboran domain. *Tectonophysics*, *722*, 507–535. https://doi.org/10.1016/j.tecto.2017.11.028

Huddlestone-Holmes, C. R., & Ketcham, R. A. (2010). An X-ray computed tomography study of inclusion trail orientations in multiple porphyroblasts from a single sample. *Tectonophysics*, *480*(1–4), 305–320. https://doi.org/10.1016/j.tecto.2009.10.021

Jabaloy, A., Galindo-Zaldivar, J., & Conzález-Lodeiro, F. (1993). The Alpujarride-Nevado-Filabride extensional shear zone, Betic Cordillera, SE Spain. *Journal of Structural Geology*, *15*(3–5), 552–569. https://doi.org/10.1016/0191-8141(93)90148-4

Jabaloy, A., & González Lodeiro, F. (1988). La deformacion en los bloques de techo y muro de los cabalgamientos de las unidades inferiores Nevado-filabrides (Cordilleras Beticas, SE. España). *Estudios geol*, *44*, 253–261.

Jabaloy-Sánchez, A. (1993). *La estructura de la region occidental de la Sierra de los Filabres (Cordilleras Béticas)* (PhD thesis, pp. 199). Universidad de Granada.

Jabaloy Sánchez, A., Padrón-Navarta, J. A., Gómez-Pugnaire, M. T., López Sánchez-Vizcaíno, V., & Garrido, C. J. (2019). Alpine Orogeny: Deformation and structure in the Southern Iberian Margin (Betics s.l.). In C. Quesada & J. T. Oliveira (Eds.), *The Geology of Iberia: A geodynamic approach*, *Regional Geology Reviews*. https://doi.org/10.1007/978-3-030-11295-0_10

Johnson, S. E. (1992). Sequential porphyroblast growth during progressive deformation and low-P high-T (LPHT) metamorphism, Cooma Complex, Australia. *Tectanophysics*, *214*(1–4), 311–339. https://doi.org/10.1016/0040-1951(92)90204-j

Johnson, S. E. (2008). The effects of strain localisation on rigid-object kinematics. In P. D. Bons, D. Koehn, & M. W. Jessell (Eds.), *Microdynamics simulation. Lecture notes in Earth Sciences* (pp. 246–252). Springer.

Johnson, S. E. (2009). Porphyroblast rotation and strain localization: Debate settled. *Geology*, *37*(7), 663–666. https://doi.org/10.1130/G25729A.1

Jolivet, L., & Faccenna, C. (2000). Mediterranean extension and the Africa-Eurasia collision. *Tectonics*, *19*(6), 1095–1106. https://doi.org/10.1029/2000TC900018

Jung, W. S., Ree, J. H., & Park, Y. (1999). Non-rotation of garnet porphyroblasts and 3-D inclusion trail data: An example from the Imjingang belt, South Korea. *Tectonophysics*, *307*(3–4), 381–395. https://doi.org/10.1016/S0040-1951(99)00105-5

Kim, H. S., & Ree, J.-H. (2013). Permo-Triassic changes in bulk crustal shortening direction during deformation and metamorphism of the Taebaeksan Basin, South Korea using foliation intersection/inflection axes: Implications for tectonic movement at the eastern margin of Eurasia during the Songrim (Indosinian) orogeny. *Tectonophysics*, *587*, 133–145. https://doi.org/10.1016/j.tecto.2012.08.033

Kirchner, K. L., Behr, W. M., Loewy, S., & Stockli, D. F. (2016). Early Miocene subduction in the western Mediterranean: Constraints from Rb-Sr multimineral isochron geochronology. *Geochemistry, Geophysics, Geosystems*, *17*(5), 1842–1860. https://doi.org/10.1002/2015GC006208

Kornprobst, J. (1971). Le socle ancien polymétamorphique dans les zones internes de la partie occidentale des chaînes bético-rifaines: Similitudes pétrographiques et constance des directions tectoniques anté-alpine. *Comptes Rendus de l'Académie des Sciences*, *272*(D), 1204–1207.

Kornprobst, J. (1974). *Contribution à L'étude Pétrographique et Structurale de la Zone Interne du Rif* (Published doctorate thesis). Notes et Mémoirs du Service Géol. 251. Editions du Services Géologiques du Maroc.

Lacombe, O., & Jolivet, L. (2005). Structural and kinematic relationships between Corsica and the Pyrenees-Provence domain at the time of the Pyrenean orogeny. *Tectonics*, *24*(1), TC1003. https://doi.org/10.1029/2004TC001673

Langenberg, C. W. (1972). Polyphase deformation in the eastern Sierra de los Filabres, N of Lubrin, SE Spain. *GUA Papers of Geology, Series*, *1*(2), 81.

Leprêtre, R., de lamotte, D. F., Combier, V., Gimeno-Vives, O., Mohn, G., & Eschard, R. (2018). The Tell-Rif orogenic system (Morocco, Algeria, Tunisia) and the structural heritage of the southern Tethys margin. *BSGF-Earth Sciences Bulletin*, *189*(2), 10. https://doi.org/10.1051/bsgf/2018009

Li, B., & Massonne, H.-J. (2018). Two Tertiary metamorphic events recognized in high-pressure metapelites of the Nevado-Filabride Complex (Betic Cordillera, S Spain). *Journal of Metamorphic Geology*, *36*(5), 603–630. https://doi.org/10.1111/jmg.12312

Liesa, C. L., & Simón, J. L. (2009). Evolution of intraplate stress fields under multiple remote compressions: The case of the Iberian Chain (NE Spain). *Tectonophysics*, *474*(1–2), 144–159. https://doi.org/10.1016/j.tecto.2009.02.002

Lonergan, L., & White, N. (1997). Origin of the Betic-Rif mountain belt. *Tectonics*, *16*(3), 504–522. https://doi.org/10.1029/96TC03937

Loomis, T. P. (1972). Diapiric emplacement of the Ronda high-temperature ultramafic intrusion, Southern Spain. *Geological Society of America Bulletin*, *83*, 2475–2496. https://doi.org/10.1130/0016-7606(1972)83[2475:DEOTRH]2.0.CO;2

Lozano-Rodríguez, J. A. (2019). *Estudio petrológico, geoquímico y geocronológico comparado de las Ofiolitas Béticas de Sierra de Baza con otras Ofiolitas Béticas* (PhD thesis, pp. 383). Universidad de Granada. Retrieved from https://digibug.ugr.es/handle/10481/54877

Marrone, S., Monié, P., Rossetti, F., Aldega, L., Bouybaouene, M., Charpentier, D., et al. (2021). Timing of Alpine orogeny and postorogenic extension in the Alboran domain, inner Rif Chain, Morocco. *Tectonics*, *40*(7), e2021TC006707. https://doi.org/10.1029/2021tc006707

Marrone, S., Monié, P., Rossetti, F., Lucci, F., Theye, T., Bouybaouene, M. L., & Najib Zaghloul, M. (2021). The pressure–temperature–time–deformation history of the Beni Mzala unit (Upper Sebtides, Rif belt, Morocco): Refining the Alpine tectono-metamorphic evolution of the Alboran domain of the western Mediterranean. *Journal of Metamorphic Geology*, *39*(5), 591–615. https://doi.org/10.1111/jmg.12587

Marroni, M., Meneghini, F., Pandolfi, L., Hobbs, N., & Luvisi, E. (2019). The Ottone-Levanto Line of Eastern Liguria (Italy) uncovered: A Late Eocene-Early Oligocene snapshot of Northern Apennine geodynamics at the Alps/Apennines Junction. *Episodes*, *42*(2), 107–118. https://doi.org/10.18814/epiiugs/2019/019009

Martínez Martínez, J. M. (1986a). *Evolución tectonometamorpfica del complejo Nevado-Filabride en el sector de unión entre Sierra Nevada y Sierra de los Filabres (Cordilleras Beticas)* (PhD thesis, pp. 1–194). Universidad de Granada. Retrieved from http://hdl.handle.net/10481/47336

Martínez Martínez, J. M. (1986b). Fabricas y texturas miloniticas. Cinematica de las traslaciones en el complejo Nevado-Filabride (Cordilleras Beticas, España). *Estudios Geológicos*, *42*(4–5), 291–300. https://doi.org/10.3989/egeol.86424-5757

Martínez-Martínez, J. M., Soto, J. I., & Balanyá, J. C. (2002). Orthogonal folding of extensional detachments: Structure and origin of the Sierra Nevada elongated dome (Betics, SE Spain). *Tectonics*, *21*(3), 3-1–3-20. https://doi.org/10.1029/2001TC001283

Massonne, H.-J. (2014). Wealth of P-T-t information in medium-high grade metapelites: Example from the Jubrique Unit of the Betic Cordillera, S Spain. *Lithos*, *208*, 137–157. https://doi.org/10.1016/j.lithos.2014.08.027

Mazzoli, S., & Martin Algarra, A. (2011). Deformation partitioning during transpressional emplacement of a 'mantle extrusion wedge': The Ronda peridotites, western Betic Cordillera, Spain. *Journal of the Geological Society*, *168*(2), 373–382. https://doi.org/10.1144/0016-76492010-126

Mazzoli, S., Martín-Algarra, A., Reddy, S. M., López Sánchez-Vizcaíno, V., Fedele, L., & Noviello, A. (2013). The evolution of the footwall to the Ronda subcontinental mantle peridotites: Insights from the Nieves Unit (western Betic Cordillera). *Journal of the Geological Society*, *170*(3), 385–402. https://doi.org/10.1144/jgs2012-105

McLachlan, G. R. (1953). Bearing of rolled garnets on the concept of 6-lineation in Moine rocks. *Geological Magazine*, *90*(3), 172–176. https://doi.org/10.1017/s0016756800064165

Michard, A., Chalouan, A., Feinberg, H., Goffe, B., & Montigny, R. (2002). How does the Alpine belt end between Spain and Morocco? *Bulletin de la Societe Geologique de France*, *173*(1), 3–15. https://doi.org/10.2113/173.1.3

Michard, A., Negro, F., Saddiqi, O., Bouybaouene, M. L., Chalouan, A., Montigny, R., & Goffe, B. (2006). Pressure-temperature-time constraints on the Maghrebide mountain building: Evidence from the Rif-Betic transect (Morocco, Spain), Algerian correlations, and geodynamic implications. *Comptes Rendus Geoscience*, *338*(1–2), 92–114. https://doi.org/10.1016/j.crte.2005.11.011

Monié, P., Galindo-Zaldivar, J., Lodeiro, F. G., Goffe, B., & Jabaloy, A. (1991). $^{40}Ar/^{39}Ar$ geochronology of alpine tectonism in the Betic Cordilleras (southern Spain). *Journal of the Geological Society*, *148*(2), 289–297. https://doi.org/10.1144/gsjgs.148.2.0289

Montel, J. M., Kornprobst, J., & Vielzeuf, D. (2000). Preservation of old U–Th–Pb ages in shielded monazite: Example from the Beni Bousera Hercynian kinzigites (Morocco). *Journal of Metamorphic Geology*, *18*(3), 335–342. https://doi.org/10.1046/j.1525-1314.2000.00261.x

Munro, M. A., & Blenkinsop, T. G. (2012). MARD-A moving average rose diagram application for the geosciences. *Computers & Geosciences*, *49*, 112–120. https://doi.org/10.1016/j.cageo.2012.07.012

Orozco, M., Álvarez-Valero, A. M., Alonso-Chaves, F. M., & Platt, J. P. (2004). Internal structure of a collapsed terrain. The Lújar syncline and its significance for the fold- and sheet-structure of the Alborán Domain (Betic Cordilleras, Spain). *Tectonophysics*, *385*(1–4), 85–104. https://doi.org/10.1016/j.tecto.2004.04.025

Orozco, M. (1971). *Los alpujarrides en sierra de gador oriental* (PhD thesis, pp. 379). Universidad de Granada. Retrieved from https://digibug.ugr.es/handle/10481/28618

Orozco, M., & Alonso-Chaves, F. M. (2012). Kilometre-scale sheath folds in the western Betics (south of Spain). *International Journal of Earth Sciences*, *101*(2), 505–519. https://doi.org/10.1007/s00531-011-0690-y

Orozco, M., Alonso-Chaves, F. M., & Nieto, F. (1998). Development of large north-facing folds and their relation to crustal extension in the Alborán domain (Alpujarras region, Betic Cordilleras, Spain). *Tectonophysics*, *298*(1–3), 271–295. https://doi.org/10.1016/s0040-1951(98)00188-7

Orozco, M., Alonso-Chaves, F. M., & Platt, J. P. (2017). Late extensional shear zones and associated recumbent folds in the Alpujarride subduction complex, Betic Cordillera, Southern Spain. *Geológica Acta*, *15*, 51–66.

Passchier, C. W., Trouw, R. A. J., Zwart, H. J., & Vissers, R. L. M. (1992). Porphyroblast rotation: *Eppur si muove*? *Journal of Metamorphic Geology*, *10*(3), 283–294. https://doi.org/10.1111/j.1525-1314.1992.tb00083.x

Peach, B. N. (1912). The geology of Ben Wyvis, Carn Chuinneag, Inchbae and the surrounding country. In *Memoirs of the Gological Survey of Scotland 93* (pp. 189). Morrison & Gibb Limited.

Pedrera, A., Ruiz-Constán, A., García-Senz, J., Azor, A., Marín-Lechado, C., Ayala, C., et al. (2020). Evolution of the South-Iberian paleomargin: From hyperextension to continental subduction. *Journal of Structural Geology*, *138*, 104122. https://doi.org/10.1016/j.jsg.2020.104122

Platt, J. P., Allerton, S., Kirker, A., Mandeville, C., Mayfield, A., Platzman, E. S., & Rimi, A. (2003). The ultimate arc: Differential displacement, oroclinal bending and vertical axis rotation in the External Betic-Rif arc. *Tectonics*, *22*(3), 1017. https://doi.org/10.1029/2001TC001321

Platt, J. P., Anczkiewicz, R., Soto, J.-I., Kelley, S. P., & Thirlwall, M. (2006). Early Miocene continental subduction and rapid exhumation in the western Mediterranean. *Geology*, *34*(11), 981–984. https://doi.org/10.1130/G22801A.1

Platt, J. P., Behr, W. M., Johanesen, K., & Williams, J. R. (2013). The Betic-Rif arc and its orogenic hinterland: A review. *Annual Review of Earth and Planetary Sciences*, *41*(1), 313–357. https://doi.org/10.1146/annurev-earth-050212-123951

Platt, J. P., & Behrmann, J. H. (1986). Structures and fabrics in a crustal-scale shear zone, Betic Cordillera, SE Spain. *Journal of Structural Geology*, *8*(1), 15–33. https://doi.org/10.1016/0191-8141(86)90014-3

Platt, J. P., Kelley, S. P., Carter, A., & Orozco, M. (2005). Timing of tectonic events in the Alpujárride Complex, Betic Cordillera, S. Spain. *Journal of the Geological Society*, *162*(3), 451–462. https://doi.org/10.1144/0016-764903-039

Platt, J. P., Vandeneeckhout, B., Janzen, E., Konert, G., Simon, O. J., & Weijermars, R. (1983). The structure and tectonic evolution of the Aguilon fold-nappe, Sierra Alhamilla, Betic Cordilleras, SE Spain. *Journal of Structural Geology*, *5*(5), 519–538. https://doi.org/10.1016/0191-8141(83)90057-3

Platt, J. P., & Vissers, R. L. M. (1989). Extensional collapse of thickened continental lithosphere: A working hypothesis for the Alboran Sea and Gibraltar arc. *Geology*, *17*(6), 540. https://doi.org/10.1130/0091-7613(1989)017<0540:ECOTCL>2.3.CO;2

Pollington, A. D., & Baxter, E. F. (2011). High precision microsampling and preparation of zoned garnet porphyroblasts for Sm-Nd geochronology. *Chemical Geology*, *281*(3–4), 270–282. https://doi.org/10.1016/j.chemgeo.2010.12.014

Porkoláb, K., Matenco, L., Hupkes, J., Willingshofer, E., Wijbrans, J., van Schrojenstein Lantman, H., & van Hinsbergen, D. J. J. (2022). Tectonic evolution of the Nevado-Filábride Complex (Sierra de Los Filábres, southeastern Spain): Insights from new structural and geochronological data. *Tectonics*, *41*(8), e2021TC006922. https://doi.org/10.1029/2021TC006922

Poulaki, E. M., & Stockli, D. F. (2022). Paleotectonic evolution of the Western Mediterranean: Provenance insights from the internal Betics, Southern Spain. *Frontiers of Earth Science*, *10*, 929502. https://doi.org/10.3389/feart.2022.929502

Poulaki, E. M., Stockli, D. F., Shuck, B., Laskari, S., & Stockli, L. (2020). Unraveling the pre-subduction stratigraphy and tectonometamorphic evolution of deeply subducted and exhumed rocks using zircon U-Pb geochronology. In *AGU Fall Meeting Abstracts* (Vol. *2020*, pp. V041-02).

Précigout, J., Gueydan, F., Garrido, C. J., Cogné, N., & Booth-Rea, G. (2013). Deformation and exhumation of the Ronda peridotite (Spain). *Tectonics*, *32*(4), 1011–1025. https://doi.org/10.1002/tect.20062

Puga, E., Díaz de Federico, A., Fanning, M., Nieto, J. M., Rodríguez Martínez-Conde, J. A., Díaz Puga, M. A., et al. (2017). The Betic ophiolites and the Mesozoic evolution of the Western Tethys. *Geosciences*, *7*(2), 31. https://doi.org/10.3390/geosciences7020031

Puga, E., Díaz de Federico, A., & Nieto, J. M. (2002). Tectonostratigraphic subdivision and petrological characterisation of the deepest complexes of the Betic zone: A review. *Geodinamica Acta*, *15*(1), 23–43. https://doi.org/10.1016/s0985-3111(01)01077-4

Reuber, I., Michard, A., Chalouan, A., Juteau, T., & Jermoumi, B. (1982). Structure and emplacement of the Alpine-type peridotites from Beni Bousera, Rif, Morocco – A polyphase tectonic interpretation. *Tectonophysics*, *82*(3–4), 231–251. https://doi.org/10.1016/0040-1951(82)90047-6

Rich, B. H. (2006). Permian bulk shortening in the Narragansett Basin of southeastern New England, USA. *Journal of Structural Geology*, *28*(4), 682–694. https://doi.org/10.1016/j.jsg.2006.01.003

Robyr, M., Vonlanthen, P., Baumgartner, L. P., & GrobetY, B. (2007). Growth mechanism of snowball garnets from the Lukmanier Pass area (Central Alps, Switzerland): A combined mu CT/EPMA/EBSD study. *Terra Nova*, *19*(4), 240–244. https://doi.org/10.1111/j.1365-3121.2007.00741.x

Romagny, A., (2014). *Evolution des mouvements verticaux n_eog_enes de la cha^_ne du Rif (Nord-Maroc): apports d'une analyse structurale et thermochronologique* (PhD thesis). Université Nice Sophia Antipolis.

Rosenbaum, G., Lister, G. S., & Duboz, C. (2002). Relative motions of Africa, Iberia and Europe during Alpine orogeny. *Tectonophysics*, *359*(1–2), 117–129. https://doi.org/10.1016/S0040-1951(02)00442-0

Rosenfeld, J. L. (1968). Garnet rotations due to major Palaeozoic deformations in Southeast Vermont. In E.-A. Zen, W. S. White, J. B. Hadley, & J. B. Thompson (Eds.), *Studies of Appalachian Geology* (pp. 185–202). Wiley.

Rossetti, F., Faccenna, C., & Crespo-Blanc, A. (2005). Structural and kinematic constraints to the exhumation of the Alpujarride Complex (Central Betic Cordillera, Spain). *Journal of Structural Geology*, *27*(2), 199–216. https://doi.org/10.1016/j.jsg.2004.10.008

Rossetti, F., Lucci, F., Theye, T., Bouybaouenne, M., Gerdes, A., Opitz, J., et al. (2020). Hercynian anatexis in the envelope of the Beni-Bousera peridotites (Alboran Domain, Morocco): Implications for the tectono-metamorphic evolution of the deep crustal roots of the Mediterranean region. *Gondwana Research*, *83*, 157–182. https://doi.org/10.1016/j.gr.2020.01.020

Rossetti, F., Theye, T., Lucci, F., Bouybaouene, M. L., Dini, A., Gerdes, A., et al. (2010). Timing and modes of granite magmatism in the core of the Alboran Domain, Rif chain, northern Morocco: Implications for the Alpine evolution of the western Mediterranean. *Tectonics*, *29*(2), TC2017. https://doi.org/10.1029/2009tc002487

Royden, L. H. (1993). Evolution of retreating subduction boundaries formed during continental collision. *Tectonics*, *12*(3), 629–638. https://doi.org/10.1029/92tc02641

Ruiz-Cruz, M. D., & Sanz-de-Galdeano, C. (2014). Garnet variety and zircon ages in UHP meta-sedimentary rocks from the Jubrique zone (Alpujárride Complex, Betic Cordillera, Spain): Evidence for a pre-Alpine emplacement of the Ronda peridotite. *International Geology Review*, *56*(7), 845–868. https://doi.org/10.1080/00206814.2014.904759

Ruiz-Fuentes, A., & Aerden, D. G. A. M. (2018). Transposition of foliations and superposition of lineations during polyphase deformation in the Nevado-Filabride complex: Tectonic implications. *International Journal of Earth Sciences*, *107*(6), 1975–1988. https://doi.org/10.1007/s00531-017-1582-6

Sánchez-Navas, A., García-Casco, A., & Martín-Algarra, A. (2014). Pre-Alpine discordant granitic dikes in the metamorphic core of the Betic Cordillera: Tectonic implications. *Terra Nova*, *26*(6), 477–486. https://doi.org/10.1111/ter.12123

Sánchez-Navas, A., Macaione, E., Oliveira-Barbosa, R. D., Messina, A., & Martin-Algarra, A. (2012). Transformation of Andalusite to Kyanite in the Alpujarride Complex (Betic Cordillera, Southern Spain): Geologic implications. *The Journal of Geology*, *120*(5), 557–574. https://doi.org/10.1086/666944

Sanislav, I. V. (2011). A long-lived metamorphic history in the contact aureole of the Mooselookmeguntic pluton revealed by in situ dating of monazite grains preserved as inclusions in staurolite porphyroblasts. *Journal of Metamorphic Geology*, *29*(2), 251–273. https://doi.org/10.1111/j.1525-1314.2010.00916.x

Santamaría-López, A., Lanari, P., & Sanz-de-Galdeano, C. (2019). Deciphering the tectono-metamorphic evolution of the Nevado-Filábride Complex (Betic Cordillera, Spain) – A petrochronological study. *Tectonophysics*, *767*, 128158. https://doi.org/10.1016/j.tecto.2019.06.028

Sanz-de-Galdeano, C. (2017). Implication of the geology of the Guadaiza and Verde valleys (Malaga Province, Betic Cordillera) on the position of the Ronda peridotites and the structure of the Alpujarride Complex. *Boletin Geologico y Minero*, *128*(4), 989–1006. https://doi.org/10.21701/bolgeomin.128.4.006

Sanz-de-Galdeano, C. (2019). Paleogeographic reconstruction of the Betic-Rif internal zone: An attempt. *Revista de la Sociedad Geologica de Espana*, *32*(2), 107–128.

Sanz-de-Galdeano, C., & Andreo, B. (1995). Structure of Sierra Blanca (Alpujarride Complex). *Estudios Geologicos*, *51*, 43–55.

Sanz-de-Galdeano, C., & López Garrido, A. C. (2016). Geometry of the contact of the peridotites of Sierra Alpujata with the Sierra Blanca succession (Alpujarride Complex, Betic internal Zone). *Geogaceta*, *60*, 7–10.

Sanz-de-Galdeano, C., & Santamaría-López, A. (2019). The lithological sequence of the Nevado-Filábride. Complex (Betic internal Zone) in the sierras Nevada and Filabres. *Revista de la Sociedad Geologica de Espana*, *32*(1), 113–126.

Sayab, M. (2005). Microstructural evidence for N-S shortening in the Mount Isa inlier (NW Queensland, Australia): The preservation of early W-E-trending foliations in porphyroblasts revealed by independent 3D measurement techniques. *Journal of Structural Geology*, *27*(8), 1445–1468. https://doi.org/10.1016/j.jsg.2005.01.013

Sayab, M., Aerden, D., Kuva, J., & Hassan, W. U. (2021). Tectonic evolution of the Karakoram metamorphic complex (NW Himalayas) reflected in the 3D structures of spiral garnets: Insights from X-ray computed micro-tomography. *Geoscience Frontiers*, *12*(3), 101113. https://doi.org/10.1016/j.gsf.2020.11.010

Sayab, M., Shah, S. Z., & Aerden, D. (2016). Metamorphic record of the NW Himalayan orogeny between the Indian plate-Kohistan Ladakh Arc and Asia: Revelations from foliation intersection axis (FIA) controlled P-T-t-d paths. *Tectonophysics*, *671*, 110–126. https://doi.org/10.1016/j.tecto.2015.12.032

Schindelin, J., Arganda-Carreras, I., Frise, E., Kaynig, V., Longair, M., Pietzsch, T., et al. (2012). Fiji: An open-source platform for biological-image analysis. *Nature Methods*, *9*(7), 676–682. PMID 22743772. https://doi.org/10.1038/nmeth.2019

Shah, S. Z., Sayab, M., Aerden, D., & Khan, M. A. (2011). Foliation intersection axes preserved in garnet porphyroblasts from the Swat area, NW Himalaya: A record of successive crustal shortening directions between the Indian plate and Kohistan-Ladakh Island Arc. *Tectonophysics*, *509*(1–2), 14–32. https://doi.org/10.1016/j.tecto.2011.05.010

Simancas, J. F. (2018). A reappraisal of the Alpine structure of the Alpujarride Complex in the Betic Cordillera: Interplay of shortening and extension in the westernmost Mediterranean. *Journal of Structural Geology*, *115*, 231–242. https://doi.org/10.1016/j.jsg.2018.08.001

Skrzypek, E., Schulmann, K., Stipska, P., Chopin, F., Lehmann, J., Lexa, O., & Haloda, J. (2011). Tectono-metamorphic history recorded in garnet porphyroblasts: Insights from thermodynamic modeling and electron backscatter diffraction analysis of inclusion trails. *Journal of Metamorphic Geology*, *29*(4), 473–496. https://doi.org/10.1111/j.1525-1314.2010.00925.x

Soto, J. I. (1991). *Estructura y evolución metamórfica del Complejo Nevado-Filábride en la terminación oriental de la Sierra de los Filabres (Cordilleras Béticas)* (PhD thesis, pp. 205). Universidad de Granada.

Spear, F. S., & Wolfe, O. M. (2021). Implications of overstepping of garnet nucleation for geothermometry, geobarometry and P–T path calculations. *Chemical Geology*, *530*, 119323. https://doi.org/10.1016/j.chemgeo.2019.119323

Spry, A. (1963). The origin and significance of snowball structure in garnet. *Journal of Petrology*, *4*(2), 211–222. https://doi.org/10.1093/petrology/4.2.211

Stampfli, G. M., & Hochard, C. (2009). Plate tectonics of the Alpine realm. *Geological Society, London, Special Publications*, *327*(1), 89e111–111. https://doi.org/10.1144/sp327.6

Stampfli, G. M., Mosar, J., Marquer, D., Marchant, R., Baudin, T., & Borel, G. (1998). Subduction and obduction processes in the Swiss Alps. *Tectonophysics*, *296*(1–2), 159–204. https://doi.org/10.1016/s0040-1951(98)00142-5

Steinhardt, C. K. (1989). Lack of porphyroblast rotation in non-coaxially deformed schists from Petrel-Cove, South Australia and its implications. *Tectonophysics*, *158*, 127–140.

ten Grotenhuis, S. M., Passchier, C. W., & Bons, P. D. (2002). The influence of strain localisation on the rotation behaviour of rigid objects in experimental shear zones. *Journal of Structural Geology*, *24*(3), 485–499. https://doi.org/10.1016/S0191-8141(01)00072-4

Timms, N. E. (2003). Garnet porphyroblast timing and behaviour during fold evolution: Implications from a 3-D geometric analysis of a hand-sample scale fold in a schist. *Journal of Metamorphic Geology*, *21*(9), 853–873. https://doi.org/10.1046/j.1525-1314.2003.00487.x

Tubía, J. M. (1994). The Ronda peridotites (Los-Reales-nappe) – An example of the relationship between lithospheric thickening by oblique tectonics and late extensional deformation within the Betic-Cordillera (Spain). *Tectonophysics*, *238*(1–4), 381–398. https://doi.org/10.1016/0040-1951(94)90065-5

Tubía, J. M., Cuevas, J., & Esteban, J. J. (2004). Tectonic evidence in the Ronda peridotites, Spain, for mantle diapirism related to delamination. *Geology*, *32*(11), 941–944. https://doi.org/10.1130/G20869.1

Tubía, J. M., Cuevas, J., & Esteban, J. J. (2013). Localization of deformation and kinematic shift during the hot emplacement of the Ronda peridotites (Betic Cordilleras, southern Spain). *Journal of Structural Geology*, *50*, 148–160. https://doi.org/10.1016/j.jsg.2012.06.010

Tubía, J. M., Cuevas, J., & Ibarguchi, J. I. G. (1997). Sequential development of the metamorphic aureole beneath the Ronda peridotites and its bearing on the tectonic evolution of the Betic Cordillera. *Tectonophysics*, *279*(1–4), 227–252. https://doi.org/10.1016/S0040-1951(97)00124-8

Tubía, J. M., Cuevas, J., Navarro-Vila, F., Alvarez, F., & Aldaya, F. (1992). Tectonic evolution of the Alpujarride Complex (Betic Cordillera, Southern Spain). *Journal of Structural Geology*, *14*(2), 193–203. https://doi.org/10.1016/0191-8141(92)90056-3

Tubía, J. M., Navarro-Vilii, F., & Cuevas, J. (1993). The Malaguide-Los Reales Nappe: An example of crustal thinning related to the emplacement of the Ronda peridotites (Betic Cordillera). *Physics of the Earth and Planetary Interiors*, *78*(3–4), 343–354. https://doi.org/10.1016/0031-9201(93)90165-6

van Hinsbergen, D. J. J., Torsvik, T. H., Schmid, S. M., Matenco, L. C., Maffione, M., Vissers, R. L. M., et al. (2020). Orogenic architecture of the Mediterranean region and kinematic reconstruction of its tectonic evolution since the Triassic. *Gondwana Research*, *81*, 79–229. https://doi.org/10.1016/j.gr.2019.07.009

Vergés, J., & Fernàndez, M. (2012). Tethys-Atlantic interaction along the Iberia-Africa plate boundary: The Betic-Rif orogenic system. *Tectonophysics*, *579*, 144–172. https://doi.org/10.1016/j.tecto.2012.08.032

Vissers, R. L. M. (1981). *A structural study of the central Sierra de los Filabres (Betic Zone, SE Spain) with emphasis on deformational processes and their relation to the Alpine metamorphism* (PhD thesis, pp. 154). GUA Papers on Geology, 1, 15.

Vissers, R. L. M., Platt, J. P., & Van der Wal, D. (1995). Late orogenic extension of the Betic Cordillera and the Alboran Domaind: A lithospheric view. *Tectonics*, *14*(4), 786–803. https://doi.org/10.1029/95tc00086

Vitale, S., Zaghloul, M. N., El Ouaragli, B., Tramparulo, F. D., & Ciarcia, S. (2015). Polyphase deformation of the Dorsale Calcaire Complex and the Maghrebian Flysch Basin Units in the Jebha area (Central Rif, Morocco): New insights into the Miocene tectonic evolution of the Central Rif belt. *Journal of Geodynamics*, *90*, 14–31. https://doi.org/10.1016/j.jog.2015.07.002

Vitale, S., Zaghloul, M. N., Tramparulo, F. D., & El Ouaragli, B. (2014). Deformation characterization of a regional thrust zone in the northern Rif (Chefchaouen, Morocco). *Journal of Geodynamics*, *77*, 22–38. https://doi.org/10.1016/j.jog.2013.09.006

Williams, J. R., & Platt, J. P. (2017). Superposed and refolded metamorphic isograds and superposed directions of shear during late orogenic extension in the Alboran Domain, southern Spain. *Tectonics*, *36*(5), 756–786. https://doi.org/10.1002/2016TC004358

Williams, J. R., & Platt, J. P. (2018). A new structural and kinematic framework for the Alboran domain (Betic–Rif arc, western Mediterranean orogenic system). *Journal of the Geological Society*, *175*(3), 465–496. https://doi.org/10.1144/jgs2017-086

Wolfe, O. M., & Spear, F. S. (2018). Determining the amount of overstepping required to nucleate garnet during Barrovian regional metamorphism, Connecticut Valley Synclinorium. *Journal of Metamorphic Geology*, *36*(1), 79–94. https://doi.org/10.1111/jmg.12284

Yeh, M. W. (2007). Deformation sequence of Baltimore gneiss domes, USA, assessed from porphyroblast Foliation Intersection Axes. *Journal of Structural Geology*, *29*(5), 881–897. https://doi.org/10.1016/j.jsg.2006.12.003

Yeh, M. W., & Bell, T. H. (2004). Significance of dextral reactivation of an E-W transfer fault in the formation of the Pennsylvania orocline, central Appalachians. *Tectonics*, *23*(5), TC5009. https://doi.org/10.1029/2003TC001593

Zevenhuizen, W. A. (1989). Quartz fabrics and recumbent folds in the Sierra-de-los-Filabres (SE Spain). *Geodinamica Acta*, *3*(1), 95–105. https://doi.org/10.1080/09853111.1989.11105177

Zwart, H. J. (1960). The chronological succession of folding and metamorphism in the Central Pyrenees. *Geologische Rundschau*, *50*(1), 203–218. https://doi.org/10.1007/bf01786838